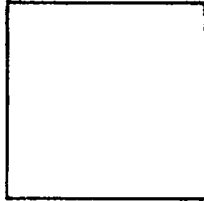


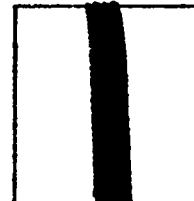
PHOTOGRAPH THIS SHEET

AD A995127

DTIC ACCESSION NUMBER



LEVEL



INVENTORY

Model Research on the Wind Loading of
Lattice Structures

DOCUMENT IDENTIFICATION

1 Mar. 55

Rept. No. AFSWP-464

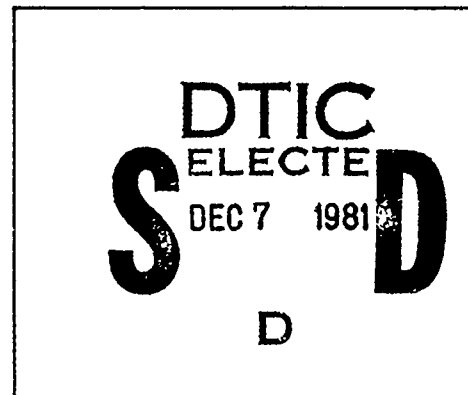
DISTRIBUTION STATEMENT A

Approved for public release;
Distribution Unlimited

DISTRIBUTION STATEMENT

ACCESSION FOR	
NTIS	GRA&I <input checked="" type="checkbox"/>
DTIC	TAB <input type="checkbox"/>
UNANNOUNCED	<input type="checkbox"/>
JUSTIFICATION	
(1 March 1955)	
BY	
DISTRIBUTION /	
AVAILABILITY CODES	
DIST	AVAIL AND/OR SPECIAL
A	

Released



DATE ACCESSIONED

DISTRIBUTION STAMP

UNANNOUNCED

81 12 02 04

DATE RECEIVED IN DTIC

PHOTOGRAPH THIS SHEET AND RETURN TO DTIC-DDA-2

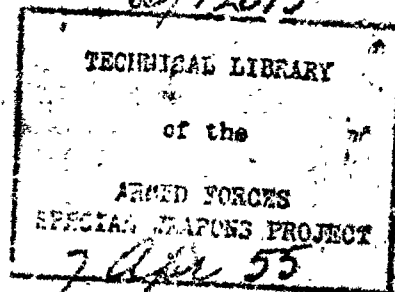
AD A995127

DISTRIBUTION STATEMENT A

Approved for public release;
Distribution Unlimited

AFSWP -
464

6/12/2013



AFSWP-464

Copy

CLEARED
FOR OPEN PUBLICATION

29 JAN 1955

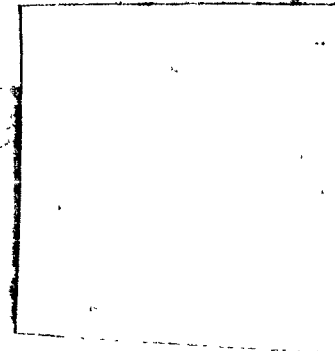
DIRECTORATE FOR SECURITY AND DEFENSE
DEPARTMENT OF STATE

MODEL RESEARCH ON THE WIND
LOADING OF LATTICE STRUCTURES

By

O. Flachsbart
H. Winter

Translated from the German
by B. L. Tucker, 5112



Statement A
Approved for public release
Distribution unlimited

AD A995127

Sandia Corporation

CONTRACTORS FOR

U.S. ATOMIC ENERGY COMMISSION

ALBUQUERQUE

NEW MEXICO

821

**Best
Available
Copy**

2 4
June 10, 1955

TO: Distribution of AFSWP-464

RE: Errata sheet for AFSWP-464

This publication should bear the following date: March 1, 1955.

1. On page 14, after the last sentence please add:

"The above designations will become clearer as they are encountered in the text and diagrams. Only the abbreviations for literature references remain to be mentioned:

AVA I I. Lieferung der Ergebnisse der Aero
Versuchsanstalt Göttingen (München und
Berlin 1921, 2nd ed 1923)

AVA II the same for (1923)

AVA III the same for 1927

AVA IV the same for 1932"

This statement originally appeared on page 18.

2. On page 41, on Fig. 15, please change call out to read

o = with plates (small)

O = with plates (large)

3. On page 47, under 4, please read $\phi = 0.458$ for $\phi = 9.458$

4. On page 63, under B, line 5, for ψ please read ψ_I

5. On page 66, under C, line 3, change expression to read $q' = \frac{1}{2}\rho v^2$

6. On page 70, paragraph 2, line 1, change expression to read $\bar{v}' = v'_{\min}$

7. On page 72, last paragraph, line 3, change expression to read
 $\psi_I = 0.9$

8. On page 76, line 7, please read e/d for e/h

9. On page 89, the Note to figure caption should read "All bars have L cross section."

10. On page 93, change expression following last 3 equations to read
"for -45° "

11. On page 101, Fig. 18a, for second note in legend, please read
"● = whole mast on smooth ground."

12. On page 107, paragraph 3, line 8, change "or box lattice" to read
"on box lattice."

13. On page 113, paragraph 2, line 2, change "sine law of sine-squared law" to read "sine law or sine-squared law."

Since the corrections to this publication are readily apparent, it was not deemed necessary to recall the document to make the above changes.

Publications, 2464-1

AFSWP-464
March 1, 1955

MODEL RESEARCH ON THE WIND
LOADING OF LATTICE STRUCTURES

By

O. Flachsbart
H. Winter

Translated from the German
by B. L. Tucker, 5112

FOREWORD

This treatise was originally published in the German journal, Der Stahlbau, under the title "Modellversuche über die Belastung von Gitterfachwerken durch Windkräfte." Part 1 appears on pages 65 to 69 of the April 27, 1934, issue and on pages 73 to 79 of that for May 11, 1934. Part 2 was printed on April 26, 1936, pages 65 to 77.

No attempt has been made to edit or interpret the original work; nor has the phraseology been changed more than the minimum for clarity. As a result, many sentences are close to their German originals in structure and length, and all of the author's repetitions are faithfully retained.

Numbers in parentheses serve as a guide to the German text.

TABLE OF CONTENTS

	<u>Page</u>
FOREWORD	3
PART 1	11
CH I -- INTRODUCTION	11
A. NOMENCLATURE	12
CH II -- AERODYNAMICS OF SOLID BEAMS AND SINGLE PLATES	15
A. MODEL RULES	15
1. The Plane Right-Angle Plate as a Model of an Unbraced Solid Beam or an Iron Gusset	15
2. Model Rules	24
3. Drag of Single-Beam Profiles	25
CH III -- TESTS ON SCHEMATIC PLANE LATTICES FOR NORMAL WINDS ($\alpha = 0^\circ$)	29
A. PARALLEL BEAMS OF INFINITE ASPECT RATIO ($\lambda = \infty$)	29
B. CONTROL TESTS ON THE INFLUENCE OF TEST ORIENTATION. MODEL SIZE, WIND VELOCITY, AND WIND TURBULENCE	33
C. PARALLEL BEAMS WITH FINITE ASPECT RATIO	36
D. THE INFLUENCE OF JUNCTIONS AND JUNCTION PLATES	39
E. CALCULATED CHANGE IN WIND LOADING DUE TO JUNCTION PLATES	40
CH IV -- TESTS FOR $\alpha = 0^\circ$ ON PLANE LATTICES WITH BARS OF VARIOUS CROSS SECTIONS	47
CH V -- TESTS ON PLANE LATTICES FOR OBLIQUE WIND INCIDENCE ($\alpha \geq 0^\circ$)	51
CH VI -- CONCLUSIONS	53

TABLE OF CONTENTS (cont)

	<u>Page</u>
PART 2 -- THREE-DIMENSIONAL LATTICES	57
CH I -- PRELIMINARY REMARKS	57
A. PURPOSE OF RESEARCH. REVIEW OF PART 1	57
B. NOMENCLATURE	58
CH II -- TWO PARALLEL LATTICES, ONE BEHIND THE OTHER	61
A. FUNDAMENTALS	61
B. TESTS ON TWO SOLID PLATES ($\phi = 1$)	63
C. PRESSURE AND VELOCITY FIELDS BEHIND A LATTICE UNDER NORMALLY INCIDENT WIND	66
D. TESTS ON TWO PARALLEL LATTICES OF LIKE PATTERN AND SOLIDARITY RATIO FOR NORMAL WINDS	70
E. OBLIQUE INCIDENCE ON LATTICE PAIRS	78
CH III -- TWO LATTICES WITH ROADBED (BRIDGES)	81
CH IV -- FOUR LATTICES IN A BOX STRUCTURE ($\lambda = \infty$)	85
A. NORMAL INCIDENCE ($\alpha = 0^\circ$)	85
B. OBLIQUE FLOWS ($\alpha \leq 90^\circ$)	92
CH V -- TESTS ON MODELS OF COMPLETE MASTS	97
CH VI -- SUMMARY AND CONCLUSIONS	103
APPENDIX A	117

LIST OF ILLUSTRATIONS

	<u>Page</u>
PART 1	
Fig. 1 -- Designation of wind forces	13
Fig. 2 -- Drag coefficient c_w for normal wind incidence ($\alpha = 0^\circ$) on plane rectangular plates of infinite aspect ratio for various Reynolds numbers	18
Fig. 3 -- Cross section of three plates of different thickness: height	19
Fig. 4 -- Normal incidence on rectangular plates $\alpha = 0^\circ$	21
Fig. 5 -- Pressure distribution along AB of an infinite plate under normal winds ($\alpha = 0^\circ$)	21
Fig. 6 -- Plane rectangular plate $\lambda = 5$. Oblique incidence from above or below	23
Fig. 7 -- Plane rectangular plate $\lambda = 5$. Oblique incidence from the side	23
Fig. 8 a-g -- Results of measurements on schematic plane lattices with $\lambda = \infty$ and $\alpha = 0^\circ$	30
Fig. 9 -- Dependence of drag coefficients on solidarity ϕ . Aspect ratio of the beams $\lambda = \infty$	32
Fig. 10 -- Some more schematic plane lattices. They were investigated for $\lambda = \infty$	35
Fig. 11 -- Dependence of drag coefficients on the aspect ratio λ for $\alpha = 0^\circ$ and schematic plane lattices	36
Fig. 12 -- Comparison drag coefficients for plates of $\lambda = \infty$ with those of $\lambda = 1$	37
Fig. 13 -- Wind loading of a 3-pronged junction	39
Fig. 14 -- Wind loading of a 4-bar junction	41
Fig. 15 -- The influence of junction plates on the wind-loading of plane schematic lattices. $\lambda = \infty$	41
Fig. 16 -- Nomenclature for calculating the effect of junction plates	42

LIST OF ILLUSTRATIONS (cont)

	<u>Page</u>
Fig. 17 -- Comparative measurements on a plane lattice. $\lambda = \infty$	48
Fig. 18 -- Model of a plane lattice girder of 'profiled' bars (bars with two-dimensional cross sections)	48
Fig. 19 -- Section model of a mast tested for $\lambda = \infty$	49
Fig. 20 -- Five bridge models tested in 1921 at Göttingen $\lambda = 1^2/F = 9.5$	52
Fig. 21 -- Combined test results for plane lattices	52

PART 2

Fig. 1 -- Shielding coefficients of two parallel plates one behind the other with normal wind incidence	64
Fig. 2a -- Distribution of total and static pressures	67
Fig. 2b -- Velocity distribution behind a ladder-type lattice	67
Fig. 3a -- Ladder structure. Lattices in line	69
Fig. 3b -- Ladder structure. Lattices transposed 1/2-field width	69
Fig. 3c -- V-structure. Lattices in line	69
Fig. 3d -- V-structure. Lattices transposed 1/2-field width	69
Fig. 3e -- N-structure. Lattices in line	69
Fig. 3f -- N-structure. Lattices transposed 1/2-field width	69
Fig. 3g -- N-structure. Lattices transposed so that the diagonal crossed, chords still in line	69
Fig. 4 -- Shielding coefficients of lattice pairs under normal incidence ($\alpha = 0^\circ$) and infinite aspect and ratio ($\lambda = 9.5$). Lattices in line	71
Fig. 5 a-e -- Shielding ratio ϕ of lattice pairs as a function of η (5 a-d, lattices in line; 5e, lattices transposed)	74
Fig. 6 a-b -- Graph of η value for technical drag calculations of lattice pairs in line; developed from Figs. 5 a-d	75

LIST OF ILLUSTRATIONS (cont)

	<u>Page</u>
Fig. 7 a-b -- Lattice pairs of type (5), $\phi = 0.458$. Oblique incidence from above (7a) and from the side (7b)	79
Fig. 8 -- Bridge model with main girders of type (5) with oblique winds from above, $\phi = 0.458$, $\frac{c}{d} = 1.44$	82
Fig. 9 -- Box structure cross section	85
Fig. 10 a-c -- Three sectional models of transmission masts	87
Fig. 11a -- Sectional model of a radio tower (Zeesner radio tower)	88
Fig. 11 b-c -- Two more sectional models of the Zeesner tower tested independently of the model of Fig. 11a	88
Fig. 12 a-c -- Three models of box-work structures with quadratic cross section and N-type bracing	89
Fig. 13 a-c -- Photographs of the three models in Fig. 10	90
Fig. 13d -- Photograph of the model in Fig. 11a	90
Fig. 14 -- Model in the wind tunnel	90
Fig. 15 a-b -- Definition sketches	92
Fig. 16 a-b -- Models of two lattice masts; (a) transmission tower; (b) line pole	97
Fig. 17 a-b -- Velocity profile over (a) rough ground plates and (b) smooth ground plates	98
Fig. 18 a-b -- Lattice towers of square cross section	101
Fig. 19 a-b -- Comparison between the proposed procedures and the current (1935) techniques for drag calculations of bridges	110
Fig. 20 a-b -- Shielding coefficients of a group of four parallel lattices, $\alpha = 0^\circ$, $\lambda = \infty$	114
Fig. 21 a-b -- Shielding coefficients of a group of four V-type parallel lattices (Fig. 8g, Part 1), $\phi = 0.234$, $\lambda = \infty$	115
Fig. 22 -- Winds from above	116
Fig. 23 -- Winds from a side	116

PART 1

CH I -- INTRODUCTION

The goal of this investigation was to obtain a broad and complete foundation for wind pressure calculations on structural lattices. Part 1 deals with plane lattices; part 2 deals with three-dimensional lattices. These researches have really contributed far-reaching clarity to the aerodynamic properties of plane and spacial lattice structures. In spite of the diversity of structural classes included in the field of lattice structures, it has been possible to express their aerodynamic characteristics in simple terms: in particular the relations of plane lattices to a spacial lattice composed of several plane sections.

In these results lies the major contribution laboratory tests can make toward answering the question of wind loading for lattice structures. The problem is not completely solved. Wind tunnel research gives only information about loading when the properties of the wind-stream are known. However, not enough is known about winds outside in storms.

In the interest of completeness, some experiments besides Göttingen data have been included. Conventional measuring techniques were used throughout, and experimental units were generally retained in the diagrams.

The author has made an effort to keep this account understandable to those without a strong foundation in aerodynamics. To avoid overloading the text, the explanations of simple concepts have been kept short. For a thorough treatment the newer texts and handbooks are recommended.*

* (3) See W. Kaufmann, Textbook of Applied Hydrodynamics, (Berlin 1934)

A. NOMENCLATURE

Wind Velocity

v [m/s] ... undisturbed wind velocity, practically identical to the wind velocity in front of the structure.

Wind Direction

α ... angle between wind direction and the normal to the lattice plane. In the text $\alpha = 0^\circ$ is often called normal incidence, and $\alpha \lesssim 0^\circ$ is labeled oblique incidence.

Physical Properties of Air*

ρ [kg s²/m⁴] ... Density = mass per unit space. For normal conditions

$$\rho \simeq 1/8 \text{ [kg} \cdot \text{s}^2/\text{m}^4\text{]}$$

μ [kg · s/m²] ... viscosity

$\nu = \frac{\mu}{\rho}$ [m²/s] ... so-called "kinematic viscosity". Usually the unit of length is [cm] and not [m], so that for convenience $\nu \approx 1/7 \text{ cm}^2/\text{s}$ can be used under normal conditions.

Geometric Properties of Plane Lattice Structures

F [m²] ... outlined area

F_r [m²] ... visible surface area (seen from the normal to the structural plane) = sum of the visible surfaces of all beams and plates = remaining surface after the empty spaces have been subtracted from the outlined area.

*Note Flachsbart uses [kg] as a unit of force; thus Mass = kg/accel.

$\phi = F_r / F$... Solidarity coefficient or fullness grade. A measure of the area density of beams in a lattice. The greater ϕ , the denser the beam coverage. A solid member has a solidarity coefficient $\phi = 1$.

Wind Pressures

$p \text{ [kg/m}^2\text{]}$... statistical pressure at any place in the wind stream, especially on the outer surface of the test structure.

$q = \frac{1}{2} \rho v^2 \text{ [kg/m}^2\text{]}$... dynamic pressure of the undisturbed wind velocity, identical with the kinetic energy of each unit space in the unaffected air stream.

Wind Forces (Fig. 1)

$P \text{ [kg]}$... resultant wind force on the structure

$W \text{ [kg]}$... component of P in the direction of v , so-called "resistance"

$A \text{ [kg]}$... component of P normal to the direction of v , "buoyancy"

$N \text{ [kg]}$... component of P normal to structure plane, "normal force"

$T \text{ [kg]}$... component of P tangential to structure plane, "tangential force."

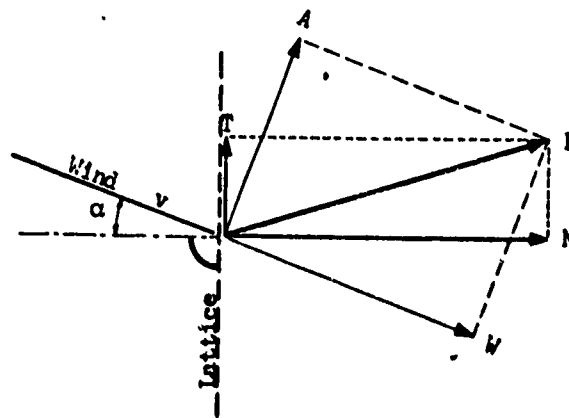


Fig. 1 -- Designation of wind forces

Relationships between wind forces derivable from Fig. 1:

- (1) $P^2 = A^2 + W^2$
- (2) $P^2 = N^2 + T^2$
- (3) $N = A \cdot \sin \alpha + W \cdot \cos \alpha$
- (4) $T = A \cdot \cos \alpha - W \cdot \sin \alpha$

For $\alpha = 0^\circ$, normal wind incidence, $W \equiv N$, $A \equiv T$

1. Dimensionless Wind Force Measures, "Drag Coefficients."

For the resulting drag (wind force), the drag coefficients depend on whether F or F_r are utilized:

$$c_p = P/qF \text{ while } c_{p_r} = P/qF_r$$

in a corresponding way for components:

$$c_w = W/qF \text{ and } c_{w_r} = W/qF_r$$

$$c_a = A/qF \text{ and } c_{a_r} = A/qF_r$$

$$c_n = N/qF \text{ and } c_{n_r} = N/qF_r$$

$$c_t = T/qF \text{ and } c_{t_r} = T/qF_r$$

These drag coefficients are related by equations based on Eqs 1 to 4 where the forces are replaced by drag coefficients: $c_p^2 = c_a^2 + c_w^2$ or $c_{p_r}^2 = c_{a_r}^2 + c_{w_r}^2$, etc.

For $\alpha = 0^\circ$, wind direction normal to the lattice plane, $c_w \equiv c_n$, $c_{w_r} \equiv c_{n_r}$, $c_a \equiv c_t$,

$$c_{a_r} \equiv c_{t_r}$$

CH II -- AERODYNAMICS OF SOLID BEAMS AND SINGLE PLATES

A. MODEL RULES

It is desirable to discuss the comparative aerodynamics of solid beams, single plates, and lattice structures. All following observations are based, unless otherwise stated, on the premise of a spacially and timely uniform wind stream.

1. The Plane Right-Angle Plate as a Model of an Unbraced Solid Beam or an Iron Gusset

Consider a rectangular plate of length l , height h , and of very slight thickness δ . The wind-facing surface of the plate then has an "aspect ratio" of $\lambda = l/h$. The solidity coefficient is $\phi = F_r'/F = 1$, since the solid wind-facing surface F_r is identical with the outlined area F . In a uniform wind stream normal to the surface ($\alpha = 0^\circ$, Fig. 1), this plate will undergo a symmetrically loaded drag force W (or, for $\alpha = 0^\circ$, an identical normal force N or P) in the direction of the air stream; the lift A (the tangential force T Fig. 1) is null:

$$W \equiv N \equiv P \neq 0 \quad A \equiv T = 0$$

therefore

$$c_w \equiv c_n \equiv c_p \neq 0 \quad c_a \equiv c_t = 0$$

Now we have three interesting questions:

- a) How do the drag and drag coefficient for normally incident air flow on a plane rectangular plate depend on λ , v , the absolute values of h and l , on surface roughness, on density, viscosity, and turbulence of the air? Since we can combine several of these quantities in the dimensionless quantity called the Reynolds Number,

(5)

$$R = \frac{v h \rho}{\mu} = \frac{v h}{\nu}$$

the question can be succinctly restated:

How does the drag coefficient depend on the Reynolds Number, the surface roughness, and turbulence?

- b) How does the drag coefficient change with λ under otherwise equal conditions?
- c) How does this relation change with oblique incidence?

The first of these questions is obviously equivalent in meaning to the question of the scalability of model measurements. The three questions are answered on the grounds of the following experiments.

For question a):

In Fig. 2 the measured c_w values as a function of R are presented for technically smooth plates. Going along the R axis in the direction of increasing R means that v , h , and ρ have been separately increased to change R , or μ was decreased. These possibilities are dynamically equivalent, as is shown in fluid mechanics, and only because they are equivalent can a single dimensionless quantity, R , be used to express a large part of an aerodynamic state. The flat plates, for which the resistance curve of Fig. 2 applies, are infinitely long plates. For such plates all stream lines are in planes normal to the plate and the stream lines are congruent, so that the complete flow pattern is contained in one of these planes. On this ground one can speak of the $\lambda = \infty$ case as "plane" or "two-dimensional" flow. As this case is experimentally feasible, the answering of question b) will be temporarily neglected.

One sees in Fig. 2, that the drag coefficient (here $c_w = \frac{\dot{W}}{q h \pi l}$, where \dot{W} designates the resistance of the plate-per-unit length) is indeed related to R , as the general law of

The above designations will become clearer as they are encountered in the text and diagrams. Only the abbreviations for literature references remain to be mentioned:

AVA I I. Lieferung der Ergebnisse der Aero Versuchsanstalt
Göttingen (München und Berlin 1921, 2nd ed 1923)

AVA II the same for (1923)

AVA III the same for 1927

AVA IV the same for 1932

similitude of hydrodynamics asserts, but over a certain R -value—approximately $R \geq 5 \cdot 10^3$ —

$c_w = \text{const}$ and is independent of R . *

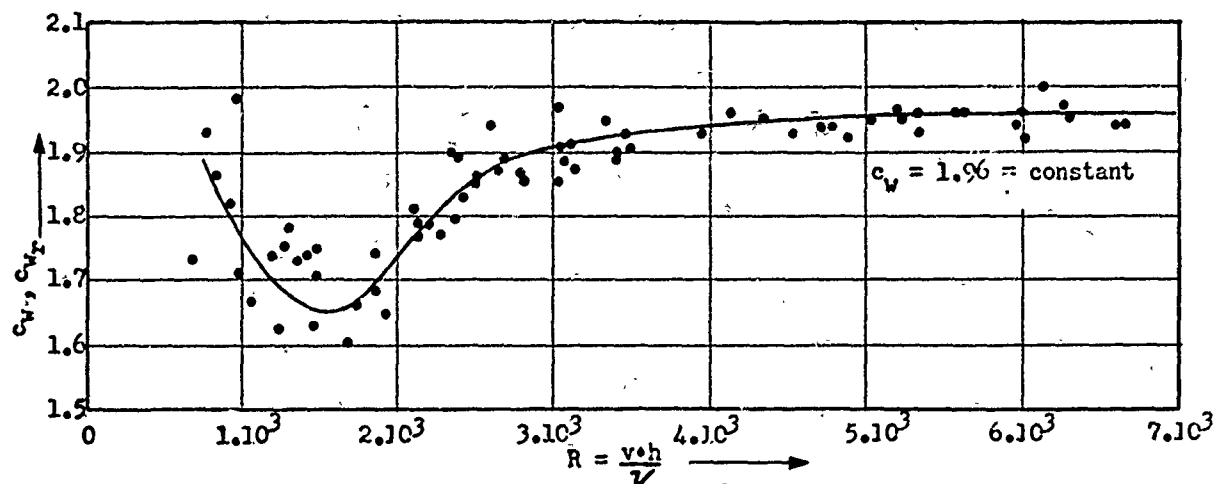


Fig. 2 -- Drag coefficient c_w for normal wind incidence ($\alpha = 0^\circ$) on plane rectangular plates of infinite aspect ratio for various Reynolds Numbers. Since these plates are solid ($\phi = 1.0$), $F \equiv F_r$, and $c_w = c_{w_r}$

This result has great practical meaning. It holds logically for every rectangular plate, only changing with the aspect ratio λ (compare Fig. 3).

Now it can be further shown that in the area where c_w is independent of R neither the roughness of the plate surface nor the degree of turbulence of the wind influence the drag on the plate. For $R > 5 \cdot 10^3$ one measurement on a plate under normally incident wind suffices for any size plate in almost any wind speed as long as the plate is geometrically similar and wind incidence angle is the same. One has only to take a test Model 1 (area F_1) in a wind v_1 giving drag W_1 to obtain c_w

$$c_w = \frac{W_1}{\frac{1}{2} \rho v_1^2 F_1}$$

* (4) In Fig. 2 the scatter of data points is rather large since the measured forces for small R -values were very small (small plates, small wind velocities). Therefore many points were taken to establish the course of the c_w -curve. A detailed publication about these measurements will appear shortly. In the range of large R -values (10^4 to 10^5) the c_w -value ($c_w = 1.96$) was measured to 1 per cent. See O. Flachsbart, Measurements on Plane and Vaulted Plates, AVA IV, S. 99

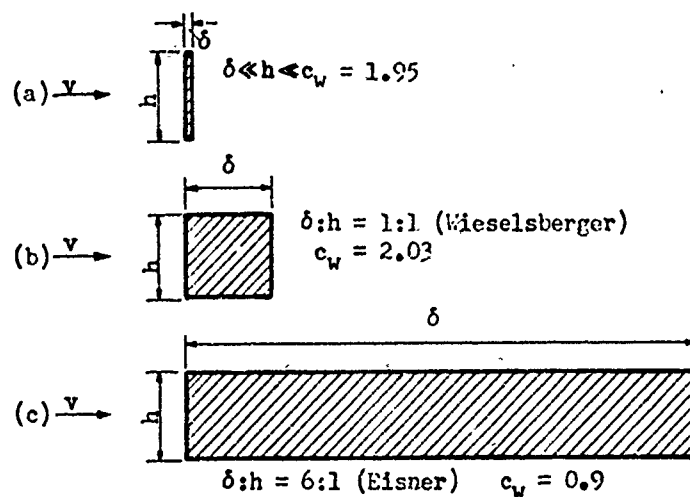


Fig. 3 -- Cross section of three plates of different thickness: height

Then a' new drag W_1^I for a new wind v_1^I can be calculated for the same plate

$$W_1^I = c_w \cdot \frac{1}{2} \rho v_1^{I^2} F_1 \text{ [kg]}$$

or a drag W_{II} for a geometrically similar Plate II (area F_{II}) for wind V_{II}

$$W_{II} = c_w \cdot \frac{1}{2} \rho v_{II}^2 F_{II} \text{ [kg]}$$

Example: Plane rectangular plate, $\lambda = \infty$, $\alpha = 0^\circ$.

In an experiment on Plate I of height $h_1 = 0.20$ m and $v_1 = 20$ m/s, the measured drag was

$W_1 = 9.8$ kg per unit length.

$$\therefore c_w = \frac{W_1}{\frac{1}{2} \rho v_1^2 h_1 \cdot "1"} = 1.96$$

For drag W_1^I on the same plate in a wind of $v_1^I = 40$ m/s, it follows with $c_w = \text{constant} =$

1.96 that:

$$W_1^I = c_w \cdot \frac{1}{2} \rho v_1^{I^2} \cdot "1" = \left(\frac{v_1^I}{v_1} \right)^2 W_1 = 39.2 \text{ kg.}$$

In a corresponding way W_{11} (drag-per-unit length on another similar plate) is calculated with $h_{II} = 1.0$ m and $v_{II} = 40$ m/s as:

$$W_{II} = c_w \cdot \frac{1}{2} \rho v_{II}^2 h_{II} \cdot "1" = 1.96 \cdot \frac{1}{16} \cdot 40^2 \cdot (1.0) \cdot "1" = 196 \text{ kg}$$

We still have to check on the Reynolds Number to make sure that $R > 5 \cdot 10^3$

$$R_1 = \frac{v_1 h_1}{\nu} = \frac{2000 \cdot 20}{1/7} = 2.8 \times 10^5$$

$$R'_1 = \frac{v'_1 h_1}{\nu} = \frac{4000 \cdot 20}{1/7} = 5.6 \times 10^5$$

$$R_{II} = \frac{v_{II} h_{II}}{\nu} = \frac{4000 \cdot 100}{1/7} = 2.8 \times 10^6$$

The condition that $R > 5 \cdot 10^3$ is therefore fulfilled in all three cases, allowing $c_w = \text{const}$ to be a valid assumption. (It should be noticed that in calculating R the length is taken in [cm] if the kinematic viscosity ν is expressed in $[\text{cm}^2/\text{s}]$ as above.)

The independence of c_w of R also holds for plates where the thickness is no longer negligibly small. For a quadratic prism ($h = \delta$) with $\lambda = \infty$, $\alpha = 0$, Wieselsberger found $c_w = 2.03$,* which is only a slight deviation from the thin plate value. For a prism where $\delta = 6h$ and $\lambda = \infty$ (Fig. 3c), $\alpha = 0^\circ$, Eisner^{6/} found the markedly small value $c_w \simeq 0.9$. A real dependence of c_w on R could not be established above $R \simeq 10^4$ for the last-named case, although it seemed likely in view of observations on long smooth plates edge-on to the air stream. The lessening of c_w for thick plates depends on the fact that the wind stream returns to the side surface after initially leaving it.

* (5) One should observe that Wieselsberger found $c_w = 2.01$ for the infinite plane plate and $\alpha = 0^\circ$. AVA II, S. 33-35.

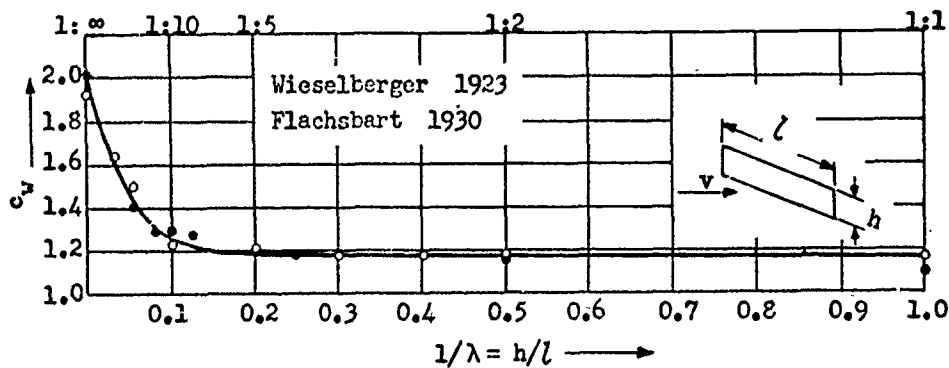


Fig. 4 -- Normal incidence on rectangular plates $\alpha = 0^\circ$. Dependence of drag coefficients c_w on aspect ratio λ . (Note that the reciprocal of λ is actually plotted above.)

(To answer question b)

Figure 4 shows, for the only interesting region $R > 5 \cdot 10^3$, that the c_w -value depends on λ for rectangular plates normal to the wind flow. This means, since $W = c_w q F$, that drag is not only proportional to the surface area, but is also significantly related to the outline of the plate. The drag on a very long rectangle is for example twice as much as the drag on a square plate of the same area.

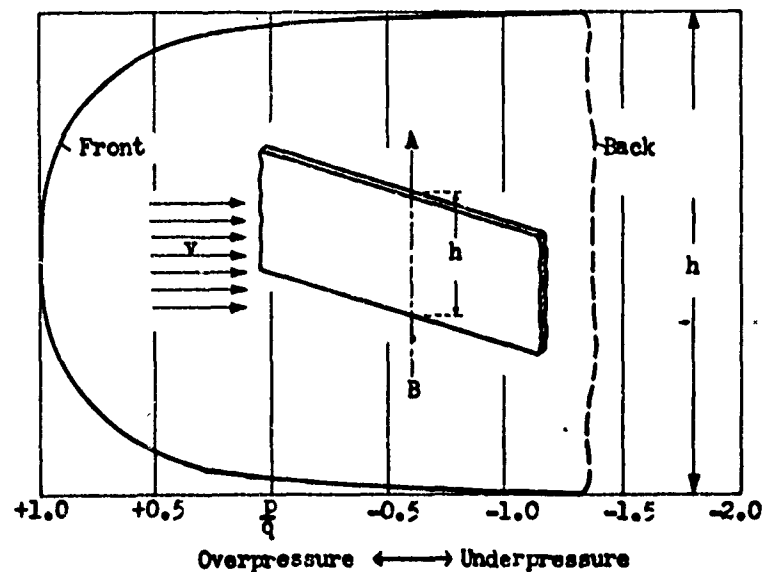


Fig. 5 -- Pressure distribution along AB of an infinite plate under normal winds ($\alpha = 0^\circ$). (From Fage and Johansen, Proc. Roy. Soc., A Vol 116, London 1927)

It is important for the understanding of later developments to have Fig. 5 on hand to delineate the distribution of wind forces for the two-dimensional case ($\lambda = \infty$) and for $\alpha = 0^\circ$. Figure 5 shows pressure distribution in a plane containing the wind direction. In conformity with the dimensionless formation of drag, the dimensionless quantity p/q replaces the normal pressure p . As one can see, the diagram represents overpressure on the windward side and underpressure on the leeward. In the middle of the forward side, $p/q = 1$ and thus the overpressure equals the dynamic pressure. As the edge of the plate is approached the overpressure declines and even becomes negative. On the back side, there is only underpressure of $1.35 q$, and therefore 35 per cent greater than the largest overpressure. It is evident that the underpressure on the leeward side exerts a greater force (and in the same direction) than the overpressure on the windward side. The average front pressure being $0.65 q$,

$$W = (0.65 + 1.35)q h \cdot "1" = 2.0 q h \text{ [kg]}$$

$$\therefore c_w = \frac{W}{qF} = \frac{W}{q h \cdot "1"} = 2.0$$

in complete agreement with the results of the drag measurements. Approximately 70 per cent of this force comes from the underpressure on the leeward side.

In view of this partition it is easily understood why the c_w -value of a plate must become smaller when λ is reduced from infinity to finite numbers. For plates of finite length, the pressure difference between the front and back induces a flow around the ends. This introduces air into the partial vacuum of the rear side and thus reduces the suction. Also the pressure on the front falls off toward the ends and further reduces the front-back pressure difference and c_w . Thus a cross section like Fig. 5 will show much higher pressure differences in the center than near the ends of the plate.

If one hinders this end flow by end plates sufficiently large and perpendicular to the incident air, then the flow patterns approach the $\lambda = \infty$ case, and λ variations are largely masked. One uses this concept to experimentally approximate plates of infinite length for test measurements.

Answer to (c)

For oblique wind incidence the independence of c_w of R above $R = 10^4$ is not seriously altered nor is the dependence of c_w on λ . Only the numerical value of c_w is changed. In general the net drag for oblique winds is not in the wind direction; a single drag coefficient no longer contains sufficient information to describe the system. One must use either c_w and c_a or c_n and c_t . How these drag coefficients for rectangular plates and $\lambda = 5$ depend upon incidence angle α is shown for winds from above in Fig. 6, and for side winds in Fig. 7.

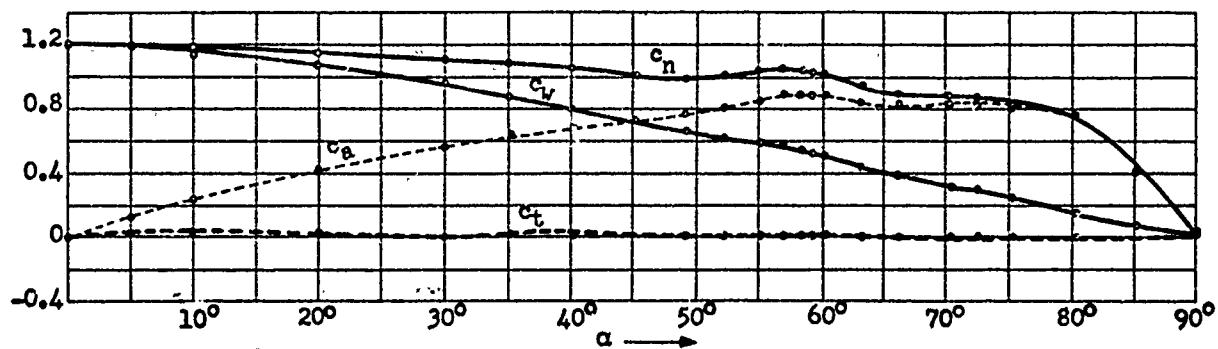


Fig. 6 -- Plane rectangular plate $\lambda = 5$. Oblique incidence from above or below

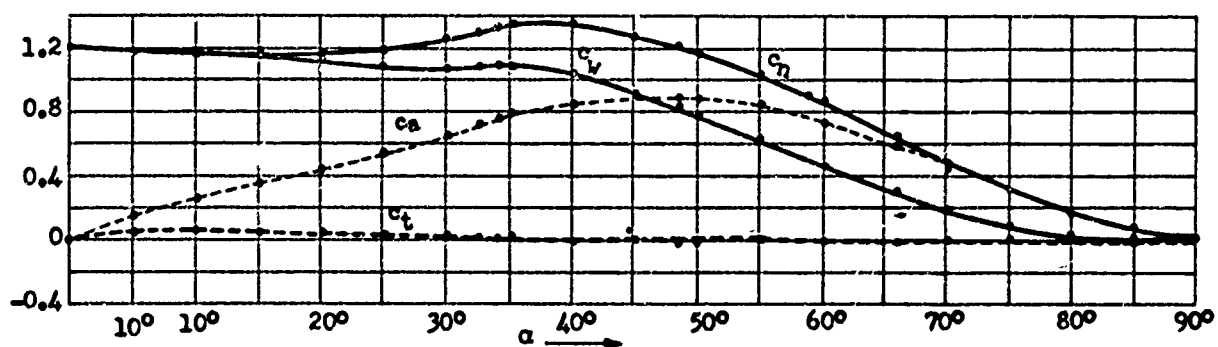


Fig. 7 -- Plane rectangular plate $\lambda = 5$. Oblique incidence from the side

The curves of c_w and c_a are not as interesting as those of c_n and c_t . We establish the important fact that the tangential forces are negligibly small, and that the normal force actually declines with growing wind angles, at first only slightly, but more strongly with large wind angles α . The small rise of c_n in the region of $\alpha = 30^\circ$ to $\alpha = 50^\circ$ for side winds rapidly falls away, so that for lattices one may say: The c_n value is in general greatest for $\alpha = 0^\circ$. For solid beams this statement is only approximately true.

For $\alpha = 0^\circ$, c_n is identical with c_w . We have the separate designation c_w since it is usually used in the literature. For oblique incidence one must examine each case to determine whether c_n and c_t or c_a and c_w should be used. For single beams c_n and c_t are recommended.

2. Model Rules

It is now of decisive importance that—always satisfying the Reynolds number condition—the independence of drag values of Reynolds number, of surface roughness and of wind turbulence is not limited to flat plates, but also holds for all bodies with sharp corners. Since the lattice constructions of engineers have, almost without exception, these properties, we can limit our observations to lattices with sharp angles. Then it follows:

The drag coefficients for lattices are to a good approximation independent of wind velocity, model size, surface roughness, density, viscosity, and turbulence of the air; they are alone dependent on the form of the lattice work and on the wind direction.

For a lattice of a certain form under a given angle of wind incidence

$c = \text{constant}$

in particular therefore

$$c_p = \text{const} \quad c_w = \text{const} \quad c_a = \text{const} \quad \text{etc.}$$

Through these simple relations, which have been established through a great number of wind tunnel tests, the transfer of model measurements is regulated by geometric similarity. They hold not only for winds uniform in space and time but—as tests have shown—also for spacially nonuniform air streams provided the comparative case has a similar nonuniformity (then v has to be specially defined, since a unified wind velocity no longer obtains). Whether they hold for strongly varying (time-wise) winds is doubtful since extensive tests have not been made. From this uncertainty come reservations for the transfer of wind tunnel data to lattices in free winds. Some remarks on this will be made in other places (Chapter III, B).

To prevent misunderstandings, it should be expressly pointed out that the law $c = \text{constant}$ does not hold:

- a) for small R -values
- b) for rounded bodies (streamlined bodies, cylinders, spheres) throughout the entire range of R -values.

In case (a) the drag coefficients are functions of R ; in case (b) functions of R , surface roughness, and wind turbulence.

The requirement of "sufficiently large Reynolds number" which is coupled to the $c = \text{constant}$ model rule is always satisfied for lattice works. "Sufficiently large" means $R \geq 5 \cdot 10^3$. The Reynolds numbers for plates and bars of real lattice works in winds of $v \geq 30$ m/s are much greater than $5 \cdot 10^3$. For the reduced members of a model one must check each case to find whether the permissible lower limit of Reynolds numbers has been passed.

3. Drag of Single Beam Profiles

Here the usual cross section form of practical beams are designated by the term beam profile. To avoid mistakes, the aspect ratio of a beam will be designated by a subscript s to distinguish it from the λ of the entire lattice.

$$\lambda = \frac{\text{structure length}}{\text{structure height}} = \text{aspect ratio of the lattice}$$

$$\lambda_s = \frac{s^2}{\phi} = \text{aspect ratio of a beam}$$

when s = beam length, and ϕ = projected surface of the beam seen in the wind direction.

For each profile c = constant. Table I shows the degree of dependence of the drag coefficient on cross-sectional profile.

One can derive from the above collection of drag coefficients that the average value is $c_w \simeq 2.0$ for $\lambda = \infty$ and normal wind incidence, and the deviation from 2.0 is small. In fact, for virtually all profiles (except type 8 #)

$$c_w = 2.0 \pm 10\%$$

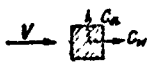
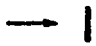

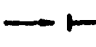

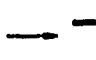
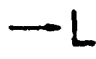

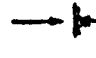
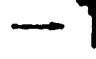
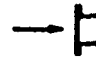
is a sufficiently accurate drag value for $\lambda_s = \infty$. *

Since different beam profiles may be used on the same lattice, their net drag coefficients will probably average out to 2.0, some drag coefficients being greater and some less than 2.0. However, $c_w = 2.0$ is the value for an infinite plate with $\alpha = 0^\circ$. Thus one must be able to use flat rectangular beams in a lattice to experimentally measure aerodynamic properties valid for most lattices for $\alpha = 0^\circ$. Useful and extensive employment of this concept will be made in the subsequent systematic investigations.

*The exceptionally small c_w -value (1.62) for the unsymmetrical L-shaped beam with the small side normal to the wind is due to the realignment of the stream lines with the trailing surface. As noticed before on the aerodynamics of thick prisms, this behavior produces a sudden reduction in drag as the trailing surface gets longer. For profile No. 6 the leading flange also produced a reduction in the dead-air zone behind the beam and thus a reduction in c_w . The small value of c_w for 4# is due to the special air flow which produces a forward pressure on the rear flange. (Compare the effect of pairs of plates in Chapter III.)

TABLE I (Part 1)

Drag Coefficients of Single Beams ($\lambda_s = \infty$)

No.	Profile and Wind Direction	C_w	C_a
1		2.03	0
2		1.96 2.01	0
3		2.04	0
4		1.81	0
5		2.0	0.3
6		1.83	2.07
7		1.99	-0.09
8		1.62	-0.48
9		2.01	0
10		1.99	-1.19
11		2.19	0

Naturally the tangential forces allow no such workable generalizations. Table 1 shows that c_a is usually virtually zero, but occasionally it takes on quite high values. In general we must expect small values for c_a for $\alpha = 0^\circ$ (it is possible in a lattice for sizable c_a values of individual beams to cancel out). Tests on models patterned from real structures confirm this view.* Only such models can in general give error-free information for oblique wind incidence (see Chapter V).

*See Chapter IV

CH III -- TESTS ON SCHEMATIC PLANE LATTICES FOR NORMAL WINDS ($\alpha = 0^\circ$)

A. PARALLEL BEAMS OF INFINITE ASPECT RATIO ($\lambda = \infty$).

To clarify the influence of structure type on drag of a lattice, schematic beams were investigated which had identical outline forms but various patterns of bracing members (see Figs. 8a to g). Figures 8a to 8b contain the test results along with a sketch of the lattice investigated. These lattices consisted of two parallel beams with the following bracing bars between: vertical bars only ("ladder type"), diagonal bars ("V" construction), vertical and diagonal bars ("N-type"). The bars were made out of flat 2mm sheets. Reinforcing plates at junctions were not used. The choice of this group of models was based on consideration of the frequency of occurrence of similar types in actual practice.

In order to obtain different values of solidarity (ϕ) for the above lattice types, both the widths of the members and their separation were varied. Which way was employed in particular tests is shown on the diagrams, as is the nomenclature for the symbols. To eliminate the influence of aspect ratio, all models had the same λ , in fact, $\lambda = \infty$.

This aspect ratio was chosen because the experience with the solid beams indicated that $\lambda = \infty$ yields the greatest drag coefficients.

The span or length of the models was generally 300mm. Only in the model group of Fig. 8b was a length of 450mm used to investigate a very small solidarity coefficient (ϕ). To obtain the effect of infinite length end plates were used. These strong plates had their leading edges rounded into semicircles. The models were hung with 1mm play close behind the leading edges of the end plates. This orientation has been tested with flat plates as models and affords a good approximation to $\lambda = \infty$.

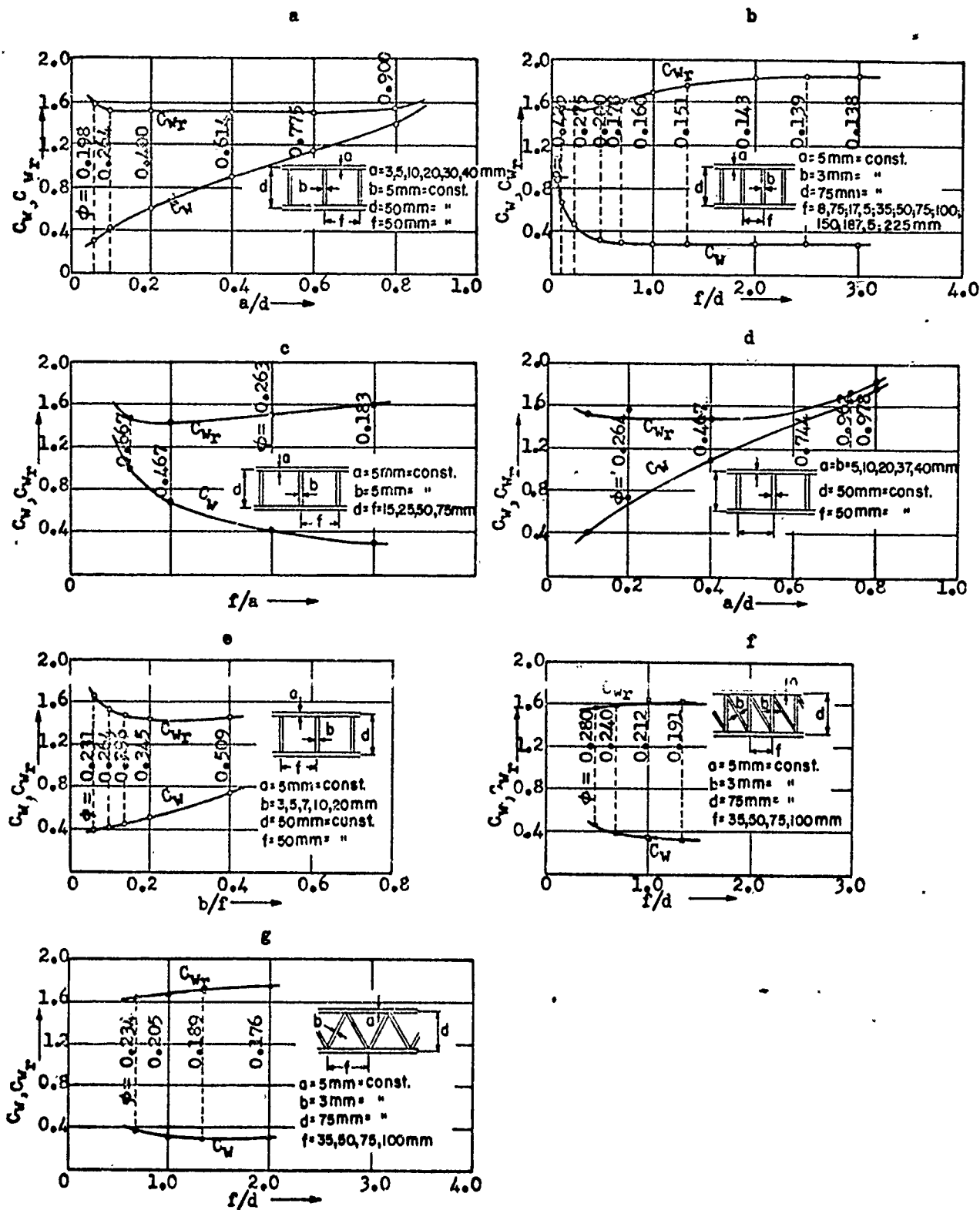


Fig. 8 -- Results of measurements on schematic plane lattices with $\lambda = \infty$ and $\alpha = 0^\circ$

The measurements were taken in the 1.20 meter wind tunnel of the Aerodynamischen Versuchsanstalt Göttingen (the so-called smaller tunnel). Each model was tested under four or five wind speeds between 10 and 30 m/s. Accidental errors of measurement were thus easily recognized. Furthermore the behavior of the drag coefficient with different velocities was obtained without further work, and it was evident whether the Reynolds number was large enough to have $c_w = \text{constant}$ and $c_{w_r} = \text{constant}$. The drag coefficients for $V = 10$ to 15 m/s must often be rejected since they still show the influence of the Reynolds number.*

In Figs. 8a to 8g the measured c_w values are presented as c_{w_r} . The two are quite different: in one case the drag force is divided by the outlined area, and in the other case the drag force W is divided by the solid projected area F_r . Included here, as in all following illustrations, are the measured points instead of average values. The scatter of measured points was in no case greater than ± 2 per cent. In general, it should be pointed out that c_w and c_{w_r} are related

$$C_w = C_{w_r} \cdot \phi$$

We can see from Figs. 8a to 8g that a survey-type graph can be constructed from these seven graphs if we plot all the c_w and c_{w_r} values against ϕ . Figure 9 represents the surprising results, which can be stated as:

The drag of a plane lattice normal to the wind of infinite aspect ratio is practically unrelated to structure pattern for a given solidarity coeff.

* (10) The reason is easy to see. The smallest bars are usually 5 mm, in some cases 3 mm, broad. Their Reynolds numbers for $V = 10$ [m/s] are

$$R = \frac{1000 \cdot (0.5)}{1/7} = 3.5 \times 10^3 \text{ for 5 mm bars}$$

$$R = \frac{1000 \cdot (0.3)}{1/7} = 2.1 \times 10^3 \text{ for 3 mm bars}$$

These R-values are not in the region for $c_w = \text{const}$. For $V = 20$ [m/s] the R-values are large enough for 5 mm bars and almost large enough for 3 mm bars.

Or:

The drag coefficient (c_w , c_{w_r}) for $\alpha = 0^\circ$ and plane lattices ($\lambda = \infty$) is a function of ϕ alone, to a close approximation.

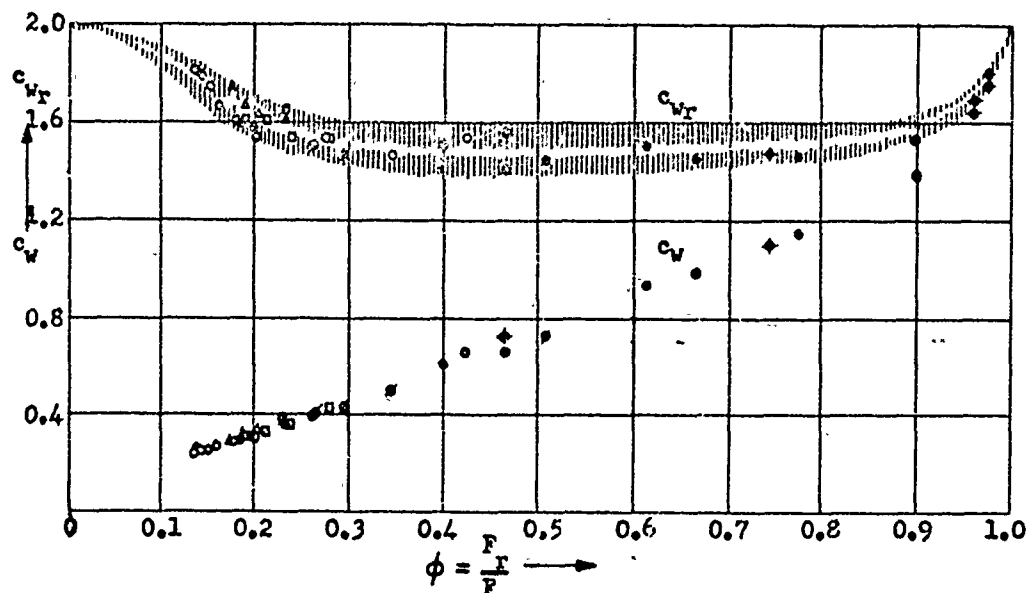


Fig. 9 -- Dependence of drag coefficients on solidarity ϕ .
Aspect ratio of the beams $\lambda = \infty$.

The small influence of structure form on drag is more evident in c_{w_r} than in c_w , and so we will limit further observations to c_{w_r} .

The meaning contained in Fig. 9 is that only one variable, ϕ , defines the drag coefficient for a lattice of given λ . This simplifies our problem significantly.*

In general, it must be remembered that our results hold only under special conditions: parallel beams, infinite or very large aspect ratio, structures without joint plates, schematic

* (11) This success shows that it was expedient from the first to investigate whole lattices. Naturally it must also be possible to construct the aerodynamics drag of the lattice from the properties of the individual bars in all configurations. In this case one must in general know both the drag of single bars as a function of λ and the effective aspect ratio of a bar in combination with the rest of the lattice. This procedure would require extraordinarily numerous measurements and would not lighten the drag calculations for the engineer.

modes, normal wind incidence. The condition that flat bars instead of bars with various cross sections were used further limits the results to normal wind incidence. Furthermore, it is not to be thought that lattices of finite length with parallel beams can be included in the rule that ϕ is the sole factor in drag coefficient determination. The effects of finite λ and $\alpha \neq 0^\circ$ must be experimentally proved. This is also true for the effects of outline form and joint plates.

Before we turn to test results it would be advisable to study some reports designed to establish the validity of model rules.

B. CONTROL TESTS ON THE INFLUENCE OF TEST ORIENTATIONS, MODEL SIZE, WIND VELOCITY, AND WIND TURBULENCE

Investigated in the common wind ranges were:

1. One and the same model with different hanging in the same wind tunnel,
2. One and the same model in three different wind tunnels,
3. A 2-1/2X model in a wind tunnel for a normal air stream,
4. A 5X model in a wind tunnel with different turbulences of the air stream.

A ladder-type structure was used.

The measurements for 1, 2, and 3, showed that no real dependence of drag coefficients on test arrangements or model size exists. (It was mentioned above that the independence of wind speed and R for every model was verified through testing at various speeds.)

These test results must be expected from model rules. They are further confirmed through the researches of Dr. Winter with the schematic models shown in Fig. 10. The

measurements from these models were markedly greater than those in Fig. 8a to 8g; the spans in Fig. 10 were 800mm. The models were also tested between end plates. These results are compatible^{12/} with Fig. 9 and with the forthcoming data of Fig. 21.*

The question whether air stream turbulence affects test results is answered "no" within certain limits by the results of 2, for the turbulence varied with the wind tunnel, but three tunnels gave identical results.

The turbulence of the Göttingen wind tunnel is slight.[†]

We have therefore introduced greater turbulence by building strong wire lattices in the air stream. Under such conditions the air speed measurements generally run into difficulties. After some not completely satisfying experiments like this, we switched to making comparative measurements independent of wind measurements. In this case the pressure distribution on and behind a 5X model was compared for different turbulences. The pressures were expressed dimensionlessly. The final results: The drag coefficients of lattices proves to be unrelated to the degree of turbulence of the wind tunnel.

This establishes the validity of model rules (in general, only for models in the constant air streams of wind tunnels). The turbulence of free wind is apparently greater, from the standpoint of mechanical similarity, than even the induced turbulence of wind tunnels. Furthermore, the wind blows in turbulent gusts, not uniform, but accelerated and twisted. It is scarcely to be assumed that this changes the drag coefficient or its independence of Reynolds number. An experimental probe of this remains to be done.

* (12) Certain small deviations observed in the control measurements find their explanation in that the end plates were not in direct contact with the lattices. Variations in this space between wall and model change the effective aerodynamic aspect ratio correspondingly.

† (13) The single means of quantitatively giving wind tunnel turbulence is the so-called "critical Reynolds number" of spheres, cylinders, or other bodies with curved outer surfaces.

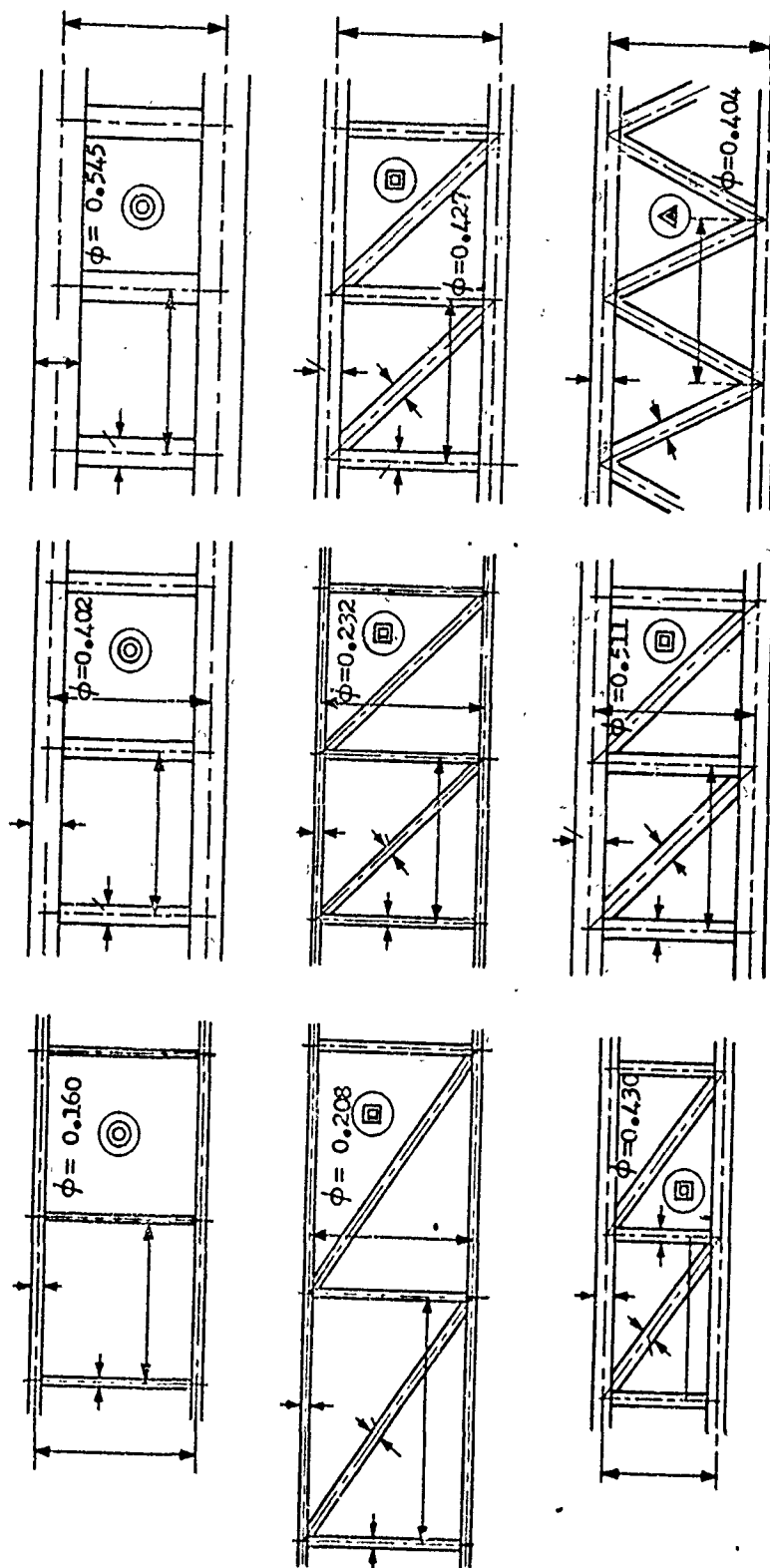


Fig. 10 -- Some more schematic plane lattices. They were investigated for $\lambda = \infty$. The test results are presented in Fig. 21. The data points are designated with the different marks accompanying each diagram above.

C. PARALLEL BEAMS WITH FINITE ASPECT RATIO

1. Influence of the Outline

It will be shown (Fig. 4) that the drag coefficient for $\alpha = 0^\circ$ is smaller for smaller values of λ . We have already considered the fall-off of drag coefficient as due to air streaming around the ends. This result can not be basically changed if the full plates are replaced by lattices. Therefore we must expect parallel-beam lattices to display the same kind of behavior as the λ is decreased. Naturally the influence of λ is greater for greater values of ϕ .

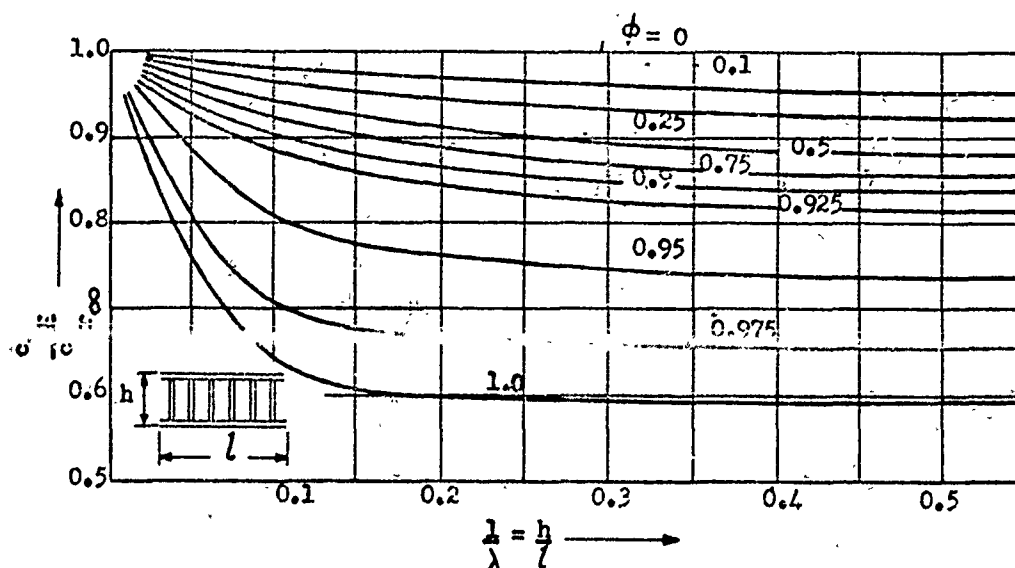


Fig. 11 -- Dependence of drag coefficients on the aspect ratio λ
 $\alpha = 0^\circ$ and schematic plane lattices

The earlier assumption is confirmed by Fig. 11. The representation in this diagram involves the reciprocal of λ and drag coefficients normalized to the $\lambda = \infty$ values. The curves for the printed ϕ values of Fig. 11 were interpolated from measured values.

Practically, one deals with $\phi < 0.5$ most of the time and the deviation is not more than 12 per cent for very short lattices, and for normally slender lattices $h/l < 0.1$ and the deviation is < 5 per cent. This is so small that the influence of aspect ratio for the average

small ϕ is negligible. The remaining error works in the direction of increased safety since

$$c_{w_r} < c_{w_{r_{\infty}}}$$

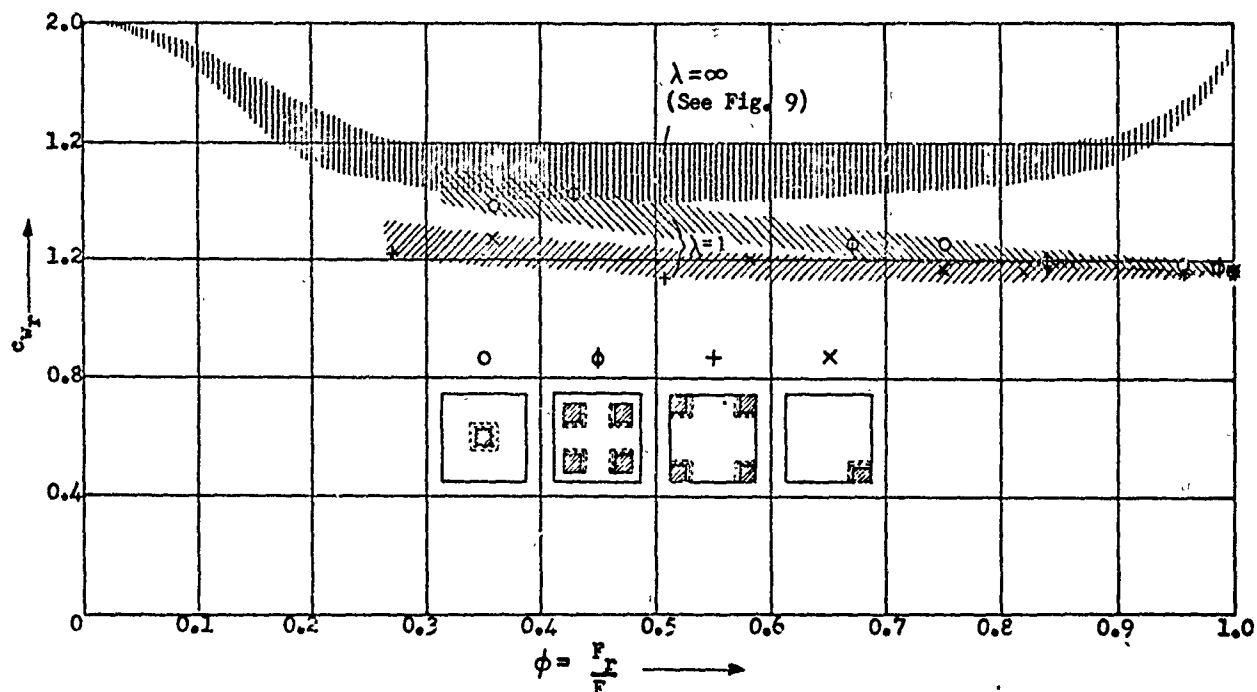


Fig. 12 -- Comparison of drag coefficients for plates of $\lambda = \infty$ with those of $\lambda = 1$. The outline area in each case is that of the original squares for the four $\lambda = 1$ test plates.

The situation for the extreme case $\lambda = 1$ (ie, square plate) is shown in Fig. 12. The ϕ values were reduced by removing shaded areas of the sketches. The first two (reading from left to right of the sketches) types of reduced squares give c - values approaching the longer lattices as ϕ is reduced. For $\phi \leq 0.3$ the difference between $\lambda = 1$ and $\lambda = \infty$ is vanishingly small.

One can now make a supposition about drag coefficients for nonrectangular lattice outlines. It is known that the greatest drag per unit length is produced by infinite plates. This

was immediately apparent in Fig. 4. Two further proofs have been introduced:

- a. In Fig. 12 the cutting of the crossed area of the right-hand square converts the original quadratic outline to a distorted outline. The measured values for the resulting angle and cruciform configurations are given in Fig. 12. They are definitely smaller than those of either rectangular lattices or squares which maintained their original outline.
- b. The solid beam (1) of Fig. 20 has a finite span and an outline deviating from the rectangular. The measured $c_{w_r} = 1.27$, therefore again smaller than the $\lambda = \infty$ value of 2.0.*

Now one might expect that the parallel beam drag coefficients would represent the maximum for all ϕ and λ values. A confirmation of this assumption will be offered later in the bridge model measurements of Fig. 20, especially types (2) to (5), whose drag coefficients are given in Fig. 21. Thus we can summarize these results as follows:

The drag coefficients of plane lattices infinite length (Fig. 9) are the largest drag coefficients obtainable with plane lattices under normally incident winds. Since the outline of the lattice work, so far as practically usable forms are concerned, plays no real role, the drag coefficients of Fig. 9 can be applied beforehand to the problem of the influence of joint plates and bar cross sections.

* (14) One defined the aspect ratio for these beams as l/h with $h = F/l$, thus here $\lambda = 9.5$, or $1/\lambda = 0.105$. It is interesting that a rectangular plate of this aspect ratio has approximately the same drag coefficient of beam (1) of Fig. 20. Therefore here a reduction to rectangular surfaces is possible through the use of the generalized definition of aspect ratio. (This is always possible if the plate outline does not deviate very strongly from rectangularity.)

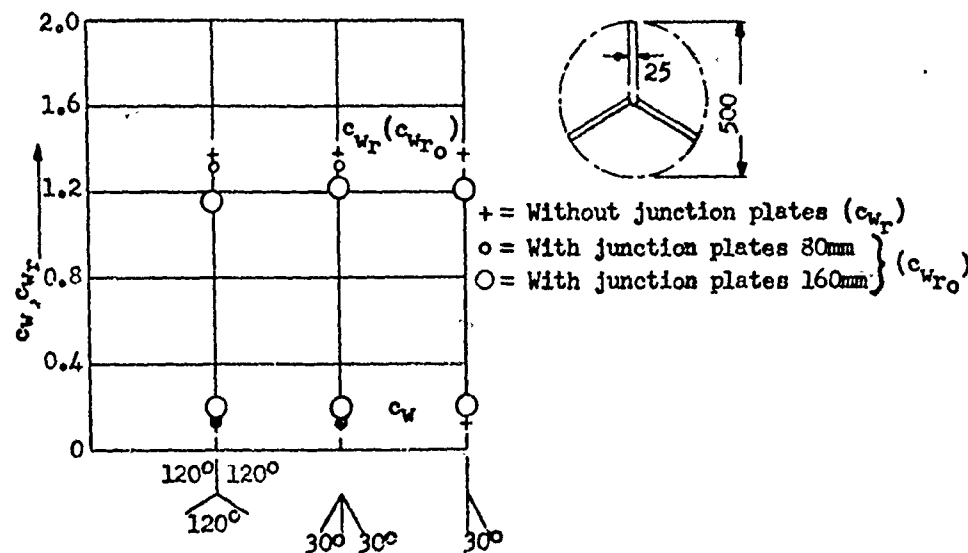


Fig. 13 -- Wind loading of a 3-pronged junction

D. THE INFLUENCE OF JUNCTIONS AND JUNCTION PLATES

So far, only networks without junction-plates have been investigated. Before investigating a whole structure with junction plates, it is expedient to test the drag of a single junction and its variation with the addition of a plate.

For this basic experiment two schematic 3- and 4-prong junction models were used. The bars were 250mm long, 25mm wide, 3mm thick. The orientation of the bars was varied with and without junction plates. The plates were circular discs of 80 and 160mm diameter. The results of the measurements are presented in Figs. 13 and 14. One can abstract the following:

1. The drag of a junction with or without plates is virtually independent* of the angles between the bars (see Fig. 13). With the joint plates the above holds as long as the ratio between plate area and bar area is not unusual. The

* (15) Excluded is the condition where the bars cover each other. In such a case there is no real function but some sort of single lattice with a degenerate function.

160mm plate exceeds this limit and in consequence shows a marked dependence of c_{w_r} on bar orientation. The extreme value of c_{w_r} deviates from the mid-value by only ± 4 per cent. One notices that c_{w_r} is smaller the more uniform the bar orientation around 360° .

2. The drag coefficient of a junction grows with the number of bars. For 3-bar joint $c_{w_r} = 1.38$; for 4-bar $c_{w_r} = 1.41$. The difference is obviously not large.
3. The c_{w_r} - value is smaller for smaller junction plates under otherwise equal conditions. The reason is that discs have a much smaller drag coefficient than bars. Without plates $c_{w_r} = 1.38$ to 1.41 . For a circular disc or plate $c_{w_r} = 1.10$ (square plates have $c_{w_r} = 1.16$). With the introduction of a joint plate the area of the lattice grows faster than the total drag.

The results here are no longer surprising. They concern two schematic, N and V, lattices with small and with large joint plates and $\lambda = \infty$. The plates have the usual commercial straight-line form. As one can see, the c_{w_r} - value declines with the introduction of the plates.

E. CALCULATED CHANGE IN WIND-LOADING DUE TO JUNCTION PLATES

We can take, as a first approximation, the combined drag as the sum of the drags at the isolated plates plus the drag of the remaining unshielded bars. The drag coefficient of the remaining bars is assumed to be the drag coefficient of a similar but "unplated" lattice, or the c_{w_r} of a lattice with vanishingly small junction plates.

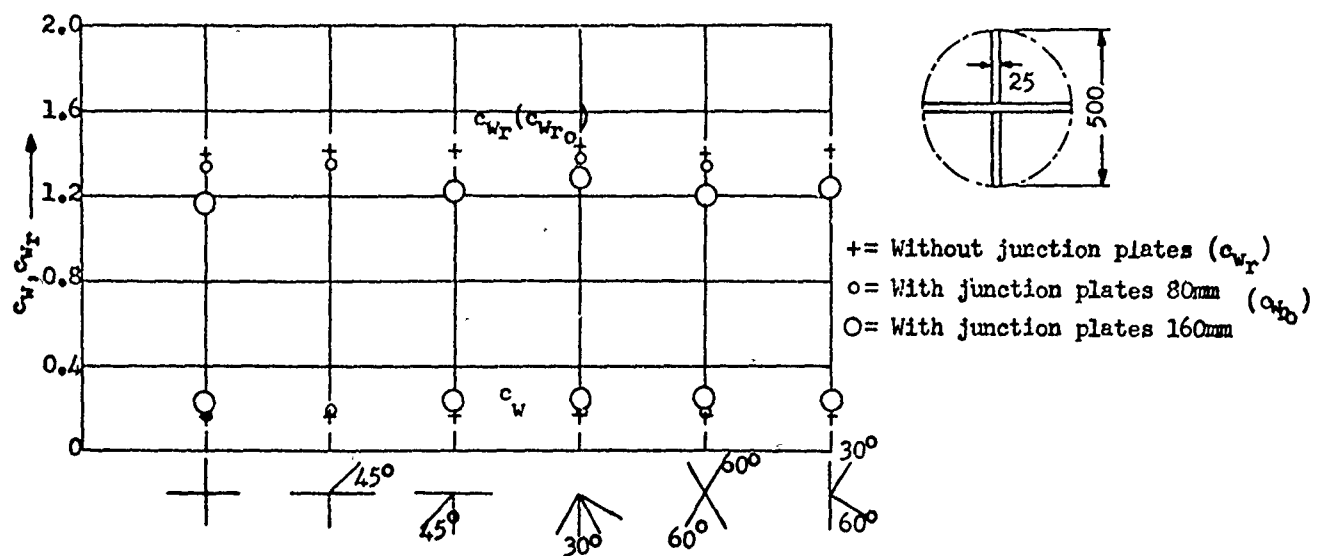


Fig. 14 -- Wind loading of a 4-bar junction

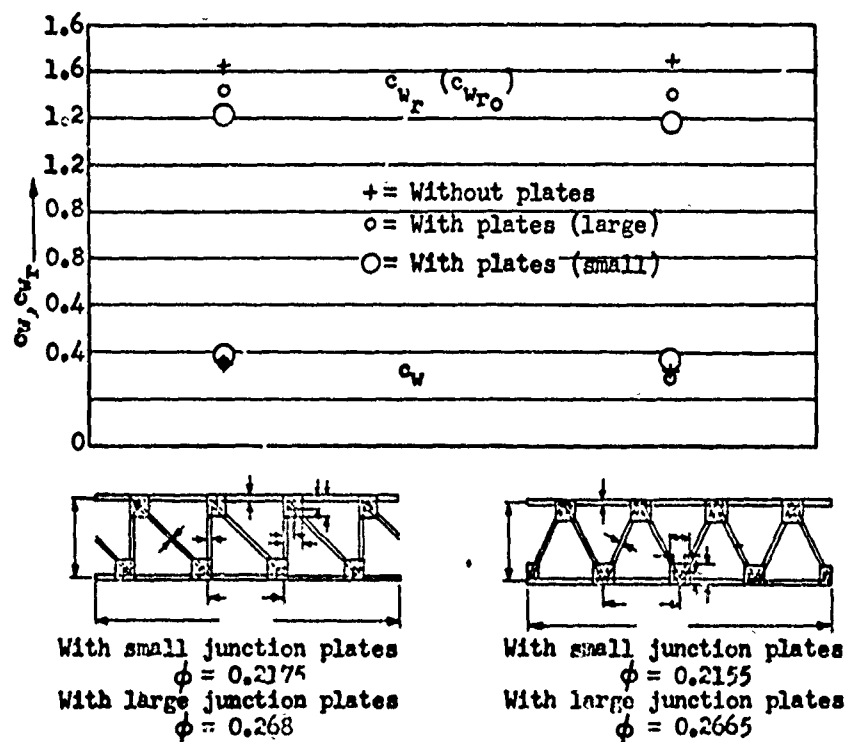


Fig. 15 -- The influence of junction plates on the wind-loading of plane schematic lattices. $\lambda = \infty$

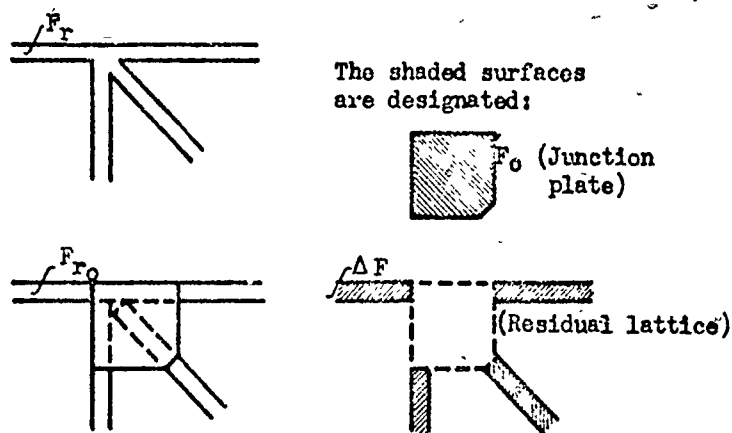


Fig. 16 -- Nomenclature for calculating the effect of junction plates

The following nomenclature will be used:

Surfaces:

F_r = Visible surface of the lattice without the plates; that is, the surface area projected in the wind direction

F_{r_o} = Visible surface area of the system, the lattice plus the (finite) junction plates.

F_o = Sum of the visible (projected) areas of all the plates

$\Delta F = F_{r_o} - F_o$ = area of lattice still visible between the plates.

Wind Forces:

W_r = drag of the lattice with area F_r

W_{r_o} = drag of the lattice with area F_{r_o}

Drag Coefficients:

$c_{w_r} = W_r / qF_r$ = drag coefficient of the projected area F_r (given)

$c_{w_{r_o}} = W_{r_o} / qF_{r_o}$ = drag coefficient of the area F_{r_o} (to be found)

$\Delta c_w = c_{w_r}$ = drag-coefficient of the area F (given)

c_{w_o} = drag coefficient of the plates alone (given)

Three-element Junctions (Fig. 13)

(a) Small (80mm) junction plates

$$\begin{aligned} F_{r_o} &= 207.3 \text{ cm}^2 & F_o &= 50.3 \text{ cm}^2 & c_{w_r} &= 1.38 \text{ (average)} \\ \Delta F &= 157 \text{ cm}^2 & c_{w_o} &= 1.10 \end{aligned}$$

$$\frac{W_{r_o}}{q} = c_{w_{r_o}} F_{r_o} = c_{w_r} \Delta F + c_{w_o} F_o$$

$$\begin{aligned} c_{w_{r_o}} &= \frac{W_{r_o}}{q F_{r_o}} = c_{w_r} \left\{ \frac{\Delta F}{F_{r_o}} + \frac{c_{w_o}}{c_{w_r}} \cdot \frac{F_o}{F_{r_o}} \right\} = c_{w_r} [0.76 + 0.797 \cdot 0.243] \\ &= 1.38 \times 0.954 \end{aligned}$$

$$c_{w_{r_o}} = 1.32 \text{ (in agreement with the measured value).}$$

(b) Large junction plates (160mm)

$$\begin{aligned} F_{r_o} &= 328.4 \text{ cm}^2 & F_o &= 201 \text{ cm}^2 & c_{w_r} &= 1.38 \text{ (average)} \\ \Delta F &= 127.4 \text{ cm}^2 & c_{w_o} &= 1.10 \end{aligned}$$

$$c_{w_{r_o}} = 1.21 \text{ (in agreement with the measurement)}$$

Four-element Junctions (Fig. 14)

In a corresponding way one finds:

(a) $c_{w_{r_o}} = 1.35$ for the juncture point with 80mm plate

(b) $c_{w_{r_o}} = 1.24$ for the juncture point with 160mm plate

Both numbers are in agreement with measurement.

Parallel Beams with N- and V-lattices (Fig. 15)

N-structure with large joint plates

$$F_{r_o} = 64.5 \text{ cm}^2 \quad F_o = 30.4 \text{ cm}^2 \quad c_{w_r} = 1.62 \quad c_{w_o} = 1.16$$

$$\Delta F = 34.1 \text{ cm}^2$$

$$c_{w_{r_o}} = \frac{c_{w_r}}{F_{r_o}} \left\{ \Delta F + \frac{c_{w_o}}{c_{w_r}} \cdot F_o \right\} = \frac{1.62}{64.5} (34.1 + 0.726 \times 30.4)$$

$$= 0.0252 \times 56.15$$

$$c_{w_{r_o}} = 1.41$$

V - work with large joint plates

$$F_{r_o} = 64 \text{ cm}^2 \quad F_o = 32 \text{ cm}^2 \quad c_{w_r} = 1.65 \quad c_{w_o} = 1.16$$

$$\Delta F = 32 \text{ cm}^2$$

$$c_{w_{r_o}} = \frac{c_{w_r}}{F_{r_o}} \left\{ \Delta F + \frac{c_{w_o}}{c_{w_r}} \cdot F_o \right\} = \frac{1.65}{64} (32 + 0.703 \times 32)$$

$$= 0.0258 \times 54.5$$

$$c_{w_{r_o}} = 1.40$$

For small plates $c_{w_{r_o}}$ is calculated in the same way and good agreement with measured values is obtained.

Thus, to a first approximation, the superposition law is valid. For plane lattices of known drag coefficients without junction plates, the change in resistance from the addition of plates is subject to close calculation along the lines of the previous examples.

Most of the junction plates of steel structures are so small in general that they scarcely alter the drag coefficients. Such plates simply add to the total area F_r and thereby

change ϕ and W . The accompanying error works in the direction of increased safety factor.

Figure 21 displays the measurements for the bridge models of Fig. 20.*

Model 3			
	F_r	F	$\phi = F_r/F$
AVA III	442 cm ²	1250 cm ²	0.354
Exact value	449 cm ²	1226 cm ²	0.366

For models (2) to (4) the behavior is that of schematic lattices with junction plates. Figure 21 shows that the test results for these models fall in the group of points for other models without junction plates.

* (16) Prof. Rein, Breslau, was good enough to recheck model (3) and supply corrected areas and ϕ 's. Consequently the c_{w_r} -value was also changed.

CH IV -- TESTS FOR $\alpha = 0^\circ$ ON PLANE LATTICES WITH BARS OF VARIOUS CROSS SECTIONS

All previous discussion pertained to lattices of flat members. It has already been mentioned that cross section apparently has small aerodynamic effect for single bars. The correctness of this assumption will be tested by the following experiments:

1. Parallel beams with N-bracing, which were previously investigated with flat rectangular bars (Fig. 8f, $\phi = 0.280$), were reconstructed with the same outline and projected areas out of equal-width angle bars (bars with L or T cross section). Figure 17 shows the different orientations of the face of the L bar which is parallel to the wind direction. Note both ($\neg \neg$) and ($\neg \neg$) orientations are used. Figure 17 shows the measured c_{w_r} beside the corresponding orientation sketch. The agreement is good. The somewhat smaller resistance of model 17c must be expected from the drag coefficient of a single bar of this type (compare Table 1).

2. Parallel beams with N-bracing as in Fig. 18.

$$\lambda = \infty \quad \phi = 0.288 \quad c_{w_r} = 1.58$$

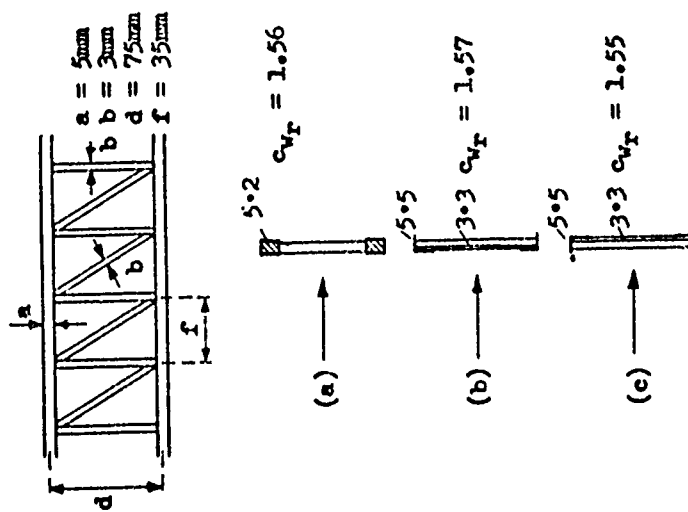
3. Lattice structure of an electric tower (model approximately 1/2 size) as in Fig. 19. Wind normal to the diagram plane. Results:

$$\lambda = \infty \quad \phi = 0.281 \quad c_{w_r} = 1.58$$

4. Model (5), a bridge member, Fig. 20.

Results:

$$\alpha = 0^\circ \quad \lambda = l^2/F = 9.5 \quad \phi = 9.458 \quad c_{w_r} = 1.47$$



a bars with square cross section
b & c bars with angle cross section

Fig. 17 -- Comparative measurements on a plane lattice. $\lambda = \infty$

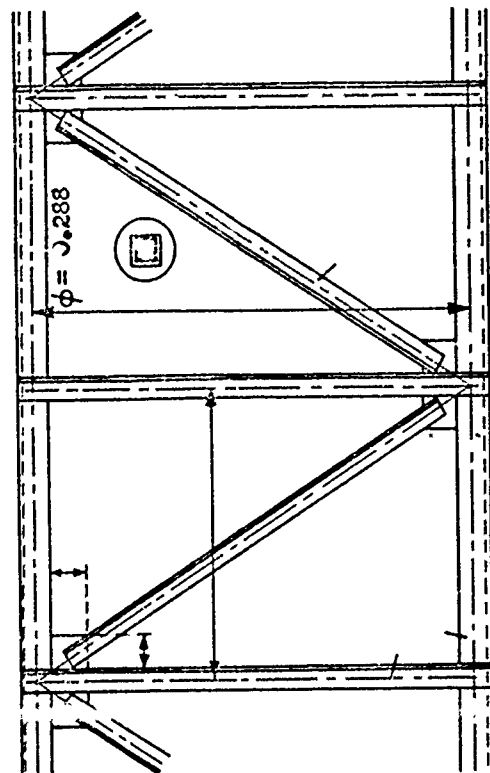


Fig. 18 -- Model of a plane lattice girder of "profiled" bars (bars with 2-dimensional cross sections). This model was tested between side walls for $\lambda = \infty$. The measured results are given in Fig. 21 with the above point-symbol.

The data from (2) through (4) are presented together in Fig. 21. They fall pretty well along the points from the schematic lattices measured earlier. For practical cases it will be satisfactory to consider the Fig. 9 values as valid for $\alpha = 0^\circ$ and plane lattices in general.

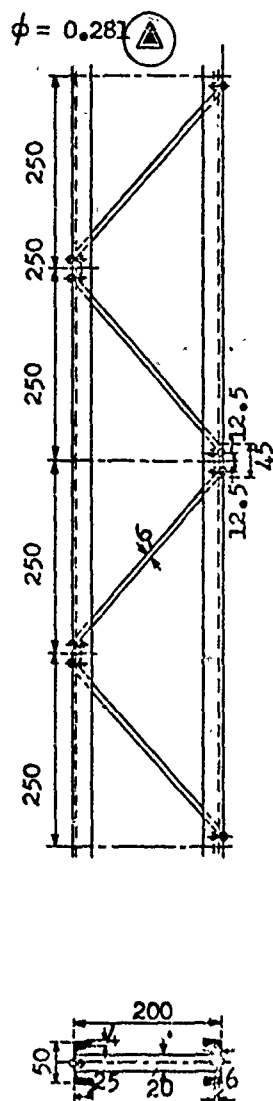


Fig. 19 -- Section model of a mast tested for $\lambda = \infty$. Results given in Fig. 21 under the above symbol.

CH V -- TESTS ON PLANE LATTICES FOR OBLIQUE WIND

INCIDENCE ($\alpha \geq 0^\circ$)

The above results have so far clarified the aerodynamics of single plane lattices that only the influence of oblique incidence remains to be tested. Such tests proceeded in 1921 on three of the bridge models of Fig. 20. These tests dealt with types (1), (4), and (5). The models were investigated for oblique incidence from above and from the side for angles up to $\alpha = 45^\circ$. The test values are presented in Figs. 22 and 23.

The results for the solid beam (1) confirm the earlier rectangular plate data (Figs. 6 and 7) for $\lambda = 5$, although the bridge beam (1) has another outline and a different aspect ratio. The agreement is complete, even to the rise of c_n above $\alpha = 30^\circ$ for side incidence. That the numerical values are different is due to the difference in aspect ratio.

Neither (4) or (5) show this rise in c_n for lateral incidence. For them, the earlier concept is valid: that c_{n_r} is maximum for small angles ($\alpha \rightarrow 0^\circ$) of incidence. One also concludes that c_{t_r} is negligibly small throughout $\alpha = 0^\circ$ to 45° , as is true for solid beams. Thus we obtain the first two of the following conclusions.

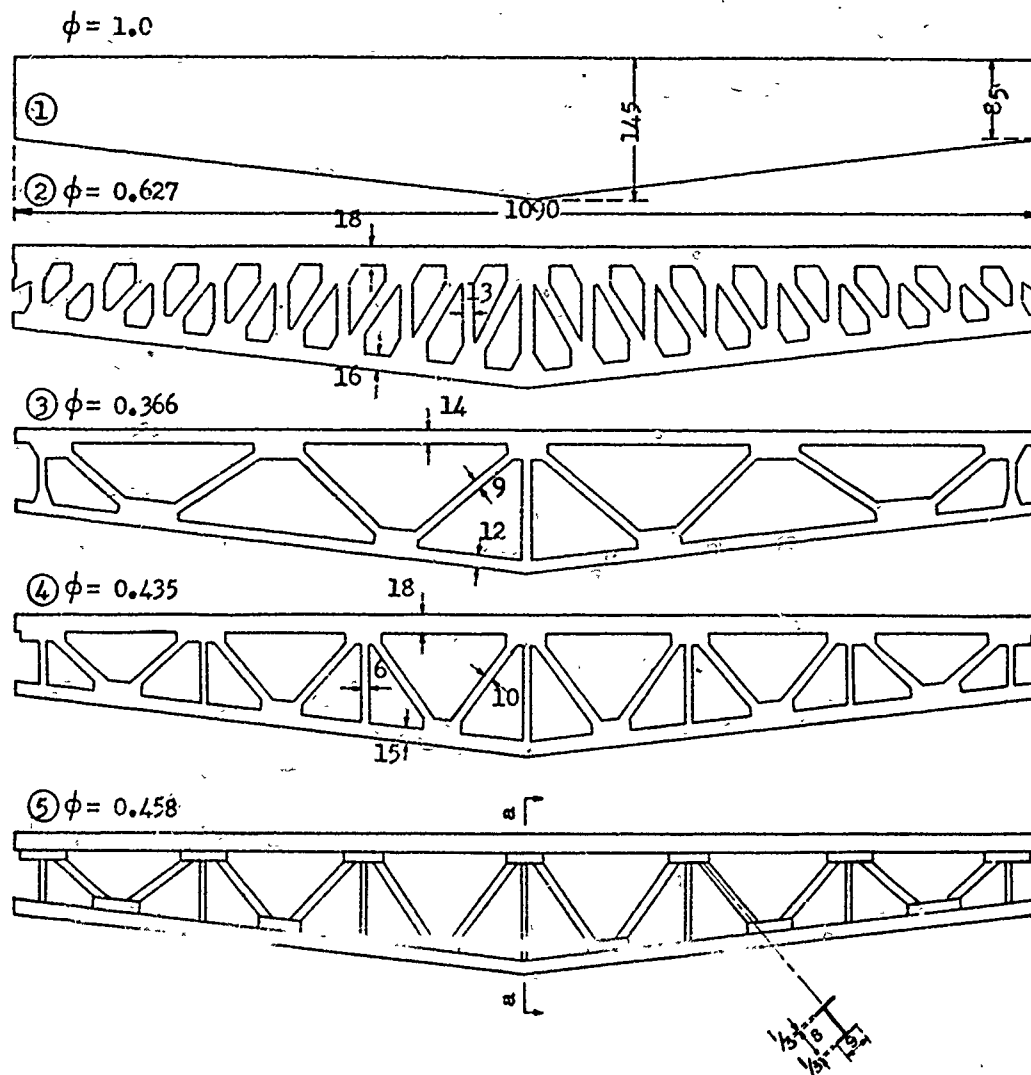


Fig. 20 -- Five bridge models tested in 1921 at Göttingen. $\lambda = l^2/F \approx 9.5$. The test results for $\alpha = 0^\circ$ of models (2) through (5) are contained in Fig. 21.

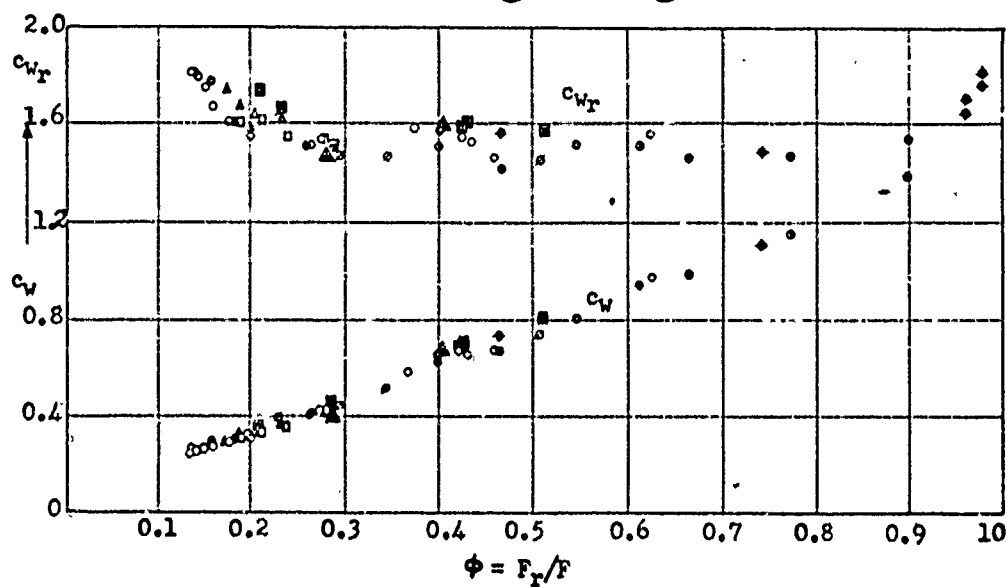


Fig. 21 -- Combined test results for plane lattices

CH VI -- CONCLUSIONS

1. The tangential force on plane lattices is generally negligibly small.
2. The normal force is a maximum for $\alpha \rightarrow 0^\circ$. It is satisfactory to base drag calculations on the $\alpha = 0^\circ$ value of c_n as a maximum. Since $c_{n_r} \equiv c_{w_r}$ for $\alpha = 0^\circ$, the term " c_{w_r} " will be used instead of the more cumbersome " c_{w_r} for $\alpha = 0^\circ$ ".
3. c_{w_r} is to a far-reaching approximation independent of structure-type, bar cross section, and outline as long as conventional structures are considered. c_{w_r} is practically dependent on the solidarity coefficient ϕ alone:

$$(7) \quad c_{w_r} = c_{w_r}(\phi)$$
4. Junction plates reduce the c_{w_r} of a lattice. The size of the reduction can be ascertained according to the ^{5/} calculations of Chapter III. So long as the plates are small, as usually is the case, it is not important to ascertain the particular influence of the plates (beyond their addition to the projected area). The resulting error will always be on the safe side, since the F_r is then the lattice area including the plate area.
5. If one knows the function $c_{w_r}(\phi)$, then it is possible to calculate W for the surface $F_r = \phi F$ and velocity v

$$W = c_{w_r} \cdot \frac{1}{2} \rho v^2 F_r [\text{kg}]$$

W is normal to the lattice plane.

6. The dependence of c_{w_r} on ϕ has to be taken from Fig. 21, in which the most important test results are presented together. If no particular data on a structure are

available, it is advisable to assume a c_{w_r} on the upper envelope of the measured c_{w_r} values. c_{w_r} is practically independent of ϕ in the interval $0.3 < \phi < 0.9$, and here the upper border of values is also a straight line $c_{w_r} = 1.6$. Outside this range, c_{w_r} climbs to $c_{w_r} = 2.0$. If one prefers a simplified, step function instead of a smooth curve, then the following table can be used:

ϕ	c_{w_r}
0 to about 0.20	2.0
0.20 to about 0.30	1.8
0.30 to about 0.90	1.6
0.90 to about 1.0	2.0

7. For practical cases these results can be still further simplified. We observe that c_{w_r} values of Fig. 9 hold for plane lattices in general, independent of outline and aspect ratio. As shown earlier, these statements are only approximately true. The approximation is better for smaller solidarity ratios ϕ . For very large ϕ values, especially $\phi = 1$, the outline and aspect ratio are clearly noticeable (Fig. 4). The drag coefficient for rectangular plates with normal incidence is $c_{w_r} = 2.0$ for $\lambda = \infty$ and $c_{w_r} = 1.16$ for $\lambda = 1$. Thus $c_{w_r} = 2.0$ holds only for large ϕ values when λ is also large. The spans of real beams deviate so much from $\lambda = \infty$ that it is satisfactory to use $c_{w_r} = 1.6$ even as $\phi \rightarrow 1$.

A corresponding simplification in the domain of smaller ϕ 's—so that one could use $c_{w_r} = 1.6$ throughout the whole range of $\phi = 0$ to $\phi = 1$ —would be desirable. However, such a simplification is unacceptable from an aerodynamic standpoint without certain restrictions. For $\phi < 0.25$, $c_{w_r} = 1.8$ is valid since very small ϕ 's are seldom encountered. For $\phi > 0.25$, the value $c_{w_r} = 1.6$ is almost always correct. Thus one obtains the following:

$$\begin{aligned} \phi < 0.25 & \quad c_{w_r} = 1.8 \\ \phi \geq 0.25 & \quad c_{w_r} = 1.6 \end{aligned}$$

8. Using the abbreviation $c_{w_r} \cdot \frac{1}{2} \rho v^2 = w$ gives the expression for drag W

$$(9) \quad W = w F_r, \text{ [kg]}$$

with $c_{w_r} = 1.6$ and $\rho = 1.2$, $\left[\text{kg/s}^2 \text{m}^4 \right]$

$$(10) \quad w = 0.1 v^2, \text{ [kg/m}^2\text{]}$$

where v is in m/s. Consequently for

$v =$	30	35	40	45	[m/s]
$v^2 =$	900	1225	1600	2025	[m ² /s ²]
$w =$	90	122.5	160	202.5	[kg/m ²]

For $c_{w_r} = 1.8$ these values for w are raised by 1.125.

9. All these investigations and conclusions apply to structures of uniform solidity coefficient. Where this condition is not fulfilled—as for trusses supporting a thick road bed—the drag on each single member with a uniform ϕ will be calculated separately.

10. Several lattices in a spacial configuration influence each other. Luckily the lattice on the windward side experiences nearly the same drag. In Part 2 of these reports the investigation of spacial structures will clarify the extent of mutual shielding.

PART 2 -- THREE-DIMENSIONAL LATTICES

CH I -- PRELIMINARY REMARKS

A. PURPOSE OF THE RESEARCH. REVIEW OF PART 1.

By spacial lattices is meant open structures made of several plane lattices. In practice virtually all structural lattices belong to this category.

The aerodynamics of single plane lattices is reported in Part 1. There the following points were brought out:

The tangential forces on single plane lattices are generally negligibly small. The normal force (drag component perpendicular to the lattice plane) reaches its greatest value, which alone is interesting technically, for a wind direction normal to the lattice plane. It is independent of structure type within practical limits of accuracy. It is likewise unaffected by beam cross section or lattice outline. The drag is proportional to the product $q \cdot F_r$, where q is the dynamic pressure and F_r is the solid projected area. The factor of proportionality has been designated C_{w_r} and called "drag coefficient." The slight dependence of drag coefficients on ϕ can be summarized:

for solidarity coeff. $\phi < 0.25$ use $C_{w_r} = 1.8$

for solidarity coeff. $\phi \geq 0.25$ use $C_{w_r} = 1.6$

Then for a given lattice, the drag W in a wind velocity V is:

$$W = C_{w_r} \cdot q \cdot F_r = C_{w_r} \cdot \frac{1}{2} \rho v^2 F_r [\text{kg}]$$

where ρ is the density of the air and $F_r = \phi \times F$. For unknown lattices, one can use $C_{wr} = 1.8$ as a somewhat rough working approximation.

Essentially C_{wr} for single plane lattices is a function of solidarity coefficient ϕ alone. And even this effect is slight for common structures, allowing $C_{wr} \approx$ constant to be useful.

Such simple results cannot be expected for three-dimensional lattices, since the mutual influences of the component beams are nonuniform. In actual fact, the aerodynamic relations cannot be put into such a simple form. The tests which we will report prove this. Nevertheless, their results are clear enough to form the groundwork for wind pressure calculations. The 'handiness' of these procedures is established because they succeeded in relating the wind loading of a spacial lattice to the drags of its components.

B. NOMENCLATURE

A number of concepts and symbols were clarified in Part 1. Some new concepts will be introduced:

e [m] = Separation between two parallel beams; usually employed in the dimensionless form e/d , where d is the distance between the two main girders of a lattice (see Fig. 2 Part 2).

C_{wrI} = drag coefficient of the windward lattice of a lattice pair.

C_{wrII} = corresponding coefficient for the leeward lattice.

$C_{wr}^{(e=\infty)}$ = drag coefficient for a single lattice—or in other words the drag coeff. of each lattice when their separation is infinite.

$\psi_I = \frac{C_{wrI}}{C_{wr}^{(e=\infty)}}$ = shielding coefficient for the forward lattice.

$\psi_{II} = \frac{C_{wrII}}{C_{wr}^{(e=\infty)}}$ = shielding coefficient for the rearward lattice.

$$\eta = \frac{\psi_{II}}{\psi_I} = \text{shielding ratio of the two lattices.}$$

P_g [kg] = net force on a spacial lattice.

W_g [kg] = resistance

A_g [kg] = buoyancy

N_g [kg] = normal force

T_g [kg] = tangential force

This terminology is the same as Part I, with the subscript "g" added to indicate spacial lattices.

$$C_{p_r} = P_g / q \cdot F_r$$

$$C_{w_r} = W_g / q \cdot F_r$$

$$C_{a_r} = A_g / q \cdot F_r$$

$$C_{n_r} = N_g / q \cdot F_r$$

$$C_{t_r} = T_g / q \cdot F_r$$

Drag coefficients for spacial lattices.

The large C is used to distinguish it from the drag coefficients for plane lattices. F_r for a spacial lattice means the projected surface of a side wall.

When it is not otherwise stated, the wind stream is assumed to be uniform in space and time.

CH. II -- TWO PARALLEL LATTICES, ONE BEHIND THE OTHER

A. FUNDAMENTALS

A pair of parallel lattices can be considered as an elementary form of a spacial lattice. It will be presupposed that the lattices are identical in type and size. This is not to say they are congruent, even though their spans, solidarity coefficients, and outlines are the same [for example, these conditions are met with N-type lattices even though the N were reversed (W) for the leeward lattice.]

Denoting the forward lattice by I, the trailing lattice by II, and the corresponding drags with W_I and W_{II} , then the combined drag is:

$$(1) \quad W_g = W_I + W_{II}$$

For normal wind incidence this force is identical with the resulting normal force N. Dividing both sides by $q \cdot F_r$ converts Eq 1 to the corresponding relation between drag coefficients:

$$(2a) \quad C_{w_r} = c_{w_{rI}} + c_{w_{rII}}$$

which can also be written

$$(2b) \quad C_{w_r} = c_{w_{rI}} \left(1 + \frac{c_{w_{rII}}}{c_{w_{rI}}} \right)$$

or

$$(2c) \quad C_{w_r} = c_{w_{rI}} (1 + \eta)$$

At first we knew none of these terms—neither C_{w_r} , nor $c_{w_{rI}}$, nor $c_{w_{rII}}$. The only information available, which is not explicitly in the equation, is the drag coefficient of a single lattice—or, in different words, when the separation is infinite (see Fig. 21 in Part 1).

We will designate this drag coefficient, which was earlier called $c_{w_r}^{(e=\infty)}$ to avoid misunderstandings. We can make one general remark about the relation between this term and the numbers $c_{w_{rI}}$ and $c_{w_{rII}}$. Apparently the fore-lattice lies in the "bow wave" of the trailing lattice, which lies in the dead air space of the leading lattice. Each of the two lattices lies in air disturbed by the presence of the other. Therefore it follows that:

$$\left. \begin{array}{l} c_{w_{rI}} \\ c_{w_{rII}} \end{array} \right\} \neq c_{w_r}^{(e=\infty)}$$

Or, more exactly

$$(3) \quad c_{w_{rI}} = \psi_I \cdot c_{w_r}^{(e=\infty)} \text{ and } c_{w_{rII}} = \psi_{II} \cdot c_{w_r}^{(e=\infty)}$$

and thus Eqs 2 converts to

$$(4) \quad \left\{ \begin{array}{l} C_{w_r} = \psi_I \cdot c_{w_r}^{(e=\infty)} \left[1 + \frac{\psi_{II}}{\psi_I} \right] \\ \text{or} \\ C_{w_r} = \psi_I \cdot c_{w_r}^{(e=\infty)} (1 + \eta) \end{array} \right.$$

Here we have $c_{w_r}^{(e=\infty)}$, a known quantity, in an expression for the drag coefficient for one lattice in the presence of another. This is a formal solution based on the aerodynamics of single beams.

Particular experiments must be made to yield information on ψ_I , ψ_{II} , and η and their dependence on separation (of lattices), ϕ , and other parameters. First one can say that the area behind a body is an area of reduced wind velocity; thus

$$\psi_{II} < 1.0$$

and so the drag on a body in the wind shadow of another is smaller than in the absence of the other body.

B. TESTS ON TWO SOLID PLATES ($\phi = 1$)

As was the case with single lattices, it is appropriate to begin with the case of $\phi = 1$.

Figure 1 presents the results of measurements on four different plate pairs, including the old data of Eiffel on discs and 2:1 rectangles, the 1921 Göttingen beams of type (1), and finally an additional measurement which we made on a rectangular plate of $\lambda = 13.6$.

The shielding coefficients, ψ , for the windward plate and ψ_{II} for the shadowed plate, are plotted against e/h = plate separation \div plate height. For ease of understanding it should be remembered that, for example, a reading $\psi_I = 0.84$ for $e/h = 3.0$ means: when the separation e between the lattice pair is 3 times the plate (lattice) height, then the fore plate experiences a drag in the wind direction which is only 84 per cent of the corresponding drag for the same plate alone but otherwise under similar conditions.

From Fig. 1 we derive the following facts:

1. The course of the ψ -curves is dependent on plate form. This is expected, since the drag of single plates has already been shown to depend strongly on the plate geometry.
2. For the plates tested ψ_I lies very near 1.0 for $e \leq 8h$. This means that even for very close spacings the rear plate has little influence on the fore plate. However, it shows simultaneously that the presence of the second plate can raise the drag of the front plate above that of a single plate (this effect is apparently stronger for elementary forms—discs, 2:1 rectangles—than for technically interesting slender beams). With growing separation, ψ_I must more and more approach unity.

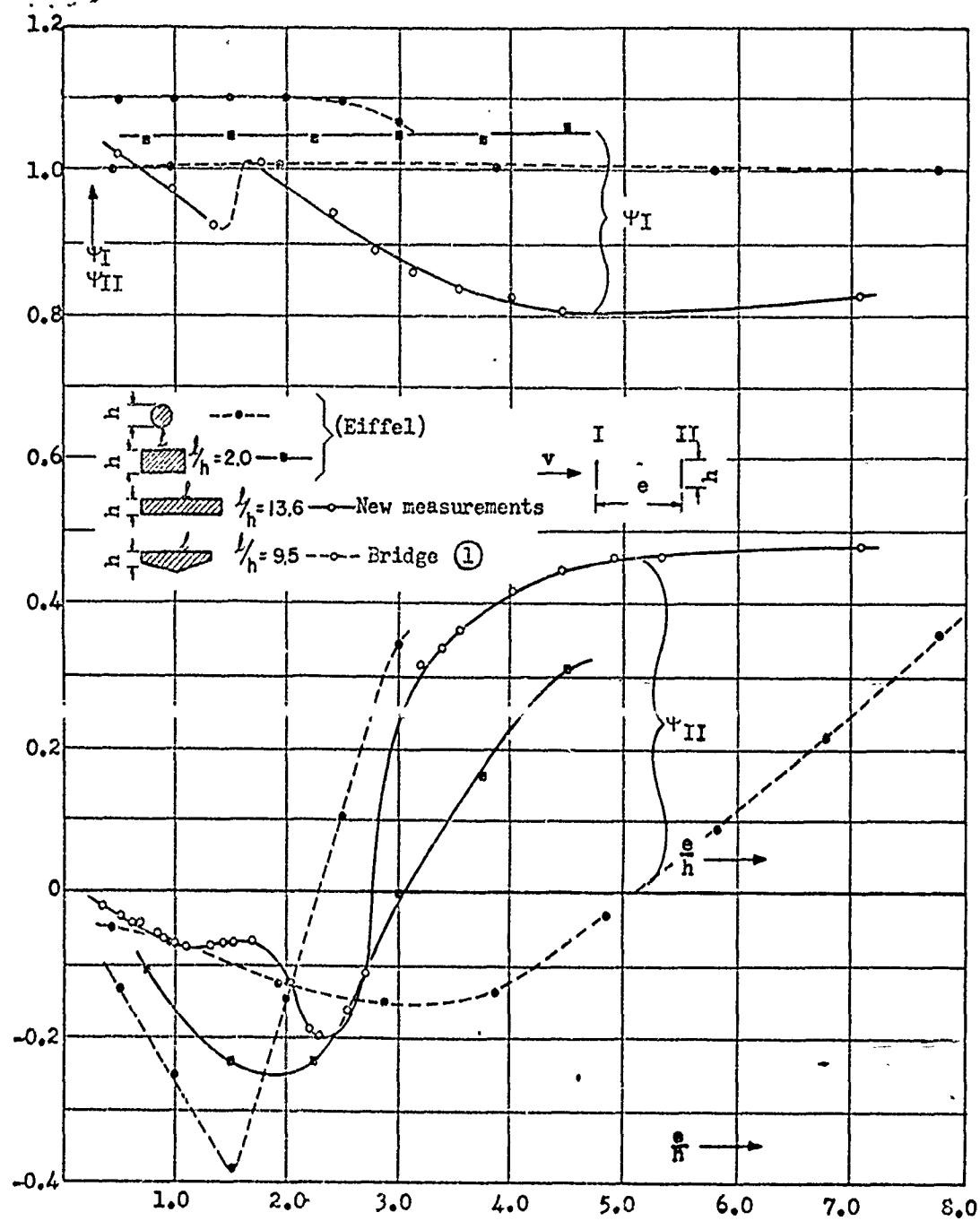


Fig. 1 -- Shielding coefficients of two parallel plates one behind the other with normal wind incidence. $\alpha = 0^\circ$; $\phi = 1.0$

3. The rear plate is strongly influenced by the fore plate. In the region of small separations—up to about 2 plate heights— ψ_{II} even takes negative values, that is: the rear plate experiences a force opposite to the wind direction. As the separation grows, ψ_{II} goes over to positive values. In this case, too, the shielding coefficient approaches a limiting value of 1.0. This limit is, however, approached slowly, as one would be inclined to assume. Even for a separation 8 times the height, the drag of the rear plate is still only around 50 per cent of that for a single plate.

On the basis of these results, we can make some pronouncements about pairs of congruent lattices, one behind the other as seen in a direction normal to their lattice planes. In this case we consider the two solid plates of Fig. 1 as part of a lattice. Then it follows: for two lattices lying one behind the other, one must expect:

for separations up to $2h$ or $5h$, $\psi_{II} < 0$, and at least for part of this range, $\psi_I > 1.0$

for greater separations $\psi_{II} \rightarrow 1.0$, $\psi_I \rightarrow 1.0$, with ψ_I approaching this limit much faster than ψ_{II}

Initially these results hold for lattices with flat bars, so-called schematic lattices. But the experience of Part 1 indicates that the data will apply to lattices with bars of more complex cross sections.

For lattices displaced so that they are no longer in line, there is no interaction for large separation, but interaction can be expected when the separation is small and when the fore lattice partially masks the trailing structure. Exact effects cannot be anticipated.

In Chapter II-4 we will see that these suppositions will be proved right. Before this is done, some remarks should be made in connection with special measurements on the flow fields behind single lattices. They will serve to make the conditions on the trailing lattice more understandable.

C. PRESSURE AND VELOCITY FIELDS BEHIND A LATTICE UNDER NORMALLY INCIDENT WIND

With the help of a small bent tube and a small static probe, the total- and static-pressure distributions (P'_{tot} and P'_{st}) were measured in five parallel planes behind a "ladder" model. From p'_{tot} and p'_{st} one obtains the point dynamic pressure $q' = \frac{1}{2}\rho v'^2$

$$q' = p'_{\text{tot}} - p'_{\text{st}} \left[\text{kg/m}^2 \right]$$

and from this the air velocity v'

$$v' = \sqrt{\frac{2q'}{\rho}} \left[\text{m/s} \right]^*$$

(The spacial pressures and velocities are primed to separate them from the undisturbed values.)

In Fig. 2a the combined and static pressure distributions are shown; in Fig. 2b the velocity distribution. The velocities were divided by the initial undisturbed velocity, and the pressures were divided by $q = \frac{1}{2}\rho v^2$. The separation of the measured planes from the ladder is given in units of ladder height.

The distribution curves show the expected wave contour with minima behind the bars and maxima behind the open spaces between bars. The waviness declines with growing

* (4) The local pressures and velocities are marked with an apostrophe to distinguish them from the corresponding quantities in the undisturbed stream (such as v and q).

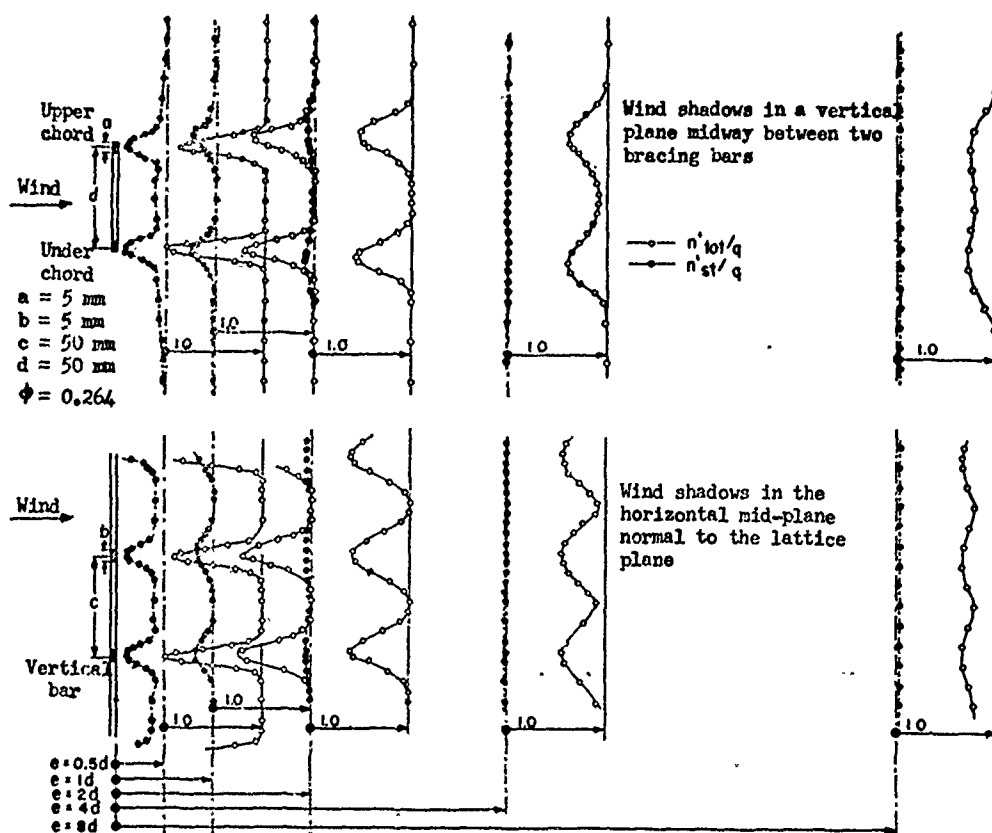


Fig. 2a -- Distribution of total and static pressures

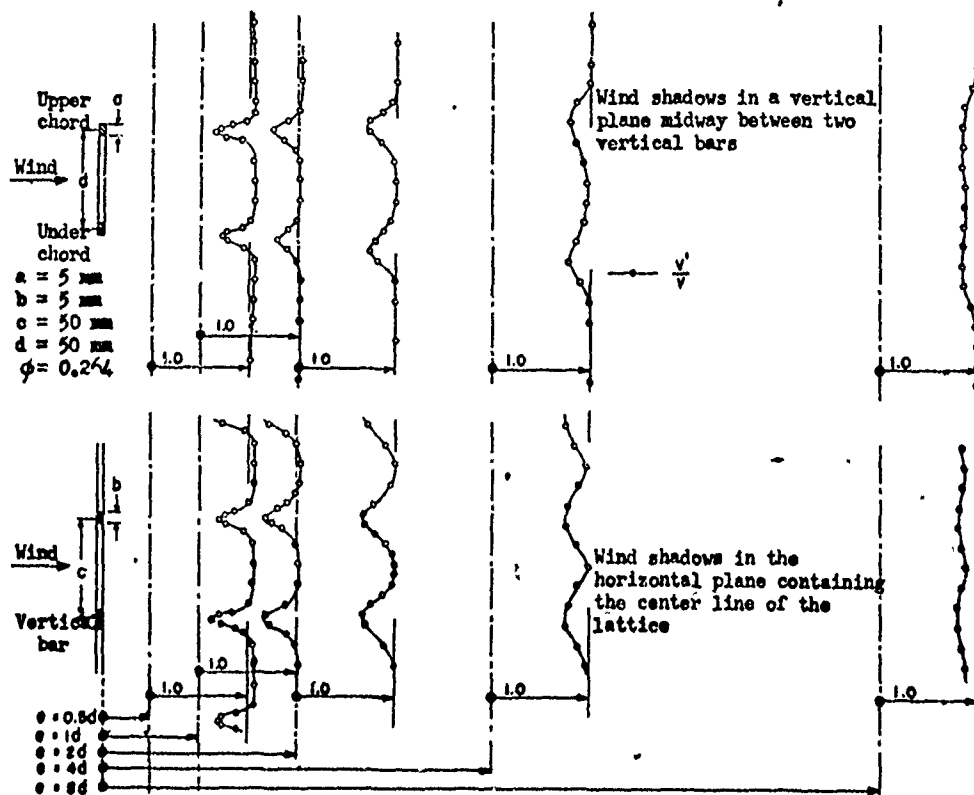


Fig. 2b -- Velocity distribution behind a ladder-type lattice

distance from the lattice. The dynamic pressure is proportionally rapidly equalized.* In comparison the total pressure and velocity equalize slowly. The spreading of the wind shadow is clearly traceable. By the time $e = 8d$, the wind shadows have joined (for thicker bars, this situation would require $e < 8d$).

The second of two lattices sees this velocity field as its incident field—as its initial or undisturbed field. If one thinks of the second of two congruent lattices in line, where \bar{v} is the average wind it experiences, then to a first approximation

$$c_{w_{rII}} \approx \left(\frac{\bar{v}}{v}\right)^2 \cdot c_{w_r}^{(e=\infty)}$$

$$\psi_{II} \equiv \frac{c_{w_{rII}}}{c_{w_r}^{(e=\infty)}} \approx \left(\frac{\bar{v}}{v}\right)^2$$

for the drag is—for sufficiently large Reynolds numbers—proportional to the square of the velocity. As a consequence of this and Figs. 2a and 2b, the following statements can be made [whose reliability is controlled by Fig. 3]:

1. The disturbance of the velocity field behind a lattice dies out slowly. Therefore the shielding effect of the forward on the rear lattice must remain notable even for wide separations. For cases which approximate the one investigated, where $\phi = 0.264$ and separation $e = 8d$,

$$\frac{\bar{v}}{v} = 0.85 \quad \psi_{II} \approx \left(\frac{\bar{v}}{v}\right)^2 \approx 0.72$$

Thus it is insignificant whether the lattices are exactly in line since the smearing of the wind shadow is large. This holds for great distances.

* (5) The slight rise in static pressure indicated in the right-hand section of Fig. 2a is a wind tunnel defect.

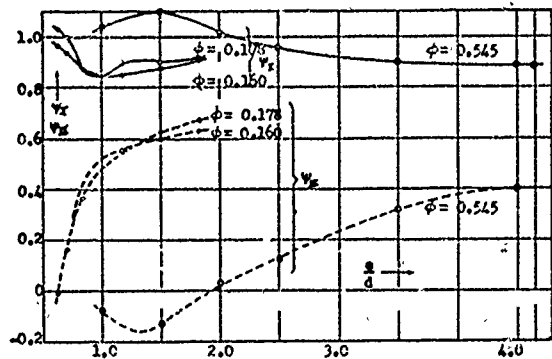


Fig. 3a -- Ladder structure. Lattices in line

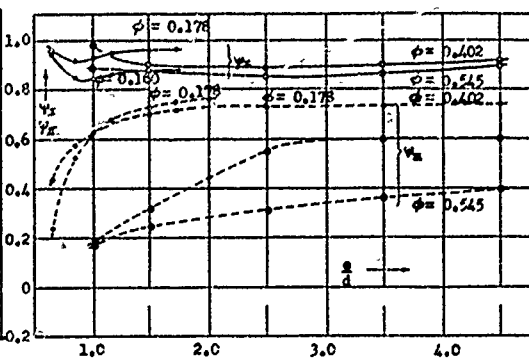


Fig. 3b -- Ladder structure. Lattices transposed 1/2-field width

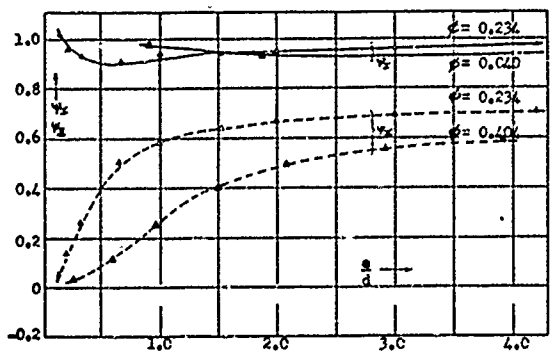


Fig. 3c -- V-structure. Lattices in line

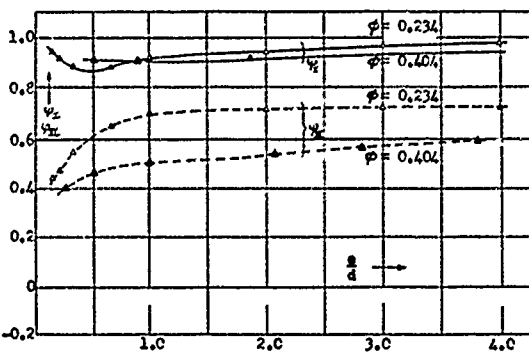


Fig. 3d -- V-structure. Lattices transposed 1/2-field width

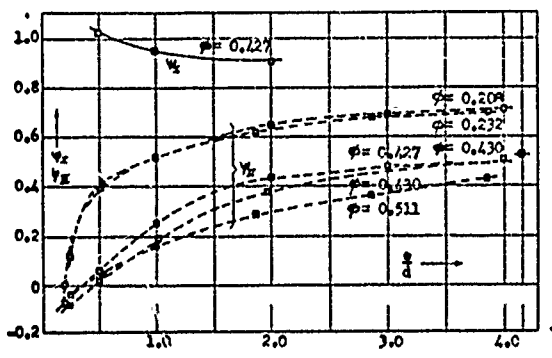


Fig. 3e -- N-structure. Lattices in line

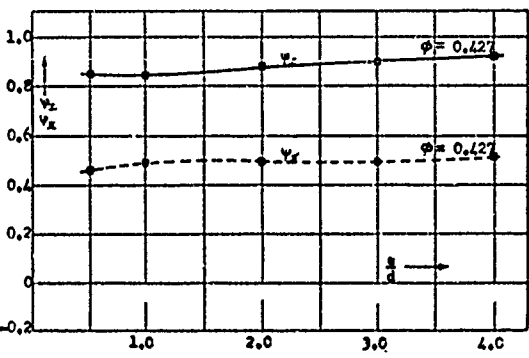


Fig. 3f -- N-structure. Lattices transposed 1/2-field width

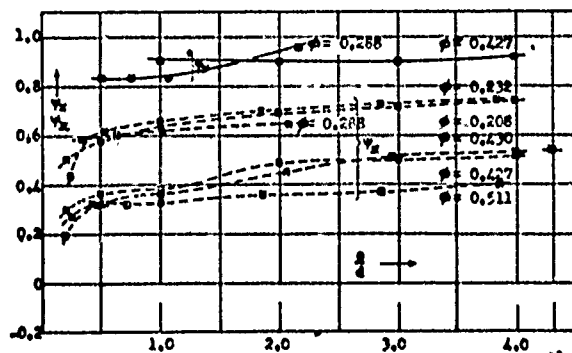


Fig. 3g -- N-structure. Lattices transposed so that the diagonals crossed; chords still in line

2. In contrast to this, it must be vital at close distances whether the lattices are in line or not. In the first case all the bars of the 2nd lattice are strongly shielded, and in the second case, they are almost equally sharply out of the wind shadows. An estimation of ψ_{II} generally runs into difficulties. The strong variations of velocity with position influences the flow patterns around the beams of the second lattice in an unpredictable way. But even if flow lines were known, the small minima would open the question of which velocity to use for aerodynamic computation. Still the lower limit of ψ_{II} for in-line lattices can be found using $\bar{v}^i = v_{\min}^i$.

With $\bar{v}^i = v_{\min}^i$ we are certainly using a smaller value than the aerodynamically true effective velocity.

$e/d = 4$	$v_{\min}^i/v = 0.78$	$\left(v_{\min}^i/v\right)^2 \approx 0.60 = \psi_{II}$
$e/d = 2$	$v_{\min}^i/v = 0.68$	$\left(v_{\min}^i/v\right)^2 \approx 0.46 = \psi_{II}$
$e/d = 1$	$v_{\min}^i/v = 0.66$	$\left(v_{\min}^i/v\right)^2 \approx 0.43 = \psi_{II}$

Similar estimates can be made for axially transposed lattices (still parallel but no longer in line). There the amount of the displacement and the type of structure will enter as parameters. In each case the ψ_{II} for displace lattices will be greater than for those in line [note that higher shielding coefficients mean less actual shielding.]

After these preliminary remarks we can turn to the results of the measurements of two lattices one behind the other.

D. TESTS ON TWO PARALLEL LATTICES OF LIKE PATTERN AND SOLIDARITY RATIO FOR NORMAL WINDS

Twelve lattice pairs were investigated, eleven schematic types of flat bar construction, and one with "profiled" bars [shapes like L, I, J, etc], all lattices were infinite ($\lambda = \infty$).

These lattices, as with the earlier experiments, were "ladder" structures: parallel beams with either V or N bracing. The results of the tests on single lattices were presented in Part 1, those for the pairs in Fig. 3a to g in Part 2. These diagrams show only shielding coefficients (ψ) and the drag coefficients must be calculated.

$$c_{w_{rI}} = \psi_I \cdot c_{w_r}^{e=\infty}$$

$$c_{w_{rII}} = \psi_{II} \cdot c_{w_r}^{e=\infty}$$

The value of $C_{w_r}^{e=\infty}$ are obtainable from Fig. 21 in Part 1. Of course, in Part 1 the designation of the quantity $C_{w_r}^{e=\infty}$ was simply C_{w_r} . The data points from similar structures of Part 1 are presented in Fig. 3, Part 2, with the same symbols (\circ , Δ , etc).

To these twelve sets of data are added the tests on four finite lattices: bridge trusses (2) through (5) of Part 1. The results are given in Fig. 4. The corresponding drag coefficients for isolated lattices are found in Fig. 21 of Part 1. The case of a pair of N - lattices with crossed diagonals was included in Fig. 3g.

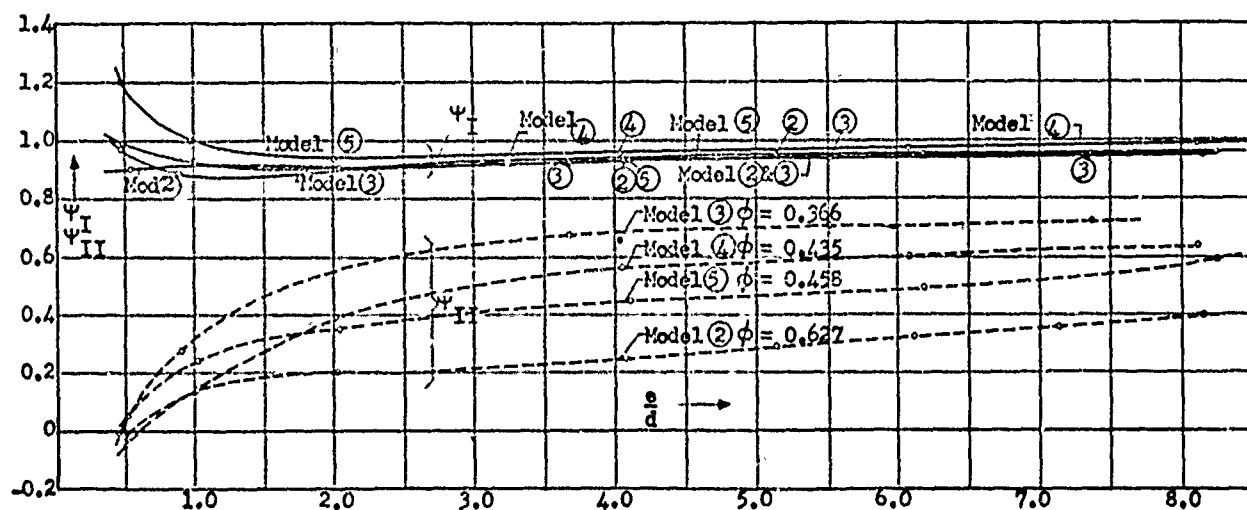


Fig. 4 -- Shielding coefficients of lattice pairs under normal incidence ($\alpha = 0^\circ$) and finite aspect ratio ($\lambda = 9.5$). Lattices in line. Model designations from Fig. 20 of Part 1. Ref. AVA-III

Not all permutations of the variables in Fig. 3 and Fig. 4 have been made. The number of parameters forced a limitation on the tests to keep them easily surveyed.

The test results conform to the predictions made on simpler considerations: slight influence on the fore lattice, strong shielding on the rear lattice.

$\psi_I = 0.8$ to 1.1 ; for normal solidarity coefficient, $\psi_I < 1.0$ in each case for $e/d > 1.0$. Even for the very large solidarity $\phi = 0.511$ and $e/d = 1.0$ the shielding coefficient ψ_I was only little greater than 1.0 . Since a separation $e/d < 1.0$ is almost never seen, $\psi_I = 0.9$ or 1.0 is a far-reaching approximation. It holds regardless of ϕ and whether or not the lattices are in line.

ψ_{II} for small separations is expectedly negative, and grows with separation, slowly approaching the limiting value of $+1.0$, so that $e/d = 8$ still gives large shielding. As one must expect from Fig. 2b, ψ_{II} is really dependent on three parameters:

Solidarity coefficient

Separation of the lattices

Orientation of the lattices to each other.

To clarify these relations Figs. 5a to 5e present the shielding coefficients versus ϕ with separation as a parameter. To allow a direct application of Eqs 2c and 4, the shielding ratio η is plotted. We have used the assumption that $\psi_I = 0.4$ for all cases where ψ_I was not measured. The corresponding points in Fig. 5 are marked (\wedge). We have limited the e/d values in these diagrams to 1.0 , 2.0 , 4.0 , and 6.0 . For transposed lattices, only the $e/d = 1.0$ case is presented. Since this oblique case is most common among lattice towers and masts where $e/d = 1.0$, this limitation is justified. In general the data of Fig. 5 can be extrapolated and interpolated to other values of e/d .

From Fig. 5 the following can be deduced: an influence of structural type exists, but it is so weak as to be negligible. No noticeable effect of bar cross section appeared. Outline and aspect ratio play no decisive roll so long as $\phi < 1$. This observation is in agreement with the aerodynamics of single lattices. Again the solidarity coefficient has significant influence, along with lattice separation and orientation. A glance at Fig. 5 shows how dominant is the influence of the solidarity coefficient.

The calculation of the resulting drag W_g of a lattice pair has to consider ϕ , separation and relative orientation.

$$W_g = C_{w_r} \cdot \frac{1}{2} \rho v^2 \cdot F_r \text{ [kg]}$$

(F_r = projected surface area of lattice!) For C_{w_r} we can use Eq 4 to write:

$$C_{w_r} = \psi_I C_{w_r}^{e=\infty} [1 + \eta]$$

ψ_I and η could be taken from Figs. 3 and 4. Both quantities are dependent on ϕ , e/d and relative position. The shielding coefficient ψ_I , as we have seen, varies so slowly compared with the other parameters that $\psi_I \approx \text{constant}$ is valid. We have the numbers between $\psi_I = 0.90$ and $\psi_I = 1.0$ to choose from; so we took

$$(5) \quad \psi_I = 1.0 = \text{constant}$$

since this value is on the safe side and simplifies the calculations. * $\psi_I = \text{constant}$ means that in the first approximation the working of the rear on the front-lattice is negligible.

* (7) In order to ascertain the η -value for lattice pairs whose ψ_I was not measured, we have set $\psi_I = 0.9$ above. It should be remarked that $\psi_I = 0.9$ gives the largest η -value obtainable for $0.9 \leq \psi_I \leq 1.0$, while $\psi_I = 1.0$ gives the largest C_{w_r} . In both bases, where ψ_I is measured, the value is chosen to give results on the safe side.

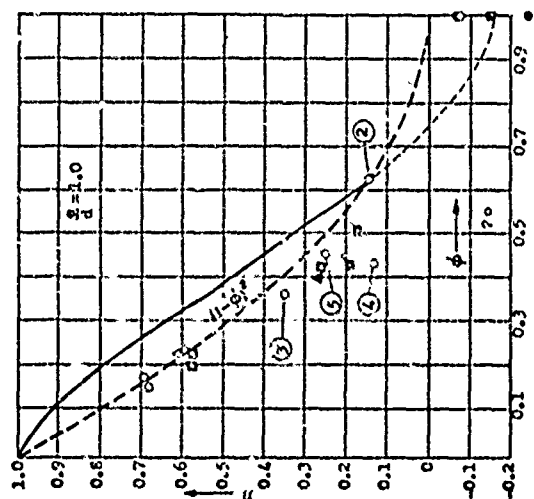


Fig. 5a

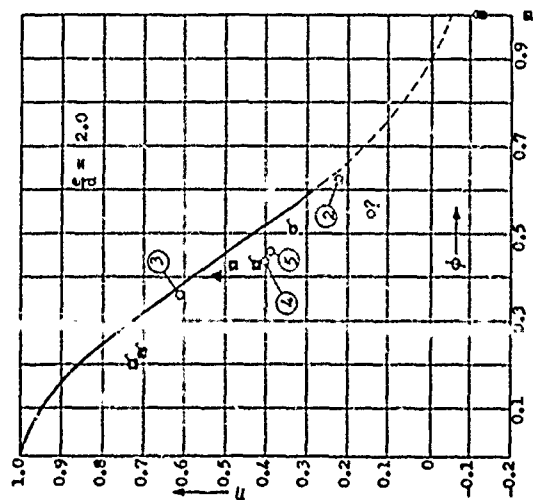


Fig. 5b

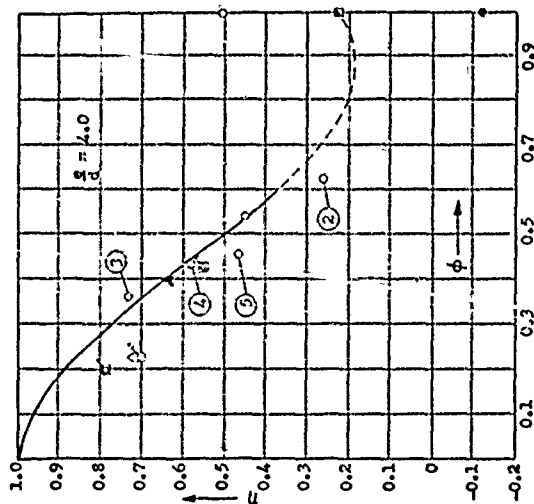


Fig. 5c

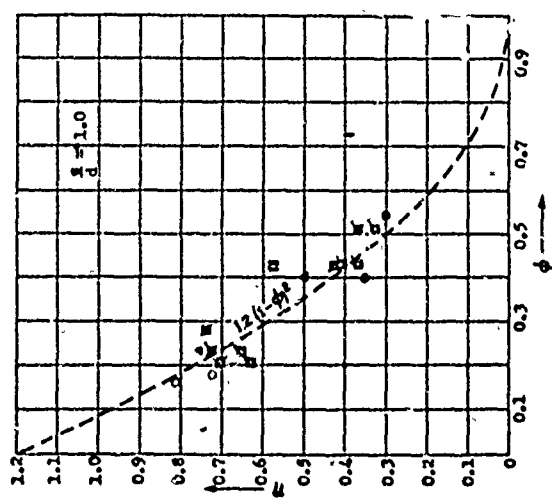


Fig. 5d

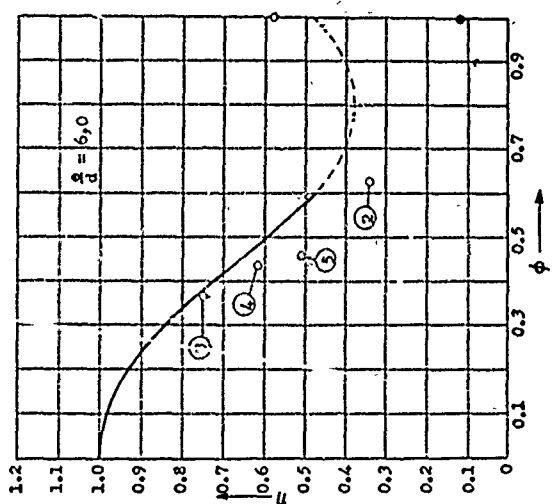


Fig. 5e

Figs. 5a - 5e -- Shielding ratio σ of lattice pairs
as a function of

Figs. 5a - 5d -- Lattices in line

Fig. 5e -- Lattices transposed

Designations of measured points for $\phi = 1.0$ are like
those in Fig. 1, and for $\phi < 1.0$ like those in Fig. 3.

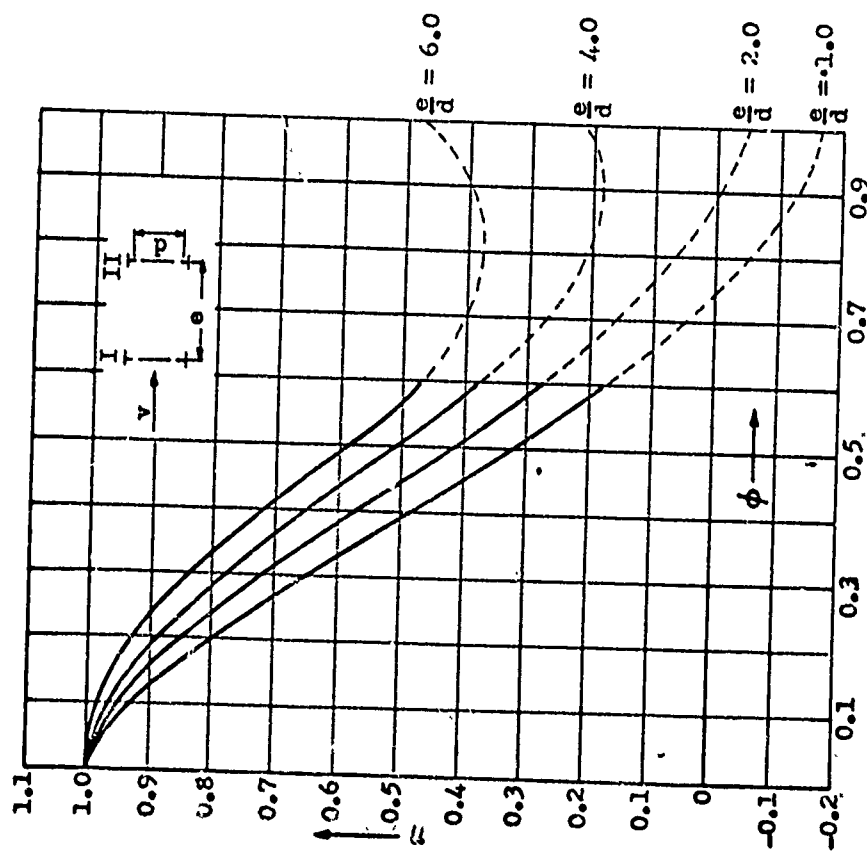


Fig. 6a

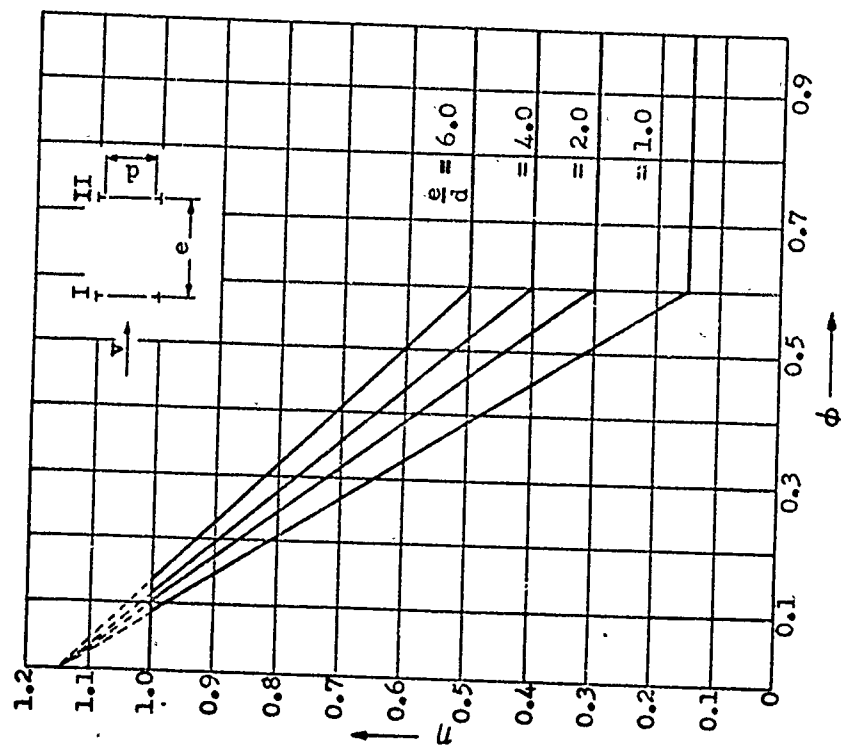


Fig. 6b

Fig. 6a -- Graph of η value for technical drag calculations of lattice pairs in line; developed from Figs. 5a through 5d. These η values to be used in Eq 7

These $\eta(\phi, e/d)$ diagrams should be further transformed for computation purposes in somewhat the following way: a simple function $\eta(\phi)$ can approximate the mid-curve of the rather scattered test points. Such approximate functions are given below:

$$\left. \begin{aligned} \eta &= (1 - \phi)^2 \text{ for lattices in line} \\ \eta &= 1.2 [1 - \phi]^2 \text{ for transposed lattices} \end{aligned} \right\} \text{ for } e/d = 1$$

These curves have been dotted in for Figs. 5a and 5c. They fit in some measure the experimental scatter, and are thus useable approximations. Their extension to greater e/h values is possible, but only by renouncing their simplicity, which alone is the real justification for the existence of such approximation formulas. Figures 5a through 5d show the curves for inline lattices (the solid curves with the thin dashed extensions). Figure 6a shows the collected curves. Generally these are NOT average curves but upper boundaries of the envelopes of the experimental points. The use of the upper limits of η values insures that η is not taken too small in calculations and amounts to a safety factor.*

The given η -curves must be qualified since the aspect ratio plays a role for $\phi > 0.6$. We have renounced the exact consequences of this dependence, since $\phi > 0.6$ scarcely occurs in practice, and the given curves show this region as a thin dashed line. For $\phi = 1$ the conditions are to some extent known. We have presented the η -value read off Fig. 1 where $d \equiv h$ for the solid plates.

For technical cases it is desirable to ignore the variation in η beyond $\phi = 0.6$, and thus to set

$$\text{for } 0.6 \leq \phi \leq 1.0 \quad \eta = \eta|_{\phi = 0.6} \approx \text{constant}$$

* (9) That the η -curve for $e/d = 1.0$ (Fig. 5a) lies somewhat high is due to accommodation of Dickmann's unpublished data. (See section III).

Then comes the last step in simplification: the substitution of the curvilinear group of Fig. 6a with a set of rectilinear approximations as in Fig. 6b.

$$(6) \quad \left\{ \begin{array}{ll} 0 \leq \phi \leq 0.1 & \rightarrow \eta = 1.0 = \text{constant} \\ 0.6 \leq \phi \leq 1.0 & \eta = \eta_{\phi=0.6} = \text{constant} \\ \text{between these areas as set of sloping lines} & \end{array} \right.$$

$$\eta \simeq 1.15 \left[1.0 - 1.45 \phi (e/d)^{3/4} \right]$$

One can proceed in a corresponding way for non-inline lattices (transposed, staggered). It is observed that one deals almost exclusively with lattices of solidarity coefficients between 0.1 and 0.6.

The drag computation for lattice pairs under normal ($\alpha = 0^\circ$) wind incidence is thus reduced to a very simple procedure. It consists of using Eq 4, which is simplified by Eq 5 to

$$C_{w_r} = c_{w_r}^{e=\infty} (1 + \eta)$$

or, if we instead of $c_{w_r}^{e=\infty}$ write c_{w_r} to

$$(7) \quad C_{w_r} = c_{w_r} (1 + \eta)$$

From Part 1 the approximate values of c_{w_r} are:

$$\begin{aligned} c_{w_r} &= 1.8 \text{ for } \phi < 0.25 \\ c_{w_r} &= 1.6 \text{ for } \phi \geq 0.25 \end{aligned}$$

η can be taken from diagrams 5 or 6.

We will consequently—after some remarks on oblique winds on lattice pairs—prove how a procedure for drag calculations of bridges and towers can be developed from drag predictions for lattice pairs.

E. OBLIQUE INCIDENCE ON LATTICE PAIRS

A bridge-type lattice pair of model (5) and $e/d = 4.12$ was tested for oblique winds both from above and from the side. Results are given in Figs. 7a and 7b, using the normal drag coefficients c_{w_r} and tangential drag coefficients c_{t_r} .

As with single lattices, the tangential force is negligible. The normal force on the leading lattice has been somewhat reduced by the presence of the second lattice.

The normal force on the second lattice grows with the obliquity of wind incidence, reaching a maximum for $\alpha = 25^\circ$, either from above or sidewise. The fall-off is gradual on either side of this maximum. That the $c_{n_{rII}}$ -curve should have this character is easy to see. Also, quantitative statements can be made if the behavior of the single lattice is known for oblique winds. However, this will not be further developed here.

It is enough to notice that the tangential forces are very small for oblique incidence, and that the normal force on the leading lattice is virtually the same as for a single lattice.

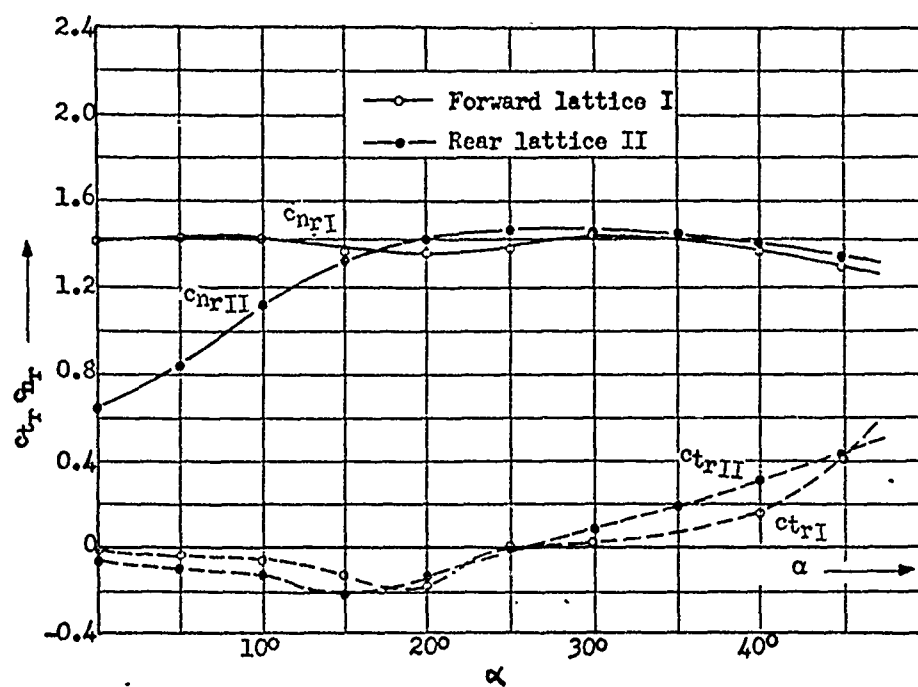


Fig. 7a

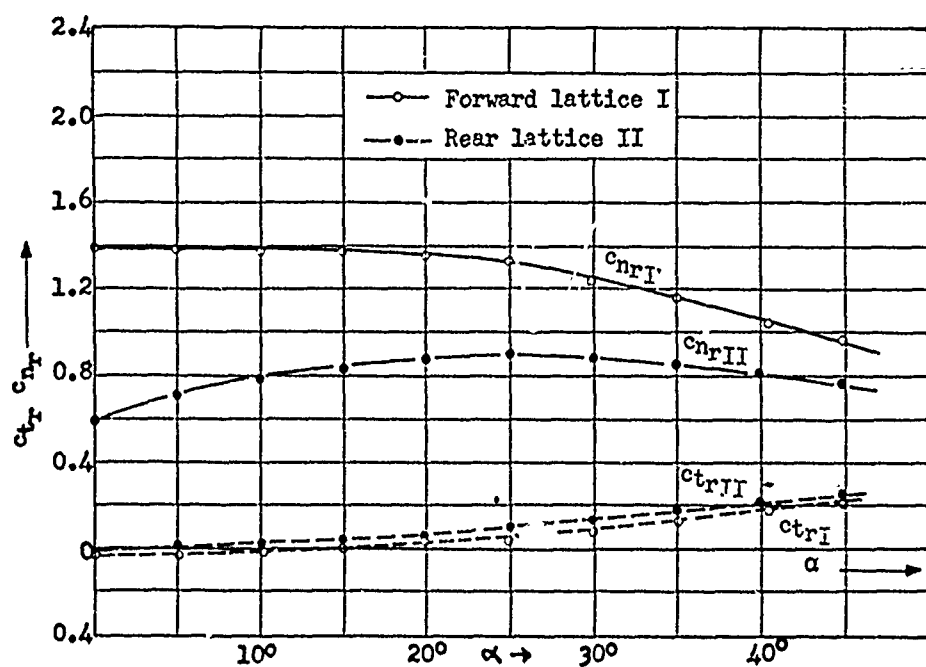


Fig. 7b

Fig. 7 -- Lattice pairs of type (5), $\phi = 0.458$. Oblique incidence from above (7a) and from the side (7b). (See sketch in Fig. 8) $e/d = 4.12$

CH III -- TWO LATTICES WITH ROADBED (BRIDGES)

The addition of a roadbed to a pair of lattices should have little effect for normal winds and small values of ϕ . Certainly the surface friction drag of the roadbed enters the picture, as well as the pressure drag if the roadbed is thicker than or between the girders [chords]. In any case, it is certain that the flow patterns will be influenced by the roadbed. But these changes and their drag changes are small compared to the total drag of the lattice pair, so that the earlier formulas for lattice pairs can be used for bridges. This is especially true since these curves were only approximations to fairly scattered data points. It must again be stated that this equating of bridge to pair data is predicated on small ϕ and normal incidence.

Luckily the conditions are not as restrictive as one might think. The limitation to $\phi < 0.6$ really excludes just the important case of $\phi = 1$. However, consider the following: a solid lattice pair with the road in the middle will have the same flow patterns as the pair alone. If the roadbed is above or below the centerline, the flow pattern will be influenced, the dead space reduced and the fore pressure on the rear plate also reduced. Both these effects lead to a reduction in total drag. Thus the curves in Fig. 6 also represent the upper limits for slender solid beam pairs with or without roadbeds. The same holds for $\phi < 0.1$ and $\phi > 0.6$. One designs somewhat uneconomically but not unsafely.

The condition of normal incidence is also no real limitation, since bridges are not subject to winds with strong vertical components, and since lateral obliquity can produce only moderate drag increases [see Fig. 7b]. Consequently the design Eq 7 for lattice pairs can be used for bridges of any solidity coefficient.

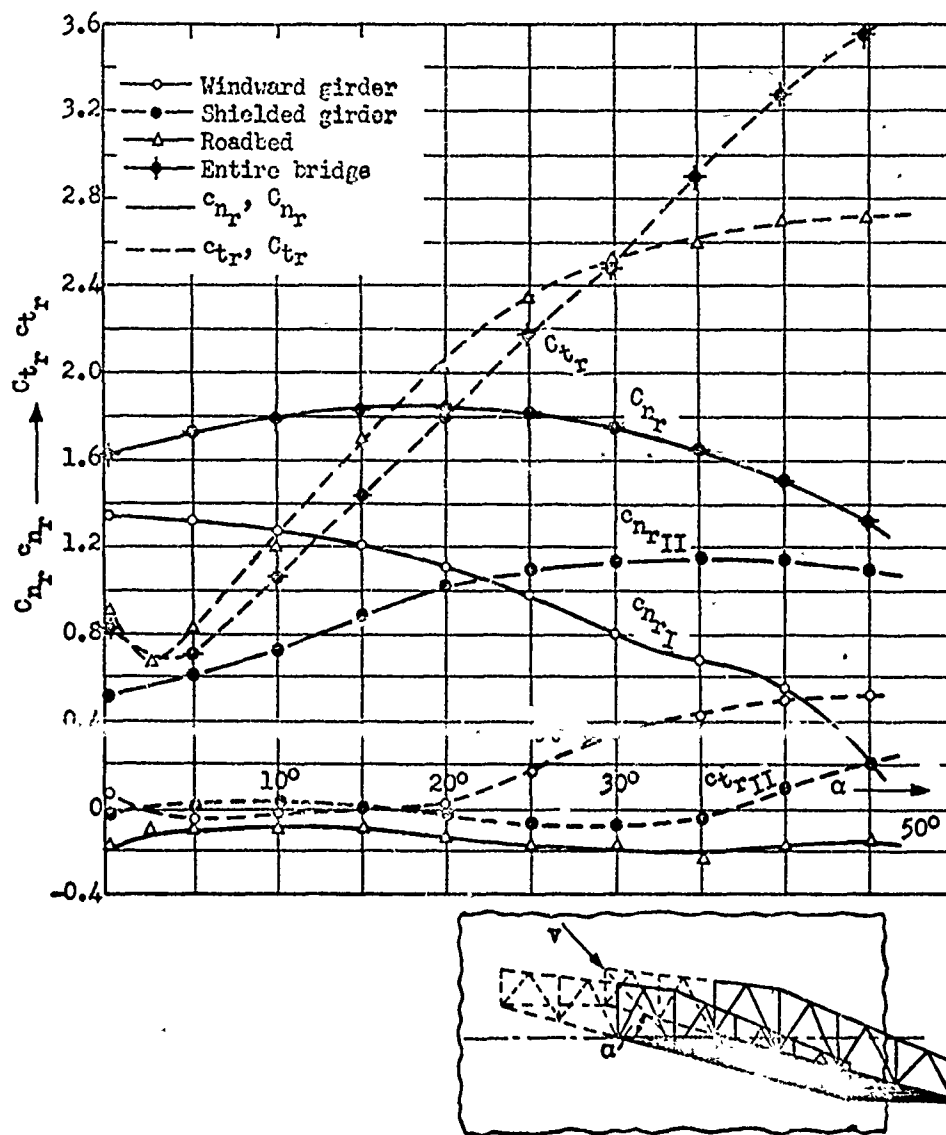


Fig. 8 -- Bridge model with main girders of type (5) with oblique winds from above, $\phi = 0.458$, $e/d = 1.44$

We made similar considerations when the test program was designed. The result of these considerations led us to discard a systematic investigation of whole bridge models, since a really new insight could not be expected. We reproduce these measurements in Fig. 8. Using Eq 7 for bridges gives $c_{w_r} = 1.46$ [from Fig. 21 of Part 1] and $\eta = \frac{\psi_{II}}{\psi_I} = 0.34$ for $e/d = 1.44$ [from Fig. 4 of Part 2].

$$C_{w_r} = 1.96$$

with $\eta = 0.43$ from Fig. 6 or Eq 6

$$C_{w_r} = 2.09$$

The measured normal drag coefficient for $\alpha = 0^\circ$ gave $c_{n_r} = 1.63$, greatest normal coefficient, for $\alpha = 20^\circ$, was 1.86. Thus one sees that in each case the calculated value lies above the measured one. It should be observed that a 20° angle of incidence from above is quite unlikely. The tangential forces are [Fig. 8] negligibly small.

Thus our conjecture on bridge calculations with lattice-pair data is supported. Still it is desirable to obtain further confirmations. O. Flachsbarth has conducted a series of tests at Hannover on bridge models. The results confirm Eqs 6 and 7 for calculation purposes.*

* (10) Figures 6a and 6b were sketched to include the Dickmann data, particularly for $\phi = 1$. The η -values for the solid pair $\lambda = 13.6$ lie - in comparison with all other $\phi = 1$ data including the Dickmann - so unusually high that we have not given them corresponding weight.

CH IV -- FOUR LATTICES IN A BOX STRUCTURE ($\lambda = \infty$)

A. NORMAL INCIDENCE ($\alpha = 0^\circ$)

Consider a square-lattice mast like that in Fig. 9. Since real towers are tapered and of declining solidity, correct use of data for $\lambda = \infty$ involves a piece-wise approximation to the tower with each piece assumed to be uniform in ϕ and cross section. Such an approach has been very accurate, and it allows the incorporation of nonuniform wind profiles.

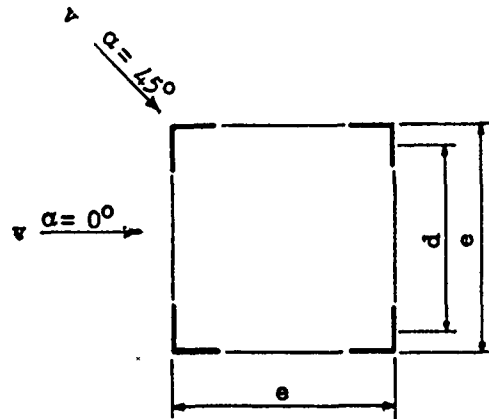


Fig. 9 -- Box structure cross section

For drag calculation of a lattice mast in an arbitrary wind field one needs only the assumption that the flow around one segment of the mast is practically independent of the flow at more distant parts. Naturally this is only an approximation, but it is good, particularly for the more permeable structures. The greatest error occurs at the mast peak, but the distortion of the total drag is slight.

Table I shows the test results for a number of partial models [those in Figs. 10 through 13]. $\alpha = 0^\circ$ means wind streams normal to the side. The placement of the models in the wind tunnel is shown in Fig. 14.

Now we must ask whether the C_{w_r} of these models approaches the C_{w_r} of similar lattice pairs; or in other words, whether the effect of the side walls parallel to the wind is negligible. The answer from experiment is affirmative: the side walls are unimportant in

TABLE I (Part 2)

Section Models of Lattice Towers With Quadratic Cross Sections

Measured						Calculated		
Model	Fig.	ϕ	α°	C_{w_r}	C_{a_r}	$\xi = \frac{C_{w_r}^{(max)}}{C_{w_r}^{(0)}}$	$C_{w_r}^{(0)} = 1.6 (1 + \eta)$ η from Fig. 6a [Bracketed Values Using $\eta = 1.2 (1 - \phi)^2$]	$C_{w_r}^{(45)} = \xi \times 1.6 (1 + \eta)$ η from Fig. 6a [$\eta = 1.2 (1 - \phi)^2$]
Transmission Line Mast	10a	0.195	0	2.74		1.01	2.50 [2.64]	$\xi = 1.1$ $\xi = 1.2$
			45	2.77				3.19 [3.12] 3.48 [3.41]
	10b	0.261	0	2.53		1.05	2.74 [2.65]	
			45	2.65				3.01 [2.92] 3.28 [3.18]
	10c	0.455	0	1.68		1.29	2.23 [2.18]	
			45	2.42				2.46 [2.41] 2.68 [2.62]
Resener Radio Tower	11a	0.214	0	2.68		1.12	2.65 [2.78]	
			45	3.00				3.14 [3.06] 3.42 [3.34]
	11c	0.182	0	2.71	0.09	1.17	2.94 [2.69]	
			7.5	2.96	0.25			
			15	3.08	0.43			
			30	3.17	0.30			
			45	3.01	0.01			3.23 [3.18] 3.52 [3.47]
	11b	0.286	0	2.40	0.02	1.22	2.67 [2.58]	
			7.5	2.55				
			22.5	2.84	0.22			
			30	2.53	0.21			2.94 [2.84] 3.21 [3.10]
			45	2.62	0.03			
X-type Box Structure	12c	0.189	0	2.62	0.05	1.10	2.91 [2.86]	
			7.5	2.77	0.27			
			15	2.60	0.59			
			22.5	2.80	0.51			3.20 [3.15] 3.50 [3.44]
			30	2.83	0.33			
			45	2.88	0.07			
	12b	0.233	0	2.56	-0.10	1.16	2.81 [2.73]	
			7.5	2.74	-0.05			
			15	2.78	+0.25			
			22.5	2.63	0.35			3.09 [3.00] 3.37 [3.28]
			30	2.55	0.21			
			45	2.96	0.02			
	12a	0.288	0	2.41	0.14	1.18	2.67 [2.58]	
			7.5	2.51	0.23			
			15		0.41			
			22.5	2.71	0.38			2.94 [2.84] 3.20 [3.09]
			30	2.79	0.24			
			45	2.85	0.03			
Calculated C_{w_r} - Measured C_{w_r} Measured C_{w_r}							10% [7%]	7% [5%] 17% [14%]

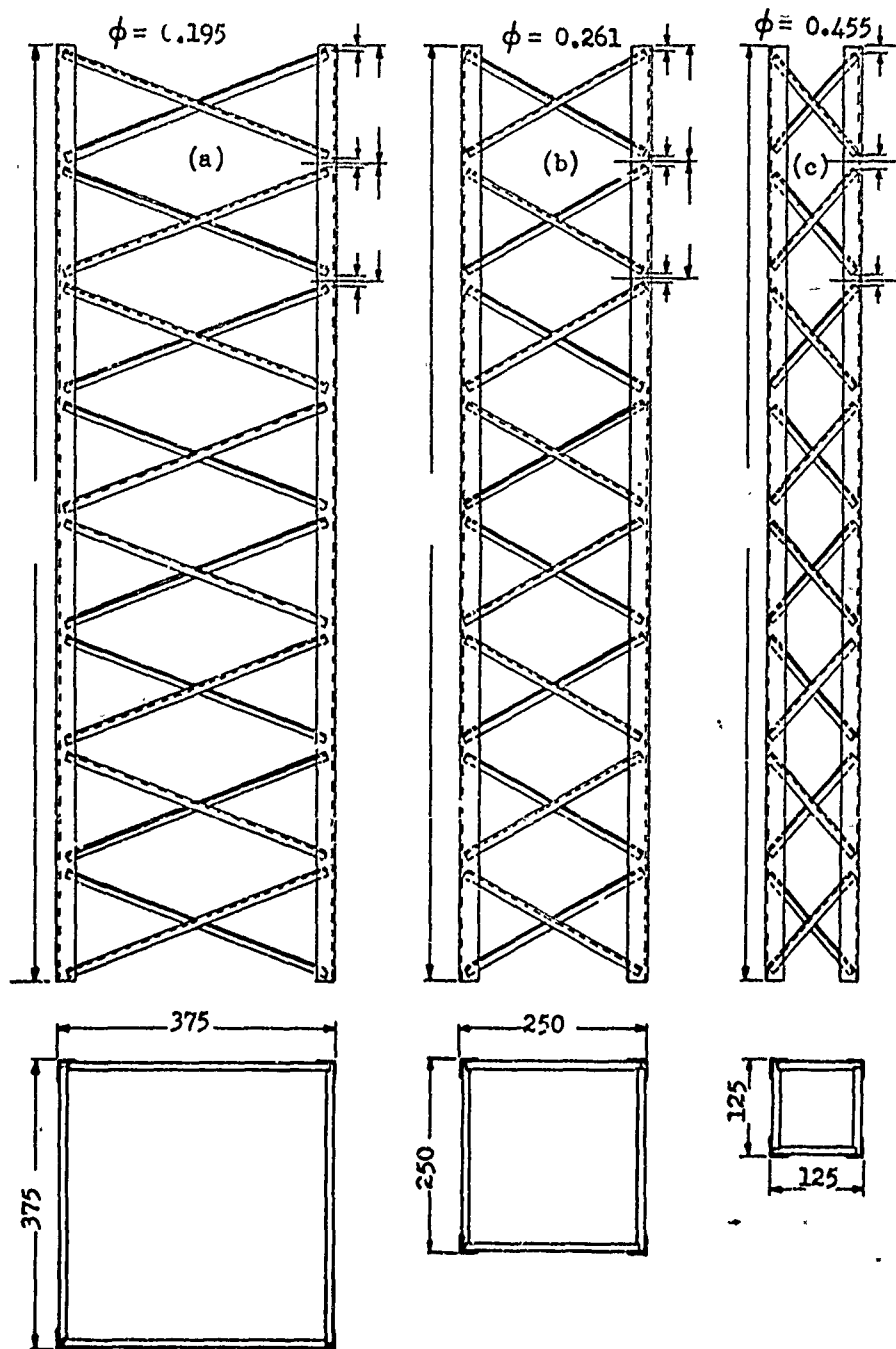


Fig. 10 -- Three sectional models of transmission masts

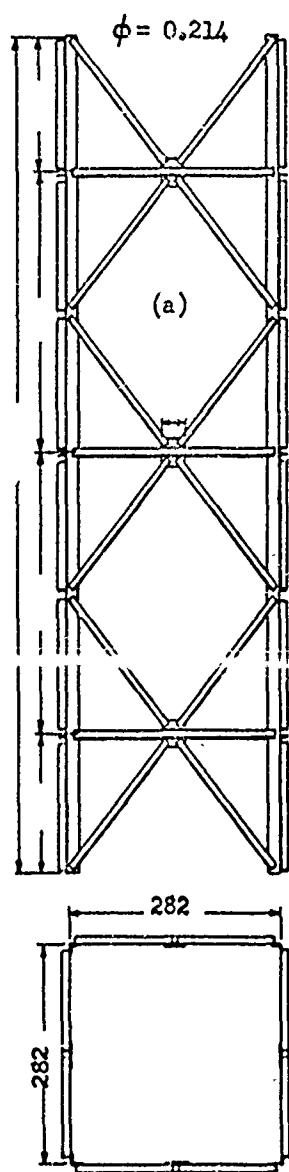


Fig. 11a -- Sectional model of a radio tower (Zeesener radio tower). Compare Fig. 13d

$$c_{wrI} \approx c_{wr1}, \quad c_{wrII} \approx c_{wr2}$$

$$c_{wrI} + c_{wrII} \approx c_{wr}$$

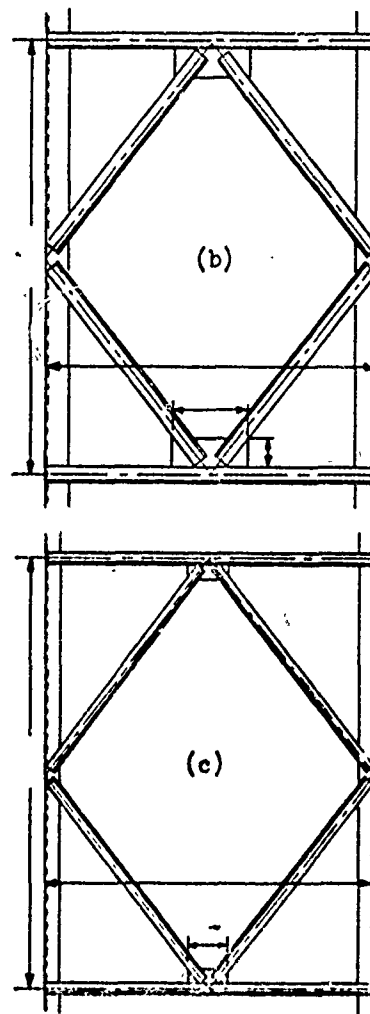


Fig. 11b, c -- Two more sectional models of the Zeesener tower tested independently of the model in Fig. 11a

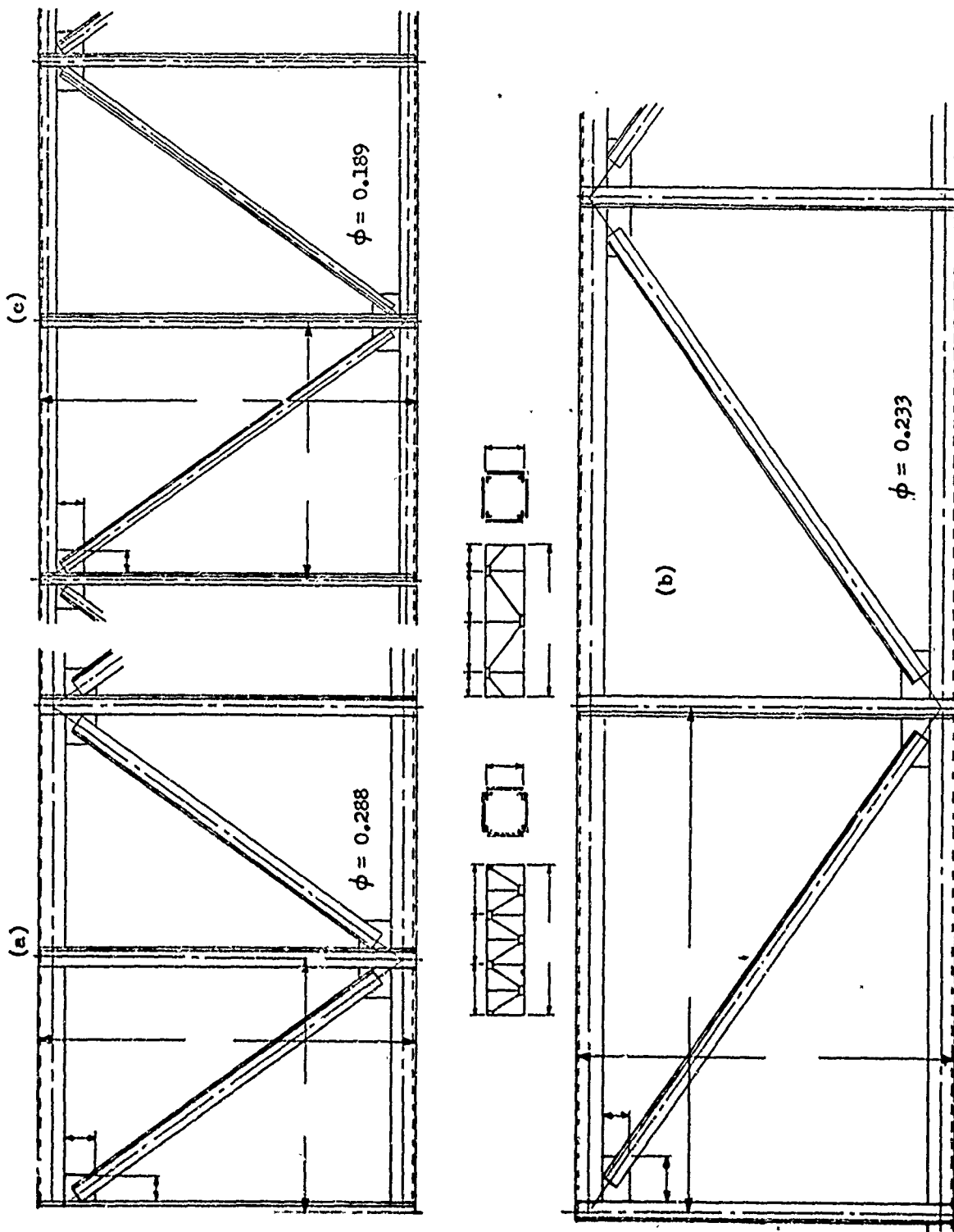


Fig. 12 -- Three models of box-work structures with quadratic cross section and N-type bracing. Note: All bars have N cross section

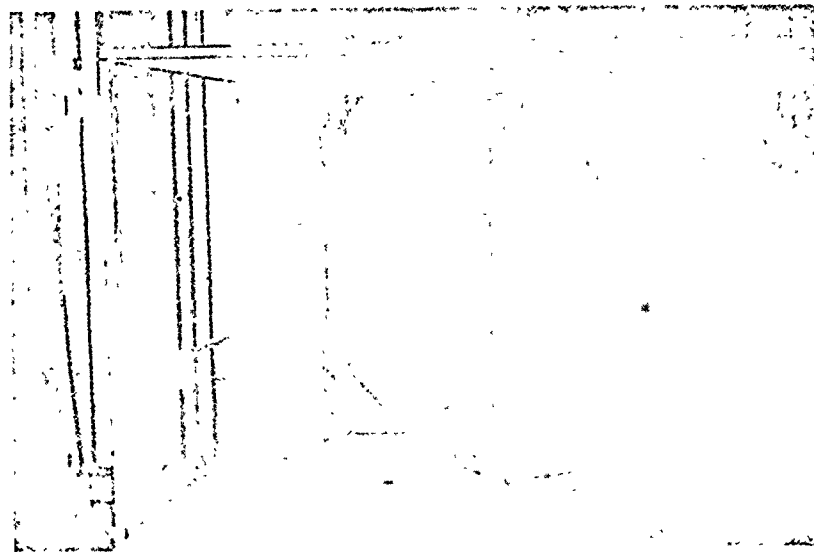


Fig. 14 -- Model in the wind tunnel.
The view is against the wind direction.
Above is the balance mechanism



Fig. 13d -- Photograph of the model in Fig. 11a

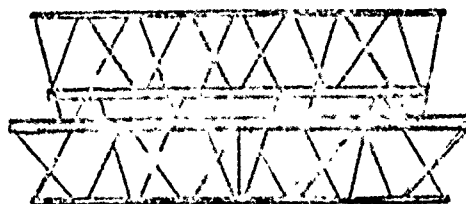
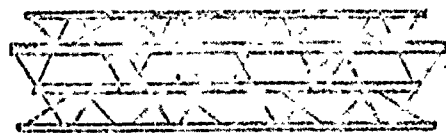
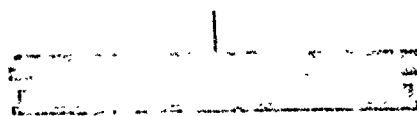


Fig. 13a-c -- Photographs of the three models in Fig. 10. The model on the right shows the thin rod used to hold the model in the wind tunnel

drag calculations. Equation 7 can be applied for the calculation of 4-lattice masts under perpendicular air stream incidence. The proof is in Table I [in comparison with section VI, 7]. An additional experimental proof might be mentioned here.

We have investigated a model [N-structure, staggered, $\phi = 0.288$] that was divided as indicated in Fig. 15a. The measurements were:

whole model	$C_{w_r} = 2.11$
mast half 2	$C_{w_{r2}} = 0.96$
<hr/>	
mast half 1	$C_{w_{r1}} = 2.11 - 0.96 = 1.15$

Earlier lattice-pair measurements for $e/d = 1$

Lattice 1	$c_{w_{rI}} = \psi_I \cdot c_{w_r} = 0.94 \times 1.58 = 1.48$
Lattice 2	$c_{w_{rII}} = \psi_{II} \cdot c_{w_r} = 0.61 \times 1.58 = 0.96$

Therefore with far-reaching exactness

$$c_{w_{rI}} \approx C_{w_{r1}} \quad c_{w_{rII}} \approx C_{w_{r2}}$$

$$c_{w_{rI}} + c_{w_{rII}} \approx C_{w_r}$$

Thus the influence of the sides of a box lattice tower is negligible, as far as $\alpha = 0^\circ$ drag is concerned.

The same is true of tangential forces; they are null for $\alpha = 0^\circ$. Table 1 shows C_{a_r} is always ≈ 0 for $\alpha = 0^\circ$.

B. OBLIQUE FLOWS ($\alpha \geq 0^\circ$)

If the wind direction swings around in the plane of the ground, all four sides contribute to the drag. Maximum drag for $\phi = .10$ to $.20$ does not always occur when $\alpha = 45^\circ$. In some cases the maxima lie between $\alpha = 25^\circ$ and $\alpha = 30^\circ$.

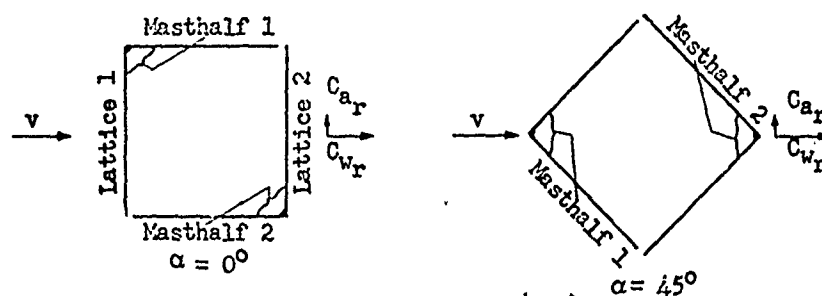


Fig. 15 -- Definition sketches

The growth of drag for oblique incidence might be predicted on simplest grounds to add 20 per cent to the total drag. It remains to be proved how the drag is divided among the mast halves. To this end, we have used the N-type model, $\phi = 0.288$, which was employed earlier.

Results:

entire model	$C_{wr} = 2.85$	} measured
mast half 2	$C_{wr2} = 1.18$	
mast half 1	$C_{wr1} = 2.85 - 1.18 = 1.67$	
mast half 2 <u>alone</u>	$C_{wr2}^{(\infty)} = 1.92$	

Therefore one obtains the following remarkable result:

The shielding coefficient of mast half 2

$$\frac{C_{wr2}}{C_{wr2}^{(\infty)}} = \frac{1.18}{1.92} = 0.615$$

which agrees with the shielding coefficient ψ_{II} of the second lattice (of a pair) under normal wind incidence ($\psi_{II} = 0.61$).

For oblique incidence the mast behaves like a lattice pair (I' and II') normal to the wind.

Let us designate:

$c_{w_{rI}}^{(0)}$ and $c_{w_{rII}}^{(0)}$ \equiv the drag coefficients of the front and back lattices when $\alpha = 0^\circ$ for the mast.

$c_{w_{rI'}}^{\max}$ and $c_{w_{rII'}}^{\max}$ \equiv the drag coefficients of the synthetic effective lattice pair for oblique incidence giving the greatest drag for the mast.

$C_r^{(0)}$ \equiv drag coefficients for whole mast for $\alpha = 0^\circ$

$C_{w_r}^{\max}$ \equiv drag coefficients for whole mast for maximum drag angle.

then three constants (ϵ_I , ϵ_{II} , and E) are defined where $\epsilon_I > 1.0$, $\epsilon_{II} > 1.0$,

$E > 1.0$ and

$$c_{w_{rI'}}^{\max} = \epsilon_I \cdot c_{w_{rI}}^{(0)}, \quad c_{w_{rII'}}^{\max} = \epsilon_{II} \cdot c_{w_{rII}}^{(0)} \quad \text{and} \quad C_{w_r}^{\max} = E \cdot C_r^{(0)}$$

Observed test results on sectional models show

$$\left. \begin{aligned} c_{w_{rI}}^{(0)} &\equiv C_{w_{r1}} = 1.45 \\ c_{w_{rII}}^{(0)} &\equiv C_{w_{r2}} = 0.96 \\ C_r^{(0)} &= C_{w_{r1}} + C_{w_{r2}} = 2.41 \end{aligned} \right\} \text{for } \alpha = 0^\circ$$

$$\left. \begin{aligned} c_{w_{rI'}}^{(\max)} &\equiv C_{w_{r1}} = 1.67 \\ c_{w_{rII'}}^{(\max)} &\equiv C_{w_{r2}} = 1.18 \\ C_{w_r}^{(\max)} &= C_{w_{r1}} + C_{w_{r2}} = 2.85 \end{aligned} \right\} \text{for } \alpha = 0^\circ$$

therefore

$$\epsilon_I = \frac{1.67}{1.45} = 1.15 \quad \epsilon_{II} = \frac{1.18}{0.96} = 1.23 \quad E = \frac{2.85}{2.41} = 1.18$$

or for a practical approximation

$$\epsilon_I \approx \epsilon_{II} \approx E$$

Thus one has the possibility, from the expression for drag number of the mast under stream incidence in the direction of the cross section diagonal

$$(8) \quad C_{w_r}^{45} = E \cdot C_{w_r}^{(0)} = \epsilon_I \cdot c_{w_{rI}}^{(0)} + \epsilon_{II} \cdot c_{w_{rII}}^{(0)} = E \cdot c_{w_r}^{(0)} (1 + \eta)$$

to immediately read the partition of drag on the two synthetic lattices and thus on each of the side walls of the real structure:

$$(9) \quad C_{w_r}^{45} = \underbrace{E \cdot c_{w_r}^{(0)}}_{\text{Contribution of windward walls (or ersatz lattice I')}} + \underbrace{E \cdot c_{w_r}^{(0)} \cdot \eta}_{\text{Contribution of the two shielded walls (or the second ersatz lattice II')}}$$

for example

$$(10) \quad W_g^{(45)} = \frac{E}{1 + \eta} \cdot W_g^{(0)} + \frac{E \cdot \eta}{(1 + \eta)} \cdot W_g^{(0)} [K_g]$$

Equation 10 follows from Eq 9 if one observes that

$$W_g^{(45)} = C_{w_r}^{(45)} \cdot \frac{1}{2} \rho V^2 F_r = \epsilon \cdot C_{w_r}^{(0)} \cdot \frac{1}{2} \rho V^2 F_r = \epsilon \cdot W_g^{(0)}$$

or

$$W_g^{(45)} = \epsilon \cdot \underbrace{C_{w_r}^{(0)} (1 + \eta)}_{W_g^{(0)}} \cdot \frac{1}{2} \rho V^2 F_r = \epsilon \cdot c_{w_r}^{(0)} \cdot \frac{1}{2} \rho V^2 F_r + \epsilon \cdot c_{w_r}^{(0)} \cdot \eta \cdot \frac{1}{2} \rho V^2 F_r$$

There is no reason to doubt that these facts (except for masts of very high ϕ 's) can be combined. Controls through further tests, however, are desirable.

For drag calculation for winds along the mast cross section diagonal—prior to corrections from further experiments—the following way will be adopted: Calculate the drag W_g^{45} in the wind direction for $\alpha = 45^\circ$, using Eq 7 to find $W_g^{(0)}$ for $\alpha = 0^\circ$ and multiplying by E. From force $W_g^{(45)}$ each of the two windward planes experiences a drag $= \frac{1}{2} \frac{E}{1 + \eta} \cdot W_g^{(0)}$ (in the wind direction). The remaining $\frac{E \cdot \eta}{1 + \eta} \times W_g^{(0)}$ is divided between the two shielded planes. The value of η can be obtained from Figs. 5 and 6; the value of E is found in Fig. 18. In general it is satisfactory to set $E = 1.1$ to 1.2 , although greater values are possible (compare Table 1, Fig. 18a and b, and the remarks for Fig. 18b in the following section).

This paper leaves out the many cases where the greatest drag is not when $\alpha = 45^\circ$ because these drags are less than 10 per cent different from 45° drag. (Compare Table I.)

The cross force (C_{a_r}) is small compared to the drag in the wind direction (C_{w_r}) also for $\alpha \neq 0^\circ$, as can be seen in Table 1.

CH V -- TESTS ON MODELS OF COMPLETE MASTS

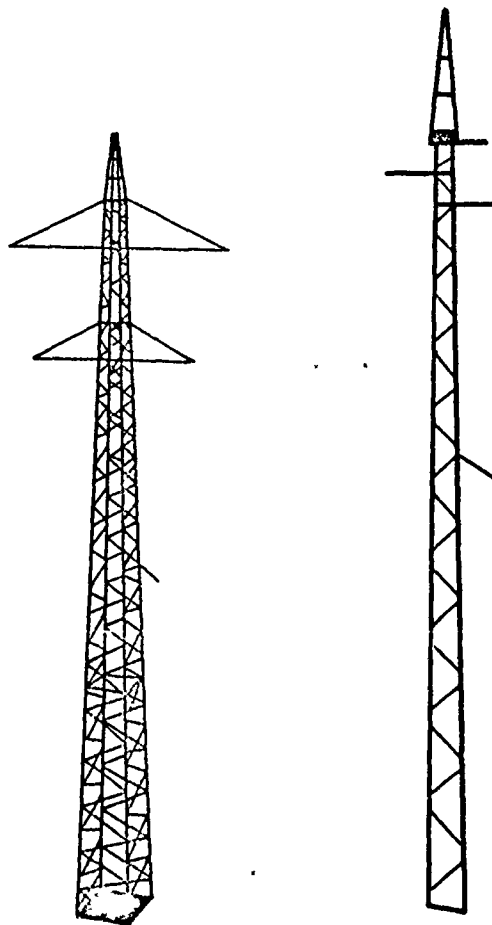


Fig. 16 -- Models of two lattice masts;
(a) transmission tower; (b) line pole

A complete model of a 100,000-volt electrical high-tension line mast was tested with and without crossbars, on smooth and rough ground plates. The height of the prototype was 25 m. Model scale was 1:50. Model height was consequently 0.50 m. Fig. 16a shows a photograph of the model. The models in Fig. 10a to c and Fig. 13a to c are sectional models which correspond to the lower, middle, and upper thirds of the mast. The velocity distribution above the ground plate for smooth and rough surfaces is to be taken from Fig. 17.

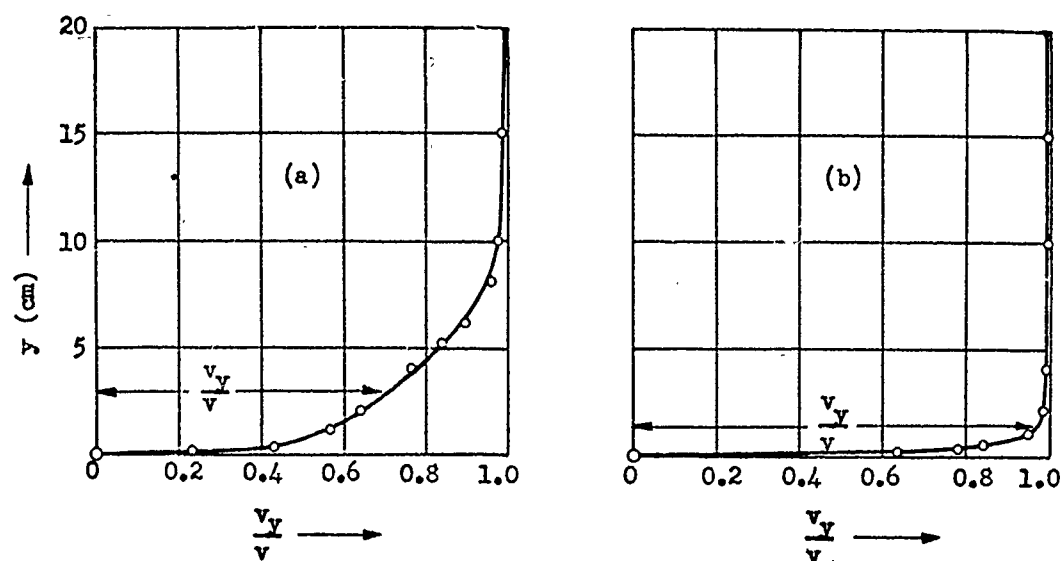


Fig. 17 -- Velocity profile over (a) rough ground plates and (b) smooth ground plates

In Table II are the measured C_{w_r} values for the electrical tower. The most important values for us are those for the tower without crossbars, since they allow direct comparison with the partial model of Fig. 10. We have calculated the C_{w_r} for $\alpha = 0^\circ$ of the tower without crossbars and for the two wind profiles of Fig. 17. The agreement in all cases was within 10 per cent.

The reliability of these calculation procedures is thus established. It has already been shown that special test results on partial models are not required for these calculations. It is sufficient to use Eq 7 with an estimation of η [from Fig. 5 or 6]. It should be noticed that this procedure not only gives information on the total resistance but also on the drag distribution along the length of the mast and thus on the torque.

The reduced resistance of the tower on rough ground is due to the reduced velocity of the wind near the ground.

In this connection, it should be remarked that drag in general is dependent on the spacial velocity distributions of the undisturbed wind. Application of test results—even when condition of aerodynamic and geometric similarity are fulfilled—is only strongly possible when the

TABLE II (Part 2)

Complete Models of Lattice Masts

MODEL		ϕ	CROSS BARS	GROUND	α°	C_{w_r}	C_{a_r}	$\xi = \frac{C_{w_r}^{(max)}}{C_{w_r}^{(0)}}$
	FIG.							
Transmission Tower	16a	0.334	Without	Smooth	0(90, 180)	2.01		1.17
					45(135)	2.35		
				Rough	0(90, 180)	1.84		1.09
					45(135)	2.01		
		0.315	With	Smooth	0(180)	2.01		
					45(135)	2.00		
					90	1.58		
				Rough	0(180)	1.90		
					45(135)	1.93		
					90	1.47		
Radio Tower		0.187	Without		0(90, usw.)	2.544	0.0295	1.42
					9	2.765	0.2335	
					18	3.060	0.2545	
					27	3.335	0.1590	
					36	3.520	0.0423	
					45	3.620	0.0917	
Line Pole	16b	0.363	Without	Smooth	0(180)	1.16		
					45(135)	1.73		
					90(270)	0.93		
				Rough	0(180)	1.15		
					45(135)	1.66		
					90(270)	0.84		
		0.386	With	Smooth	0(180)	1.22		
					20(160)	1.28		
					45(135)	1.63		
					65(115)	1.54		
					90(270)	0.85		
				Rough	0(180)	1.15		
					45(135)	1.30		
					90(270)	0.83		

velocity profiles are the same. Applied to the problem of a lattice mast on the ground this implies that the ground frictional boundary layer has to be approximated in the wind tunnel in order to obtain valid model results.

The rise in total resistance with increase in α from 0° to 45° for the electric tower on a rough ground plate was around 9 per cent $[(2.01 - 1.84)/1.84 \approx .09]$, for a smooth ground plate the rise was 17 per cent. In other words, in one case $E = 1.09$, in the other $E = 1.17$. These values correspond then to expectations derived from partial model tests. It is notable that Katzmayer and Seitz* have obtained slightly greater E-values. Both authors found $E = 1.42$ for a wooden wireless tower model of scale 1:30. The solidarity coefficient of a side wall was $\phi = 0.137$. For $\alpha = 0^\circ$ $C_{w,r} = 2.544$, which is covered by our results [compare Table 1 and 2]. It is thus more striking that a really higher value was found for $\alpha = 45^\circ$. Rejecting experimental error as the explanation, then the reason may be the difference between customary wood construction, with its use of two \parallel bars, and usual steel construction. Such double bars have markedly higher resistance under oblique incidence from above or below. Such oblique incidence can occur from the end flow up over the peak of the mast or from the separation of the ground layer—even when the initial wind was horizontal. The effect on either profiled or flat bars is unimportant. Both effects are stronger for $\alpha = 45^\circ$ than for $\alpha = 0^\circ$ (since ϕ is at least as large for 45° as for $\alpha = 0^\circ$, the real permeability of this mast for oblique incidence is less). Therefore, a wood structure with double beams can have a larger E-value than those found by us. The magnitude of the increase in E due to double bars is not completely clarified. The following, however, should be noted:

* (12) Wind Pressure on Lattice Towers of Quadratic Cross Section (Baning 15, 1934, p 218-221). Two series of tests on the influence of fluctuating wind streams (once the dynamic pressure changed ± 30 per cent and the wind direction by ± 15 per cent, both with a period of about 1 sec) gave the important result that such fluctuations do not influence the exactness of the measurements.

Katzmayr and Seitz did not employ force measurements on the entire model to measure drag, but used readings on a high section of the model, with the help of a special but not described testing method. This method avoided breaking the model into sections.

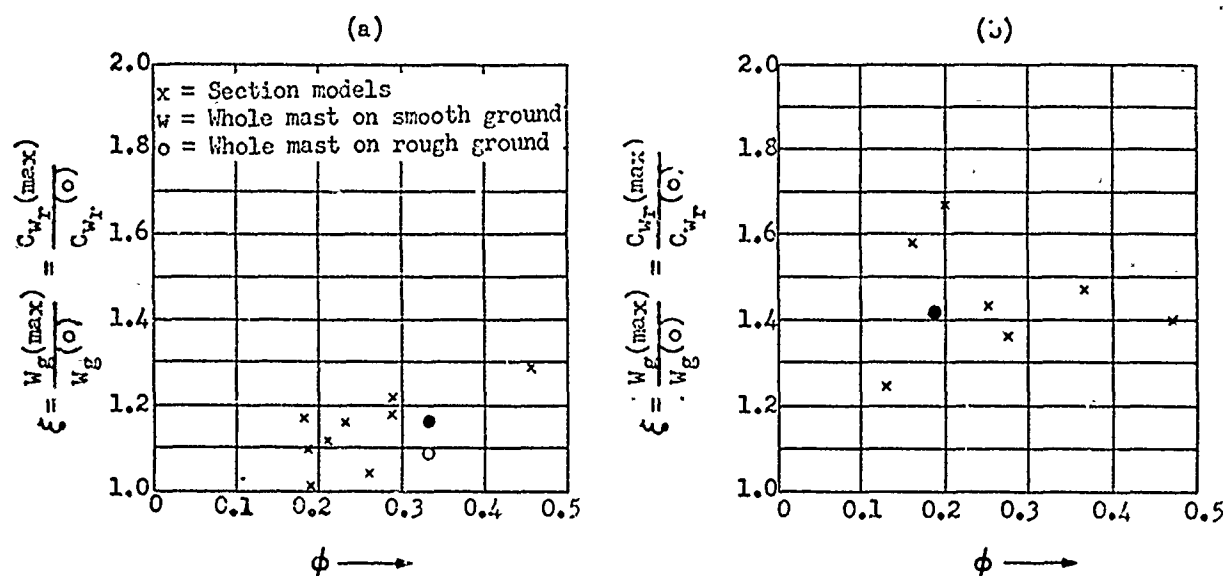


Fig. 18 -- Lattice towers of square cross section. No cross bars. Tests of Katzmayr and Seitz

In Figs. 18a and 18b the data of Katzmayr and Seitz is shown. The scatter of data points is rather large, a regular variation with ϕ is uncertain, so that we cannot conclude that unknown variables are at work determining the E-value. It would be welcome to have these questions clarified. Until then, it must be assumed provisionally that $E > 1.2$ can occur, especially for double-bar construction. It will be sufficient in such cases to set $E = 1.3$ or 1.4 . The value $E \approx 1.3$ is in agreement with our values, particularly for large solidarity coefficients ($\phi = 0.455$). For a quadratic prism ($\phi = 1.0$) Wieselsberger found for $\lambda = \infty$ that $E = 1.072$ while, with $\lambda = 5$, $E = 0.835$. Therefore, even a reduction in drag is possible with finite λ and oblique incidence.

The influence of cross arms on drag is slight as long as the projected area of the arms is relatively small, as is shown in Table II.

Table II contains, besides the data for high-tension towers and radio spires, the corresponding results for the model of a smaller (line) pole (scale 1:20, model height 0.575 m) illustrated in Fig. 16b. This pole is not three-dimensional, but is included for comparison with other towers.

CH VI -- SUMMARY AND CONCLUSIONS

1. While the drag coefficients c of single beams in uniform air streams are practically dependent alone on the solidarity coefficient ϕ , the drag coefficient C of a spacial lattice under similar conditions is a function of three variables: solidarity coefficient, ratio of lattice-plane separation to lattice height (e/d), and orientation of the lattice patterns to each other (congruent, in-line, etc). If τ symbolizes orientation, then one can write the relation:

$$(11) \quad C = C(\phi, e/d, \tau)$$

By spacial structures are meant open work formed by similar plane lattices.

2. If C is in particular the drag coefficient C_{p_r} ; then, according to definitions, the net force on a 3-d lattice in a uniform wind stream impinging at angle α is

$$P_g = C_{p_r} \cdot \frac{1}{2} \rho v^2 \cdot F_r \text{ [kg]}$$

(ρ = density, F_r = projected surface area of the lattice).

Corresponding equations hold for normal force, tangential force, resistance, and lift.

With an arbitrary angle of incidence, Eq 11 becomes

$$(12) \quad C = C(\phi, e/d, \tau, \alpha)$$

and also

$$\left. \begin{array}{l} P_g \\ W_g \\ A_g \\ N_g \\ T_g \end{array} \right\} \text{ really dependent on } \phi, e/d, \tau, \alpha, \rho, v, F_r$$

This applies when the gas velocity field is uniform in space and time, a condition assumed here unless otherwise stated. For nonuniform winds other parameters must be introduced. For single lattices both e/d and τ are discarded.

3. Two lattices of equal outline, equal structure type, and equal ϕ , form a lattice pair when they lie parallel to each other so that their outlines coincide (in-line) when viewed along the perpendicular to their planes. The lattice patterns don't necessarily have to be congruent. Each of the two lattices affects the drag of the other, as compared to the drag of one lattice alone.

The difference, of course, is a reduction for the shielded lattice and an increase for the leading lattice. The wind shadow of the forward member is very far-reaching, so that the rear lattice is still shielded even if it is quite far behind. For large lattice separation it is unimportant whether the patterns are congruent or not. For small separations the congruency of pattern reduces the drag, since the wind shadows coincide with corresponding bars on the rear lattice.

4. If one designates the resistance of the two lattices for normal incidence with W_I and W_{II} , then the combined drag W_g for the pair is [from Eqs 1 through 4]:

$$W_g = W_I + W_{II} = \psi_I W + \psi_{II} W = \psi_I W \left\{ 1 + \frac{\psi_{II}}{\psi_I} \right\}$$

and the drag coefficient (combined)

$$C_{w_r} = \psi_I \cdot c_{w_r} \left(1 + \frac{\psi_{II}}{\psi_I} \right) = \psi_I \cdot c_{w_r} (1 + \eta)$$

Here W means the drag, $c_{w_r} \equiv c_{w_r}^{(e=\infty)}$ which is the drag coefficient of a single isolated lattice.

On experimental grounds, the shielding coefficient of the fore lattice can be very well approximated as

$$\psi_I = 1.0$$

The shielding coefficient ψ_{II} of the second lattice and the shielding ratio of η of the two lattices are then practically equivalent numerically. The expression for C_{w_r} simplifies to

$$(7) \quad \boxed{C_{w_r} = c_{w_r} (1 + \eta)}$$

The values of c_{w_r} are available in Fig. 21, Part 1, and Figs. 7 and 8. The values of η lie in Figs. 5 and 6 of Part 2. For approximations:

$$(13) \quad \left. \begin{array}{l} c_{w_r} = 1.6 \\ \eta = (1 - \phi)^2 \end{array} \right\} \text{Lattices in-line}$$

$$\left. \begin{array}{l} c_{w_r} = 1.6 \\ \eta = 1.2 (1 - \phi)^2 \end{array} \right\} \text{Lattices displaced}$$

Oblique incidence on a lattice pair is shown in Figs. 7a and 7b.

For both single and paired lattices, the tangential forces are negligible under either normal or oblique incidence. Aspect ratio and outline of the lattice make no real difference.

5. The wind loadings of bridges with two main lattices and of lattice towers are traceable to the wind loadings of lattice pairs. Through Eq 7 and the shielding ratio, η , the bridge and mast drags are further related to the loadings of single lattices. Lattice masts [4-sided] under diagonal wind incidence are equivalent only to an imagined lattice pair. To aerodynamically designate this "ersatz" pair, the further quantity E is introduced.

6. The drag calculation of a twin-lattice bridge can use Eq 7. In the absence of special measurements use:

$$\text{for } \phi < 0.25, \quad c_{w_r} = 1.8$$

$$\text{for } \phi \geq 0.25, \quad c_{w_r} = 1.6$$

Since almost all bridges have ϕ exceeding 0.25, it is safe to assume

$$c_{w_r} = 1.6 = \text{constant}$$

so that the formula simplifies to

$$(14) \quad C_{w_r} = 1.6 (1 + \eta)$$

η is obtained from Eq 6 or Fig. 6, designates the road width and d the distance between the chords or the height of the bridge.

The approximate drag portion between the two main lattices is directly readable from the formula

$$C_{w_r} = c_{w_r} [1 + \eta] = \underbrace{c_{w_r}}_{\text{forward}} + \underbrace{c_{w_r} \eta}_{\text{leeward}}$$

for example with $c_{w_r} = 1.6$

$$C_{w_r} = \underbrace{1.6}_{\text{forward lattice}} + \underbrace{1.6\eta}_{\text{leeward lattice}}$$

For an estimation, one can again use $\eta = (1 - \phi)^2$ (in any case for lattices in line, which is true for almost all bridges). For design calculations the use of Figs. 6a and 6b, which are upper limits of experimentally scattered values, will incline the results to the safe side. The η -value of Fig. 6b in combination with Eqs 7 or 14 fixes the total resistance of the bridge with certainty, even for $\phi = 1.0$. However, the drag distribution for $\phi = 1.0$ is no longer that given by Fig. 6b and the approximation formula. Actually, the rear lattice experiences (for small e) negative drag, and Fig. 6b can't give this because its values for η have been made +.

The aerodynamics of solid-wall bridges thus merits further investigation. To the extent of Dickmann's researches this problem was attacked. For all true bridges* with two solid wall beams the preceding design formula gives practical information on the maximum total drag and its distribution. Besides, it has already been borne out that the greatest normal force occurs, not with normal incidence, but with oblique incidence. The drag forces derived from Eqs 7 or 14 are normal to the lattice planes. The tangential forces remain negligible.

7. The drags of lattice masts are derivable from drags of sectional models [a single section with the same structure and ϕ], with compensation for the ground posts, since they are usually different from the higher portions of the tower. The sum of the drags of each section gives the total drag and also the center of force.

For a tower of square cross section composed of four lattices the drag for $\alpha = 0^\circ$ is the same as for lattice pairs calculated by formula (7). This means that the drag is due almost entirely to the faces normal to the wind; the drag of planes parallel to the wind is practically nil. η is presented in Figs. 5 and 6. Usually masts have a square cross section ($e/d = 1.0$). If the lattice patterns are reversed, then the approximation formula must use a graph to obtain η , such as Fig. 5e which gives the upper values of η . Also the curves in Figs. 5a and 6a for $e/d = 1.0$ are satisfactory because they too are higher than the test points. One can ignore the unequal drag distribution on box lattice towers when $\alpha = 0^\circ$, if one uses Eq 7 and the curves at $e/d = 1.0$ in Fig. 6a. This is, of course, an approximation. Also for $\phi < 0.25$ it usually is satisfactory to set $c_{w_r} = 1.6$, as can be seen in the last third of Table I. In this section of Table I, the C_{w_r} values are presented [note here the designation is $C_{w_r}^{(0)}$ since here $\alpha = 0^\circ$]—values calculated with Eq 14 $C_{w_r} = 1.6 (1 + \eta)$, with η

* (16) Concerning calculations for lattices of nonuniform ϕ , one should refer to the remarks in Section VI, 9 of Part I.

taken from Fig. 6a where $e/d = 1.0$. Equally good results are obtained if one sets $\eta = 1.2$
 $(1 - \phi)^2$. Basically, one naturally is more certain using $c_{w_r} = 1.8$ for $\phi < 0.25$.

For oblique incidence [$\alpha \geq 0^\circ$] the resistance of a box lattice grows. Usually the maximum is for $\alpha = 45^\circ$, although sometimes for smaller angles. For technical calculations $\alpha = 45^\circ$ is assumed to give the maximum drag. Then from Eq 8

$$W_g^{(max)} = W_g^{(45)} = E W_g^{(0)}$$

The value of E has to be measured (as in Fig. 18). In general $E = 1.1$ to 1.2 (see Table I).
 For constructions utilizing two parallel bars instead of one, the E-value is raised to 1.3 or 1.4 . The expression for $W_g^{(45)}$ gives the drag distribution on the individual lattices directly [Eqs 9 and 10].

The lift or force normal to the wind direction (C_{a_r}) is negligible for all α 's.

6. The aerodynamics of spatial lattices is in some measure clarified by these results. Also the basic outlines of improved calculation techniques are brought out by the new knowledge. It is probably useful to once more write out the drag calculation procedure without the mass of supporting evidence.

a. Drag Calculation for a Bridge with Two Main Girders

(Assumption: the main girders are of uniform ϕ)*

Given: the solidarity coefficient ϕ of each girder

= projected area F_r of each girder

$$c_{w_r} = 1.6$$

Air density ρ {for normal conditions $\rho = \frac{1}{8} [\text{kg s}^2/\text{m}^4]$ }

Assumed peak wind velocity v (≈ 35 or 40 m/s)

* (17) Where this condition is not fulfilled, the parts of uniform ϕ must be calculated separately.

Calculation: The drag on the bridge is

$$W_g = C_{w_r} \cdot \frac{1}{2} \rho v^2 F_r = C_{w_r} q F_r \text{ [kg]}$$

directed normal to the girder (lattice) plane

C_{w_r} is from (7) or (14)

$$C_{w_r} = c_{w_r} (1 + \eta) = 1.6 (1 + \eta)$$

thus

(15)

$$W_g = 1.6 (1 + \eta) q F_r \text{ [kg]}$$

η is taken from Eq 6 or Fig. 6. η is dependent on ϕ and e/d where e is road width and d the girder height (actually d = distance between the mid-points of the chords of the principle girder lattices, and thus is very close to the lattice height).

The portion of this total drag is:

$$W_I = 1.6 q F_r \text{ on the windward lattice}$$

$$W_{II} = 1.6 \eta q F_r = \eta W_I \text{ on the leeward girder.}$$

[Notice: The use of Fig. 6b will give very safe (high) drag predictions for $\phi > 0.6$, but is unsatisfactory for predicting drag portion.]

To compare the above calculations with the current (1935) techniques, we must write

$$W = 1.6 (1 + \eta) q \text{ [kg/m}^2\text{]}$$

in the form

$$W_g = W F_r \text{ [kg]}$$

The German pressure formula is

$$W_g = w_o F_r \text{ [kg]}$$

with $w_o = 150 \text{ [kg/m}^2\text{]}$ for loaded bridges and $w_o = 250 \text{ [kg/m}^2\text{]}$ for unloaded bridges.

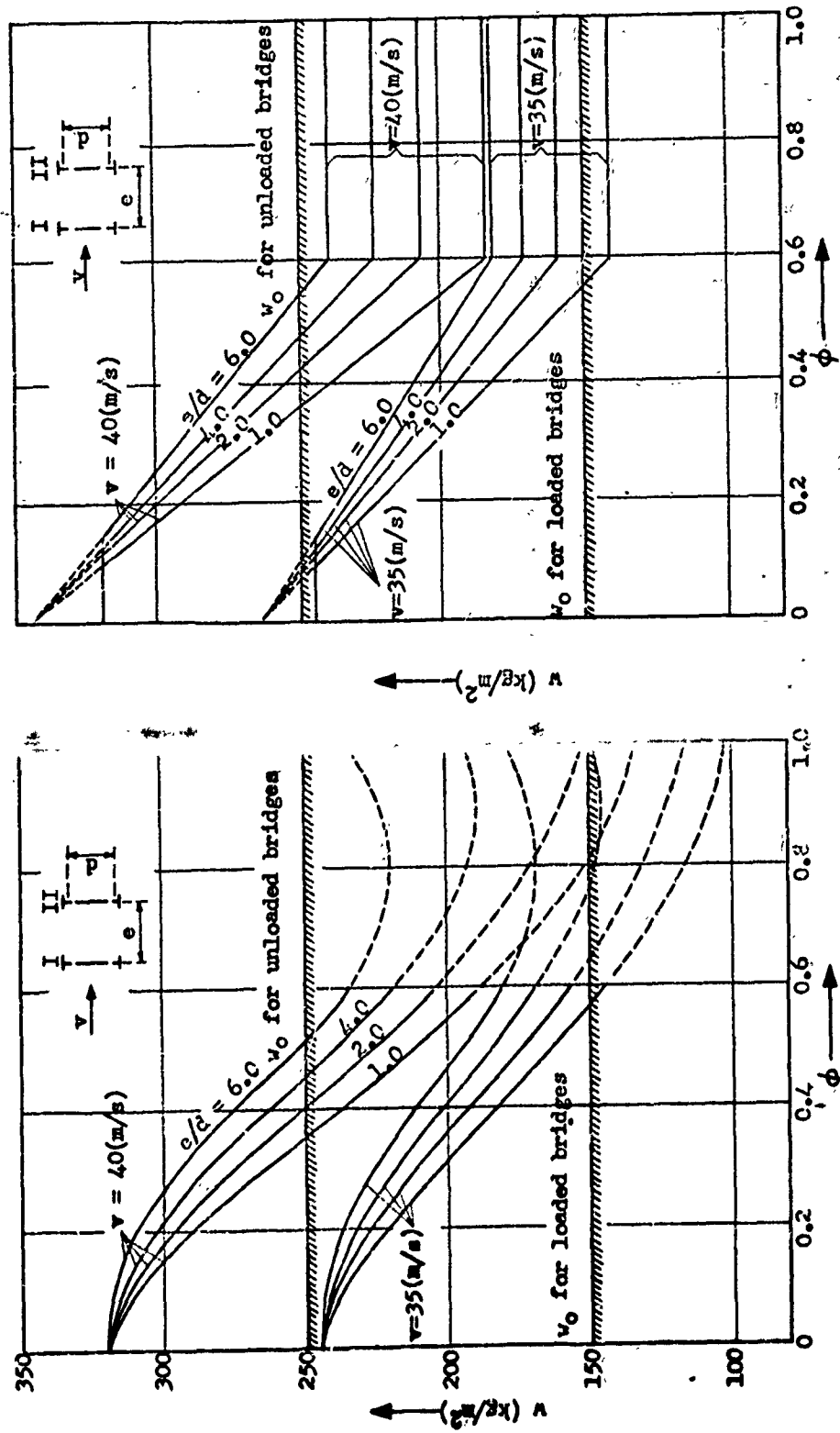


Fig. 19 -- Comparison between the proposed procedures and the current (1935) techniques for drag calculations of bridges. Fig. 19a corresponds to Fig. 6a, and Fig. 19b corresponds to Fig. 6b.

We have calculated w -curves for $v = 35 \text{ m/s}$ and $v = 40 \text{ m/s}$ from Figs. 6a and 6b and presented them in Figs. 19a and b along with w_0 values. One can see that no allowance is made by the old method for either ϕ or bridge width, and that no means is offered to give the drag partition among the two main girders.

b. Drag Calculations for Lattice Towers of Square Cross Section

Given: Solidarity coefficient ϕ of each side

Projected area F_r of each side

$c_{w_r} = 1.6$ (in place of more exact values)

Air density ρ

Further requirements: The distribution of wind velocity v as a function of height y above the ground.

Procedure: Divide the mast into sections of uniform ϕ , cross section, and incident wind. Calculate the drag for each section as follows:

Normal incidence to a side wall ($\alpha = 0^\circ$)

Combined drag in wind direction

$$W_g^{(0)} = C_{w_r}^{(0)} \cdot \frac{1}{2} \rho v^2 F_r = C_{w_r}^{(0)} q F_r \text{ [kg.]}$$

where F_r is the projected area of one side wall of the section.

With

$$C_{w_r}^{(0)} = c_{w_r} (1 + \eta)$$

it follows

(18)

$$W_g^{(0)} = c_{w_r} (1 + \eta) q F_r \text{ [kg]}$$

or with $c_{w_r} = 1.6$

$$(19) \quad W_g^{(0)} = 1.6 (1 + \eta) q F_r \text{ [kg]}$$

η is taken from Fig. 6a for $e/d = 1.0$, or one can set

$$\eta = 1.2 (1 - \phi)^2$$

It comes out approximately

$$1.6 q F_r = \frac{1}{1 + \eta} \cdot W_g^{(0)} \text{ on the fore wall}$$

$$1.6 \eta q F_r = \frac{1}{1 + \eta} \cdot W_g^{(0)} \text{ on the rear wall}$$

These forces are (to a high approximation) normal to the wall surfaces. The walls parallel to the wind experience practically no loading.

Air Stream along the Cross Section Diagonal ($\alpha = 45^\circ$). The net force in the wind direction

$$(20) \quad W_g^{(45)} = E W_g^{(0)} \text{ [kg]}$$

$E = 1.1$ to 1.4 . For steel construction usually $E = 1.1$ to 1.2 , particularly when no double bars are used [two close parallel bars where one "profiled" bar is normally employed]. Where double bars occur [wood construction] $E > 1.2$ should be used. (This question is not completely clarified.)

The combined force is divided approximately

$$E \cdot 1.6 q F_r = \frac{1}{1 + \eta} \cdot W_g^{(45)} \left\{ \begin{array}{l} \text{for the two windward} \\ \text{sides} \end{array} \right.$$

$$E \eta \cdot 1.6 q F_r = \frac{\eta}{1 + \eta} \cdot W_g^{(45)} \left\{ \begin{array}{l} \text{for the two leeward} \\ \text{sides} \end{array} \right.$$

The forces are in the wind direction.

The integration of each section's drag gives the total mast drag and its distribution and torque.

If one undertakes a critique of contemporary drag calculations; then, before all, it must be stated that the so-called sine law of sine-squared law fails to give the observed increase in drag for oblique incidence and there is no insight into the drag partition between the individual walls.

. In conclusion it must be pointed out once more that these results apply only to spacial lattice-works composed of plane lattices and which are uninfluenced by terrain and neighboring structures. In such cases no far-reaching predictions can be made and further tests are recommended.

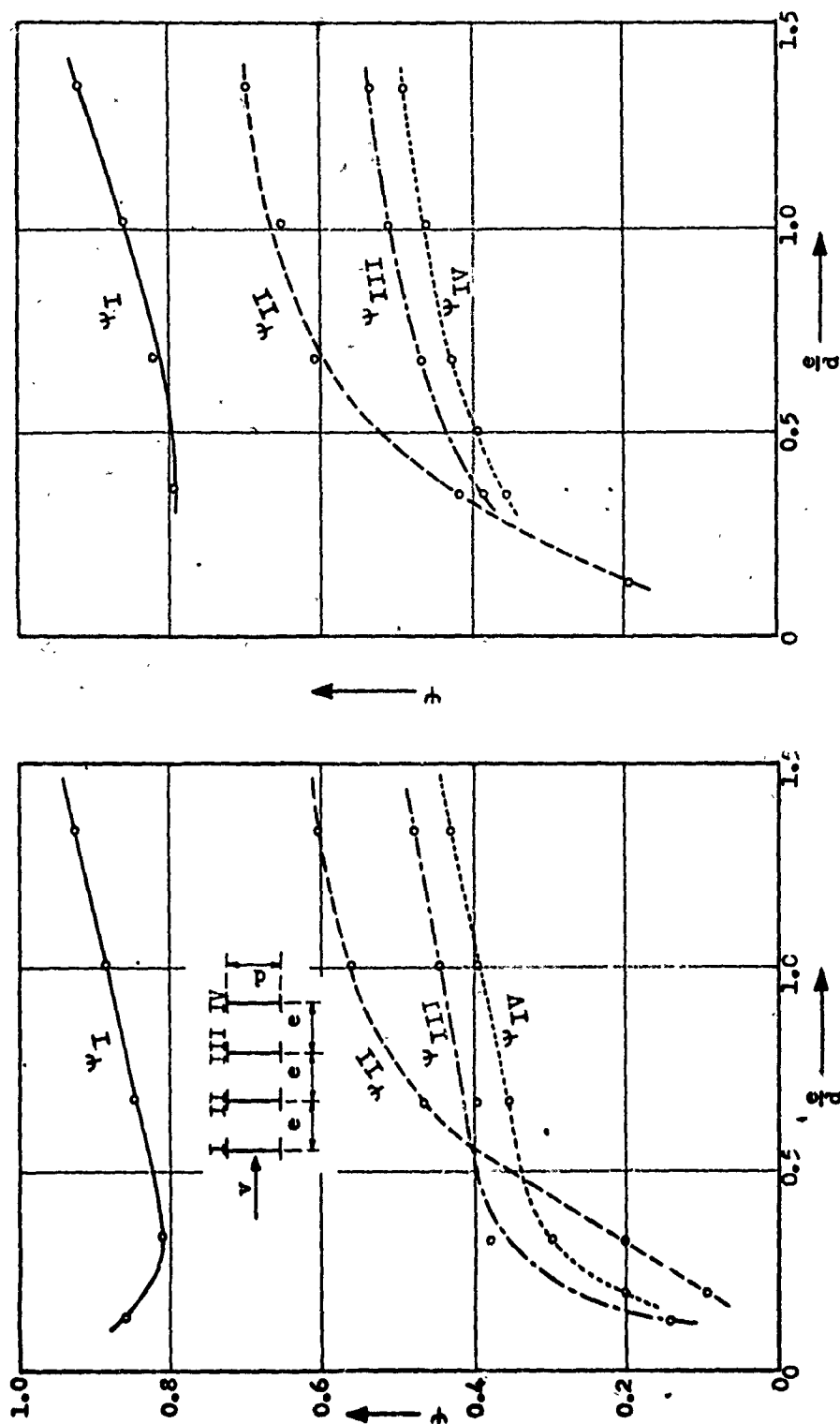


Fig. 20 -- Shielding coefficients of a group of four parallel lattices, $\alpha = 0^\circ$, $\lambda = \infty$. The lattices are shown in Fig. 8b of Part 2, $\phi = 0.178$. At left (Fig. 20a) all beams are in line; at right, each beam is transposed $1/2$ x field width compared to the previous one. "Field-width" is the height of the lattice

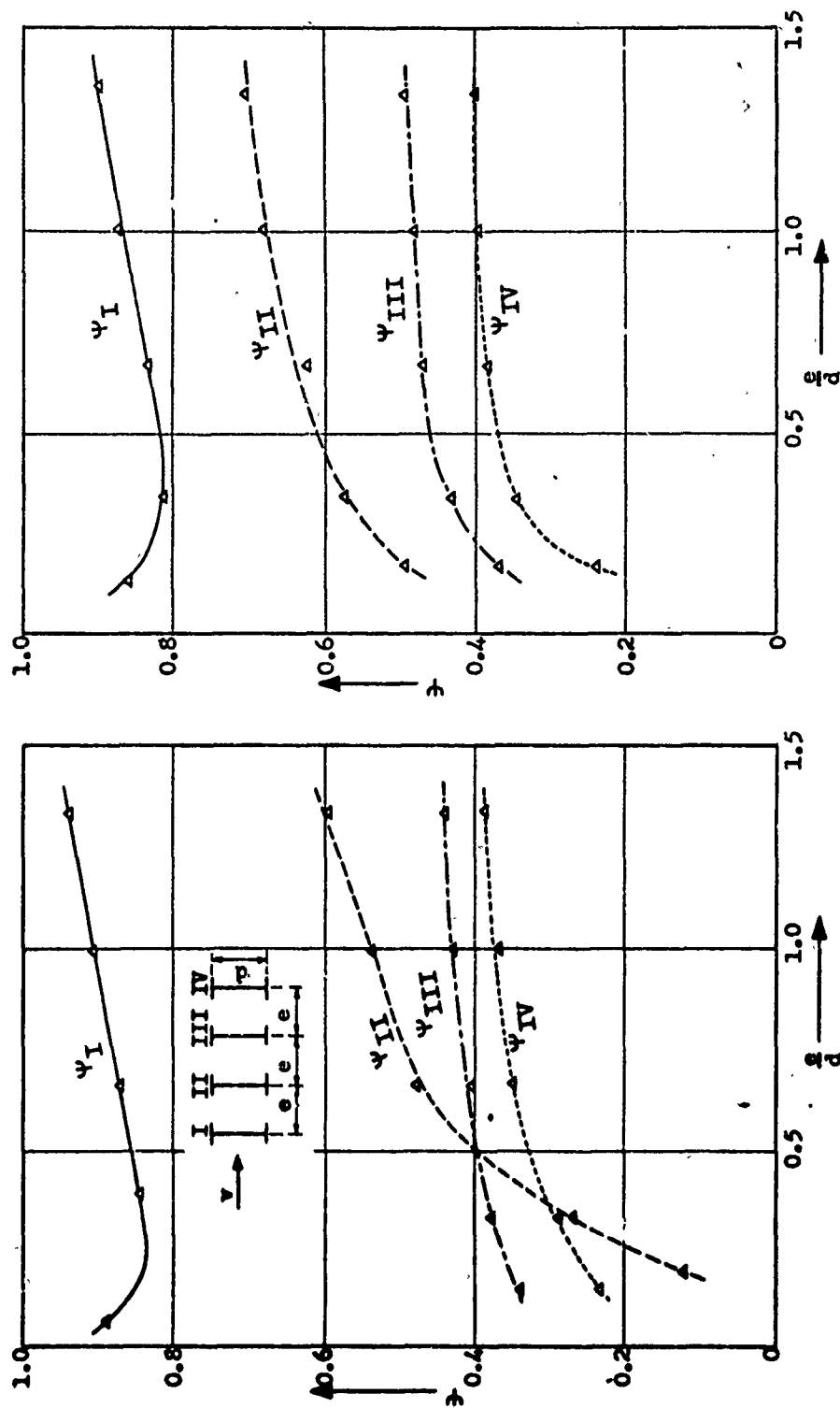


Fig. 21 -- Shielding coefficients of a group of four V-type parallel lattices (Fig. 8g, Part 1), $\beta = 0.234$, $\lambda = \infty$. Fig. 21a, lattices in line; Fig. 21b, each lattice transposed $1/2 \times$ "field width" ($1/2 \times$ height) with respect to the adjacent lattice

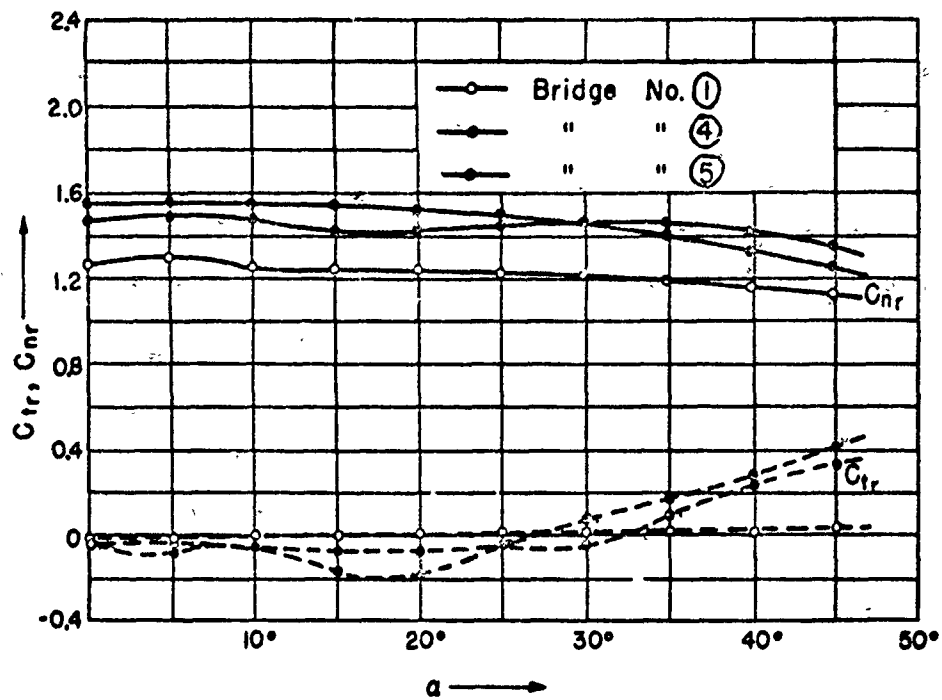


Fig. 22 -- Winds from above

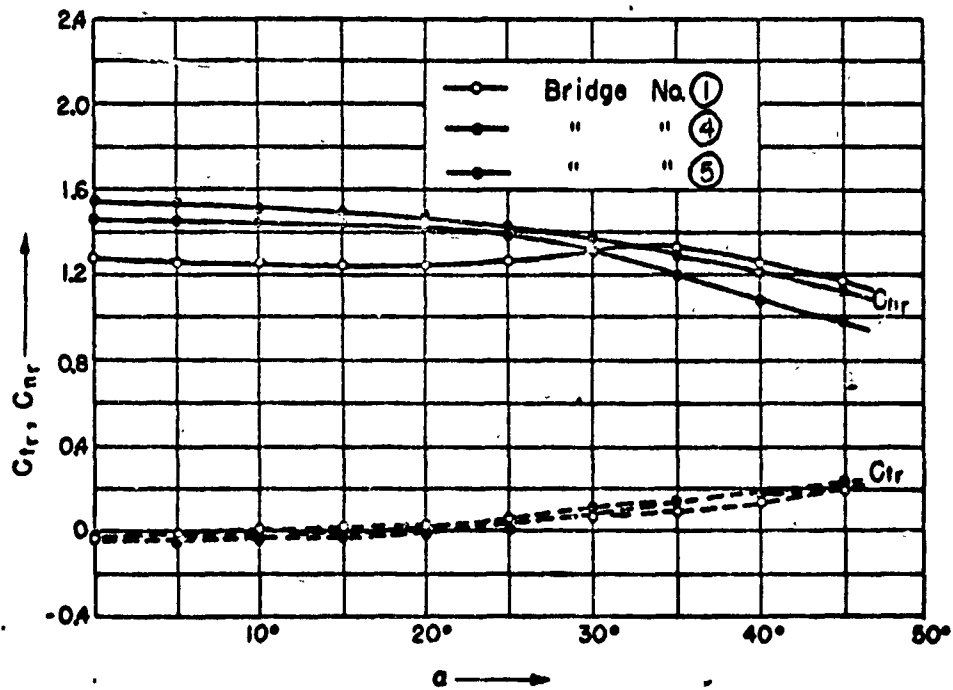


Fig. 23 -- Winds from a side

APPENDIX A

In Figs. 20 and 21 we include results from measurements on four equidistant parallel identical lattices, with $\lambda = \infty$.

These data have some interest for bridges with more than two main girders. These results are presented in an appendix because they may be subject to test errors. The models were investigated in a small tunnel with a free air stream. Since the free streamlines spread out laterally, the uniformity of the velocity field becomes more and more distorted with increasing distance from the tunnel throat. Both effects lead to a reduction in resistance. Control measures were not taken. However, the errors are probably so small that the results are a sufficient approximation to the true conditions.

The single beams are known from Part 1 (see Figs. 8b and 8g, Figs. 9 or 21). For the same type beam the notation is retained here for the corresponding test points. Figs. 20 and 21 show shielding coefficients ψ against separation e/d .

One uses the drag coefficients and resistance in the known way. Example: Resistance W_{III} of beam III for separation e/d and given orientation (transposed or in-line). One takes ψ_{III} from Fig. 20 or 21 and adds the c_{w_r} of an isolated beam to obtain the drag coefficient and resistance of the III beam in combination with the group.

$$c_{w_{rIII}} = \psi_{III} c_{w_r}; \quad W_{III} = c_{w_{rIII}} q F_r \text{ [kg]}$$

INITIAL DISTRIBUTION

- 1 W. A. MacNair, 5000
- 2 S. C. Hight, 5100
- 3 E. F. Cox, 5110
- 4 G. E. Hansche, 5140
- 5 M. L. Merritt, 5111
- 6-7 J. D. Shreve, Jr., 5112
- 8 G. T. Pelsor, 5121
- 9 R. O. Frantik, 5131
- 10 W. D. Wood, 5132
- 11 S. H. Dike, 5133
- 12 R. F. Brodsky, 5141
- 13-14 A. Y. Pope, 5142
- 15 W. E. Schorr, 1215-2
- 16 Walker Bleakney, Princeton University
- 17 C. W. Lampson, BRL
- 18 G. K. Hartmann, NOL
- 19 C. J. Aronson, NOL
- 20 E. B. Doll, SRI
- 21 R. J. Hansen, MIT
- 22 F. M. Duggan, MIT
- 23 E. A. Witmer, MIT
- 24 N. M. Newmark, University of Illinois
- 25 R. S. Stillwell, University of Illinois
- 26 J. S. McNown, University of Michigan
- 27 B. G. Johnston, University of Michigan
- 28 H. L. Bowman, Drexel Institute of Technology
- 29 E. H. Smith, E. H. Smith & Company
- 30 UCRL, Livermore; Attn: Margaret Folden
- 31 P. Fine, DMA/AEC
- 32 R. L. Corsbie, DBM/AEC
- 33 C. Beck, Construction Division, USAEC
- 34 Director, J Division, LASL
- 35 J. E. Fitzgerald, American Machine & Foundry Company
- 36 S. J. Fraenkel, Armour Research Foundation
- 37 J. O. Jackson, Pittsburg-Des Moines Steel Company
- 38-39 K. Zebb, Cooperative Wind Tunnel
- 40-41 K. D. Bird, Cornell Aeronautical Laboratory
- 42-47 Ira H. Abbott, NACA, Washington
- 48 Technical Information Service, USAEC, Attn: Jean M. O'Leary
- 49-88 Document Room

INITIAL DISTRIBUTION (cont)

Through Technical Library Branch AFSWP Headquarters

ARMY

- 89 Assistant Chief of Staff, G-3, D/A, Washington 25, D. C., Attn: Deputy Chief of Staff, G-3 (RR&SW)
- 90 Assistant Chief of Staff, G-4, D/A, Washington 25, D. C.
- 91 Chief of Ordnance, D/A, Washington 25, D. C., Attn: ORDTX-AR
- 92-94 Chief Signal Officer, D/A, P & O Division, Washington 25, D. C.
- 95 The Surgeon General, D/A, Washington 25, D. C., Attn: Chairman, Med R & D Board
- 96-97 Chief, Chemical Officer, D/A, Washington 25, D. C.
- 98 The Quartermaster General, CBR Liaison Officer, R & D Division, D/A, Washington 25, D. C.
- 99-100 Chief of Engineers, D/A, Washington 25, D. C., Attn: ENGNB
- 101 Chief of Transportation, Military Planning & Intelligence Division, Washington 25, D. C.
- 102-104 Chief, Army Field Forces, Ft. Monroe, Va.
- 105 President, Board #1, OCAFF, Ft. Bragg, N. C.
- 106 President, Board #2, OCAFF, Ft. Knox, Ky.
- 107 President, Board #4, OCAFF, Ft. Bliss, Texas
- 108-109 Commander-in-Chief, FECOM, APO 500, c/o P. M., San Francisco, Calif., Attn: ACofS, J-3
- 110 Commandant, Command & General Staff College, Ft. Leavenworth, Kansas, Attn: ALLIS(AS)
- 111 Secretary, The AA & GM Branch, The Artillery School, Ft. Bliss, Texas, Attn: Lt. Col. Albert D. Epley, Dept of Tactics and Combined Arms
- 112 Commanding General, Medical Field Service School, Brooke Army Medical Center, Ft. Sam Houston, Texas
- 113 Director, Special Weapons Development Office, OCAFF, Ft. Bliss, Texas
- 114 Commanding General, Research & Engineering Command, Army Chemical Center, Maryland, Attn: Deputy for RW & Non-Toxic Material
- 115-116 Commanding General, Aberdeen Proving Grounds, Maryland, Attn: Director, Ballistics Research Lab.
- 117-119 Commanding General, The Engineer Center, Ft. Belvoir, Va., Attn: Assistant Commandant, Eng School
- 120 Commanding Officer, Engineer Research & Development Laboratory, Ft. Belvoir, Virginia, Attn: Chief, Tech Intelligence Branch
- 121 Commanding Officer, Picatinny Arsenal, Dover, N. J., Attn: ORDBB-TK
- 122-123 Commanding Officer, Chemical & Radiological Laboratory, Army Chemical Center, Maryland, Attn: Tech Library
- 124 Commanding Officer, Transportation R & D Station, Ft. Eustis, Virginia
- 125 Director, Technical Documents Center, Evans Signal Laboratory, Belmar, N. J.
- 126 Director, Waterways Experiment Station, P. O. Box 631, Vicksburg, Miss., Attn: Library
- 127 Director Operations Research Office, Johns Hopkins University, 7100 Connecticut Avenue, Chevy Chase, Maryland, Washington 15, D. C.

NAVY

- 128-129 Chief of Naval Operations, D/N, Washington 25, D. C., Attn: OP-36
- 130 Chief of Naval Operations, D/N, Washington 25, D. C., Attn: OP-374(OEG)
- 131 Director of Naval Intelligence, D/N, Washington 25, D. C., Attn: OP-922V

INITIAL DISTRIBUTION (cont)

NAVY (cont)

- 132 Chief, Bureau of Medicine & Surgery, D/N, Washington 25, D. C., Attn: Special Weapons Defense Division
- 133 Chief, Bureau of Ordnance, D/N, Washington 25, D. C.
- 134 Chief, Bureau of Ships, D/N, Washington 25, D. C., Attn: Code 348
- 135 Chief, Bureau of Yards & Docks, D/N, Washington 25, D. C., Attn: P-312
- 136 Chief, Bureau of Supplies & Accounts, D/N, Washington 25, D. C.
- 137-138 Chief, Bureau of Aeronautics, D/N, Washington 25, D. C.
- 139 Chief of Naval Research, D/N, Washington 25, D. C., Attn: LTJG F. McKee, USN
- 140 Commander-in-Chief, U. S. Pacific Fleet, FPO San Francisco, California
- 141 Commander-in-Chief, U. S. Atlantic Fleet, U. S. Naval Base, Norfolk 11, Va.
- 142-145 Commandant, U. S. Marine Corps, Washington 25, D. C., Attn: Code A03H
- 146 Superintendent, U. S. Naval Postgraduate School, Monterey, California
- 147 Commanding Officer, U. S. Naval Schools Command, U. S. Naval Station, Treasure Island, San Francisco, California
- 148 Commanding Officer, U. S. Fleet Training Center, Naval Base, Norfolk 11, Va., Attn: Special Weapons School
- 149-150 Commanding Officer, U. S. Fleet Training Center, Naval Station, San Diego, California, Attn: (SPWP School)
- 151 Commanding Officer, Air Development Squadron 5, VX-5, U. S. Naval Air Station, Moffett Field, California
- 152 Commanding Officer, U. S. Naval Damage Control Training Center, Naval Base, Philadelphia, Pa., Attn: ABC Defense Course
- 153 Commanding Officer, U. S. Naval Unit, Chemical Corps School Army Chemical Training Center, Ft. McClellan, Alabama
- 154-156 Commander, U. S. Naval Ordnance Laboratory, White Oak, Silver Spring 19, Maryland, Attn: EE, EH, and R
- 157 Commander, U. S. Naval Ordnance Test Station, Inyokern, China Lake, Calif.
- 158 Officer-in-Charge, U. S. Naval Civil Engineering Research and Evaluation Laboratory, U. S. Naval Construction Bn. Center, Port Hueneme, Calif, Attn: Code 753
- 159 Director, U. S. Naval Research Laboratory, Washington 25, D. C.
- 160 Commanding Officer & Director, U. S. Navy Electronics Laboratory, San Diego 52, California, Attn: Code 4223
- 161-162 Commanding Officer, U. S. Naval Radiological Defense Laboratory, San Francisco, California, Attn: Tech Info Division
- 163 Commanding Officer & Director, David W. Taylor Model Basin, Washington 7, D. C., Attn: Library
- 164 Commander, U. S. Naval Air Development Center, Johnsville, Pa.
- 165-166 Director, Office of Naval Research Branch Office, 1000 Geary Street, San Francisco, California

AIR FORCE

- 167 Assistant for Atomic Energy, Headquarters USAF, Washington 25, D. C., Attn: DCS/O
- 168 Director of Plans, Headquarters USAF, Washington 25, D. C., Attn: War Plans Division
- 169 Director of Requirements, Headquarters USAF, Washington 25, D. C., Attn: AFDRQ-SA/M

INITIAL DISTRIBUTION (ccnt)

AIR FORCE (cont)

- 170 Director of Research & Development, DCS/D, Headquarters USAF, Washington 25, D. C., Attn: Combat Components Division
- 171-172 Director of Intelligence, Headquarters USAF, Washington 25, D. C., Attn: AFOIN-1B2
- 173 The Surgeon General, Headquarters USAF, Washington 25, D. C., Attn: Bio. Defense Br., Prev. Med Division
- 174 Commander, Strategic Air Command, Offutt AFB, Omaha, Nebraska, Attn: Special Weapons Branch, Inspector Division, Inspector General
- 175 Commander, Tactical Air Command, Langley AFB, Va., Attn: Doc Security Br.
- 176 Commander, Air Defense Command, Ent AFB, Colorado
- 177-178 Commander, Air Materiel Command, Wright-Patterson AFB, Dayton, Ohio, Attn: MCAIDS
- 179 Commander, Air Training Command, Scott AFB, Belleville, Ill. Attn: DCS/O GTP
- 180 Commander, Air Research & Development Command, P. O. Box 1395, Baltimore, Maryland, Attn: RDDN
- 181 Commander, Air Proving Ground Command, Eglin AFB, Florida, Attn: AF/TRB
- 182-183 Director, Air University Library, Maxwell AFB, Alabama, Attn: CR-5464
- 184 Commander, Crew Training Air Force, Randolph Field, Texas, Attn: 2GTS, DCS/O
- 185 Commander, Headquarters, Technical Training Air Force, Gulfport, Miss., Attn: TA & D
- 186-187 Commandant, Air Force School of Aviation Medicine, Randolph AFB, Texas
- 188-190 Commander, Wright Air Development Center, Wright-Patterson AFB, Dayton, Ohio, Attn: WCOESP
- 191-192 Commander, AF Cambridge Research Center, 230 Albany Street, Cambridge 39, Mass., Attn: CRW, Atomic Warfare Directorate and CRQST-2
- 193-195 Commander, AF Special Weapons Center, Kirtland AFB, New Mexico, Attn: Library
- 196 Commandant, USAF Institute of Technology, Wright-Patterson AFB, Dayton, Ohio, Attn: Resident College
- 197 Commander, Lowry AFB, Denver, Colorado, Attn: Dept of Armament Training
- 198 Commander, 1009th Special Weapons Squadron, Headquarters USAF, Washington 25, D. C.
- 199-200 The RAND Corporation, 1700 Main Street, Santa Monica, California, Attn: Nuclear Energy Division

OTHER DOD AGENCIES

- 201 Assistant Secretary of Defense, Research & Development, DOD, Washington 25, D. C., Attn: Tech Library
- 202 United States National Military Representative, Headquarters SHAPE, APO 55, c/o P. M., New York, New York, Attn: Col. J. P. Healy
- 203 Director, Weapons Systems Evaluation Group, OSD, Rm 2E1006, The Pentagon, Washington 25, D. C.
- 204 Commandant, Armed Forces Staff College, Norfolk 11, Va., Attn: Secretary
- 205-210 Commanding General, Field Command, AFSWP, P. O. Box 5100, Albuquerque, New Mexico

21.

INITIAL DISTRIBUTION (cont)

OTHER DOD AGENCIES

- 211-212 Commanding General, Field Command, AFSWP, P. O. Box 5100, Albuquerque, New Mexico, Attn: Tech Training Group
- 213-221 Chief, Armed Forces Special Weapons Project, Washington 25, D. C.
- 222 ASTIA, Document Service Center, U B Building, Dayton 2, Ohio, Attn: DCS-SA
(No Restricted Data to this Addressee)

OTHERS

- 223 Director, National Bureau of Standards, Washington, D. C., Attn: Security Officer
- 224 Chief, Forest Service, Department of Agriculture, Washington, D. C.
- 225 Dr. Hans H. Bleich, Department of Civil Engineering, Columbia University, New York, New York
- 226 Dr. Clayton Oliver Dohrenwend, Office, Graduate Division, Rensselaer Polytechnic Institute, Troy, New York
- 227 Dr. L. S. Jacobsen, 668 Cabrillo Street, Stanford University, Palo Alto, Calif.
- 228 Dr. Merit P. White, Department of Engineering, University of Massachusetts, Amherst, Mass.
- 229 Professor Harry A. Williams, Stanford University, Palo Alto, Calif.